Title
Regulation of isoprenoid precursor pathways in Listeria monocytogenes

Author
Lee, Eric David

Publication Date
2019

Peer reviewed|Thesis/dissertation

Regulation of isoprenoid precursor pathways in *Listeria monocytogenes*

By

Eric David Lee

A dissertation submitted in partial satisfaction of the

requirements for the degree of

Doctor of Philosophy

in

Infectious Diseases and Immunity

in the

Graduate Division

of the

University of California, Berkeley

Committee in charge:

Professor Daniel A. Portnoy, Chair
Professor Jeffery Cox
Associate Professor Laurent Coscoy
Professor Jay D. Keasling

Fall 2019

Abstract

Regulation of isoprenoid precursor pathways in *Listeria monocytogenes*

by

Eric David Lee

Doctor of Philosophy in Infectious Diseases and Immunity

University of California, Berkeley

Professor Daniel A. Portnoy, Chair

Listeria monocytogenes is a facultative, Gram-positive intracellular pathogen that is also a model organism for studying bacterial pathogenesis. Much of the appeal of using *L. monocytogenes* as a model organism derives from the fact that much of the knowledge gained from studying *L. monocytogenes* pathogenesis or metabolism can be applied to other pathogens that are more difficult to work with or manipulate. However, the unique aspects of *L. monocytogenes* biology are equally fascinating and still shed light on the host cell processes that help protect against infections.

Isoprenoids are a diverse class of compounds produced by all forms of life and are synthesized from essential precursors derived from either the mevalonate pathway or the nonmevalonate pathway. Most organisms have one pathway or the other, but *L. monocytogenes* is unique because it encodes all of the genes from both pathways. Other scientists reported that the mevalonate pathway was essential for growth, but here we report that the nonmevalonate pathway was sufficient for growth anaerobically. Deleting the mevalonate pathway gene *hmgR* (Δ*hmgR*) impaired bacterial growth in all *L. monocytogenes* strains studied, but the laboratory strain 10403S grew significantly slower than two lineage I strains, FSL N1-017 and HPB2262 Aureli 1997. The faster anaerobic growth of the lineage I strains was initially traced to a difference in the nonmevalonate pathway enzyme GcpE, and then chimeric proteins were constructed to precisely identify the molecular basis of this phenotype. Three amino acid residues, K291T, E293K, and V294A were shown to be necessary and sufficient to increase the anaerobic growth rate of 10403S Δ*hmgR*. However, these mutations did not map to GcpE in a way that provided any obvious mechanistic insights to how the enzyme function was altered. Even though the nonmevalonate pathway was found to function anaerobically, we were unable to identify conditions where deleting the nonmevalonate pathway impaired *L. monocytogenes* growth of any strain. Given the fitness cost of maintaining all seven genes in the nonmevalonate pathway, it is likely that there are yet unidentified anaerobic growth conditions that require the nonmevalonate pathway. This work showed that, contrary to previous reports, the mevalonate pathway is not essential

for *L. monocytogenes* growth anaerobically, although it is still essential for growth aerobically.

After finding specific mutations in GcpE that altered growth, we were also interested in understanding the broader networks regulating the nonmevalonate pathway in *L. monocytogenes*. The difference in anaerobic growth rates between 10403S Δ*hmgR* and lineage I Δ*hmgR* mutants indicated that it could be possible to find suppressor mutations that increased 10403S Δ*hmgR* growth rate. 10403S Δ*hmgR* cultures were passaged anaerobically, and fast-growing suppressor mutants began arising after three passages, which was noted by the observation that cultures initially required four or five days to reach stationary phase, but later only required two days to reach stationary phase. Whole genome sequencing of these cultures identified mutations in several genes, but the most common mutations were in the histidine kinase of a two-component system LisRK. We demonstrated that the suppressor mutations altered rather than disrupted LisRK signaling, but were unable to identify specific genes in the regulon that were responsible for the increased rate of anaerobic growth. This work showed that multiple mutations can be made that alter the rate of *L. monocytogenes* growth using the nonmevalonate pathway. The previously identified mutations in GcpE likely directly change enzyme kinetics, allowing for increased flux through the nonmevalonate pathway, but the additional mutations identified here likely change gene expression levels or alter metabolite concentrations at points upstream or downstream of the nonmevalonate pathway itself.

“Dig where you stand.”

- Sven Lindqvist

Dedication

To my parents who supported me every step of the way,

and have always challenged me to wonder, “Why?”

Table of Contents

List of Figures and Tables

Acknowledgements

Portnoy Lab: Where to start. **Aaron**, you taught me everything I know about cloning. **Jon**, you taught me how to have fun in lab and in grad school. I still remember meeting both of you during the IDI recruitment weekend and give you a lot of credit for me ending up at Berkeley in the first place. **Gabe**, you taught me that, as scientists, we should be just as fastidious as our bacteria. Thank you for mentoring me during my rotation and bringing a positive attitude to work every single day.

For **everyone in the lab**, past and present, thank you for contributing the special place that is the Portnoy Lab. Thanks to Thomas, Michelle, Susy, Qiongying, and Chen for generously sharing your knowledge when I first joined the lab. You created a culture of scientific excellence combined with lots of fun that Bret, Brittney, and I have tried to carry on. For everyone who joined afterwards: Alex, Freddy, Sam, Raf, Ying, John, and Victoria; thank you for everything you've contributed to my science as well, it's up to you to keep the spirit of the Portnoy Lab alive and well. The environment has changed over the years, but from our parties in Barker, to BBQs on the lawn, to adventures around the Bay Area, every one of you have made it fun to show up and do science each day.

Kathleen: Third time's the charm. It's been an absolute blast working with you over the past year and a half, and I'll miss the enthusiasm and energy that you bring to lab every day. Your ceaseless and fearless curiosity have brought me so much joy, and I hope I've been able to give back a tiny fraction of what I've received as your mentor. Watching your growth as a scientist and knowing that I had some tiny part in that is one of the things I've proudest of from my time in graduate school. I can't wait to see where you're headed.

Brittney: Extra special thanks to you for everything you've done as a lab mate, bay mate, and friend over the years. From welcoming me into the PMB cohort to literally teaching me how to streak out bacteria, it's hard to capture how much you've impacted my graduate school experience in just a few sentences. We've been through a lot and seen a lot of changes through graduate school, and I'm thankful that I've been able to share that with you and Bret.

Dan: Shortly before I joined the lab, you said to me, "I just don't think you're hungry enough." I don't think that chip on my shoulder ever went away, and I hope that the work I've done over the past five years has at very least challenged that idea.

In one of my favorite articles about 'how to do' graduate school, the author advises picking a mentor who is a good scientist and a good mentor. Anyone reading this thesis surely recognizes the first is true. Scientifically, I honestly can't count the number of times I stubbornly ignored one of your suggestions for months, and once I finally did it, it led to a major step forward in my research. I think many outside the lab may not recognize what you offer as a mentor as readily. Your generosity and commitment to supporting your trainees, regardless of whether we are going into academia, is unparalleled in my experience at Berkeley. Wherever I end up after graduate school, I hope that I can do as much for my future mentees as you've done for me.

I would be remiss to talk about graduate school without mentioning everyone outside the lab who shaped this experience as well. All the people in **IDI/MCB/PMB**, thank you for your friendships along the way. There are too many of you to mention individually (although special shout-out to Domi, Alyssa, Huntly, and Claire), and I look forward to keeping in touch well past graduate school. To the **Cal Sailing Club** community, thanks for helping me discover a love of windsurfing, and to the **CAYAC** choir at First Pres, thanks for helping me rediscover my love of music. Finally, thank you to everyone in the **Science Policy Group at Berkeley**. The work we've done over the past few years has been essential in shaping my future career aspirations, and I hope that I'll have the opportunity to work with many of you as colleagues in the future.

Eric David Lee
Curriculum Vitae

EDUCATION

University of California, Berkeley Berkeley, CA
PhD, Infectious Diseases and Immunity December 2019
Regulation of isoprenoid precursor pathways in *Listeria monocytogenes*
Daniel A. Portnoy (Chair), Jeffery Cox, Laurent Coscoy, Jay Keasling

Columbia University in the City of New York New York, NY
B.A., *magna cum laude*, Chemistry Department Honors, Biochemistry May 2014

RESEARCH EXPERIENCE

University of California, Berkeley Berkeley, CA
Doctoral candidate; Professor Daniel A. Portnoy September 2014 - present
- Discovered that the nonmevalonate pathway of isoprenoid precursor biosynthesis functions anaerobically in the bacterial pathogen *Listeria monocytogenes*
- Studied role of the nonmevalonate pathway for growth in the bacterial pathogen *Listeria monocytogenes*, using human tissue culture and mouse models

Columbia University New York, NY
Research assistant; Professor Brent R. Stockwell August 2012 - May 2014
- Identified acetyl-CoA carboxylase 1 (ACC1) as an essential regulator of caspase-independent cell death, and demonstrated that inhibition of the cystine-glutamate exchange regulator system x_c^- induces ferroptotic cell death pathways

AWARDS & SCHOLARSHIPS

UC Center of Sacramento - Winner of STEM Solutions in Public Policy Competition (2019), proposal was developed into California Assembly Bill AB-1178
UC Berkeley - Student Leadership Award (2018)
UC Berkeley - Spath Scholarship (2014)
UC Berkeley - Art and Mary Fong Graduate Fellowship in the Health Sciences (2014)
American Society of Microbiology - Student and Postdoctoral Travel Award (2017)
National Science Foundation - Graduate Research Fellowship Program Honorable Mention (2015, 2016)

PUBLICATIONS

Lee ED, Navas KI, Portnoy DA. "The nonmevalonate pathway of isoprenoid biosynthesis supports anaerobic growth of *Listeria monocytogenes*." (*Infection & Immunity*, *in review*)

Dixon SJ, Winter GE, Musavi LS, **Lee ED**, Snijder B, Rebsamen M, Superti-Furga G, Stockwell BR. "Human haploid cell genetics reveals roles for lipid metabolism genes in nonapoptotic cell death." (*ACS Chemical Biology* 2015)

Dixon SJ, Patel DN, Welsch M, Skouta RS, **Lee ED**, Thomas A, Gleason C, Tatonetti N, Slusher BS, Stockwell BR. “Pharmacological inhibition of cystine-glutamate exchange induces ER stress and ferroptosis.” (*eLife 2014*)

SCIENCE COMMUNICATION

California Academy of Science – Nightlife (presenter)
Grounds for Science – April 25, 2019
Berkeley Science Review – Spring 2018, Spring 2019
California Assembly Health Committee – April 2, 2019
California Senate Health Committee – July 3, 2019
Catalyzing Advocacy in Science and Engineering – March 24-27, 2019
Alliance for Global Health and Science – Makerere University, Kampala, Uganda July 22, 2018 - August 3, 2018

Chapter 1

An introduction to *Listeria monocytogenes*

1.1 *Listeria monocytogenes*, an intracellular pathogen

Listeria monocytogenes is a Gram-positive, facultative intracellular pathogen that grows in diverse environments. During infection, *L. monocytogenes* is taken up by professional phagocytic cells or induces its own uptake into nonphagocytic cells. After entering a cell, the virulence factor Listeriolysin O (LLO) forms a pore in the host cell vacuole, allowing *L. monocytogenes* to escape the vacuole and spread to the host cytosol (1). Once *L. monocytogenes* reaches this replicative niche, it rapidly proliferates, growing at almost the same rate in the cytosol as it does in rich media. It then secretes the protein ActA, which polymerizes host actin and allows the bacterium to propel itself into neighboring cells to continue replicating (Fig. 1.1) (2).

Due to its fast doubling time, the relative ease of genetic manipulation, and the wide variety of *in vitro* and *in vivo* assays to analyze virulence, *L. monocytogenes* is a model organism for understanding bacterial pathogenesis (3). The conserved set of host pathways exploited by many bacterial pathogens has meant that studying *L. monocytogenes* has shed light on the strategies used by many clinically significant intracellular pathogens such as *Chlamydiae*, *Salmonellae*, and *Mycobacterium tuberculosis* (4,5). Outside of pathogenesis, *L. monocytogenes* has also contributed to our broader understanding of immunology and cancer biology (6).

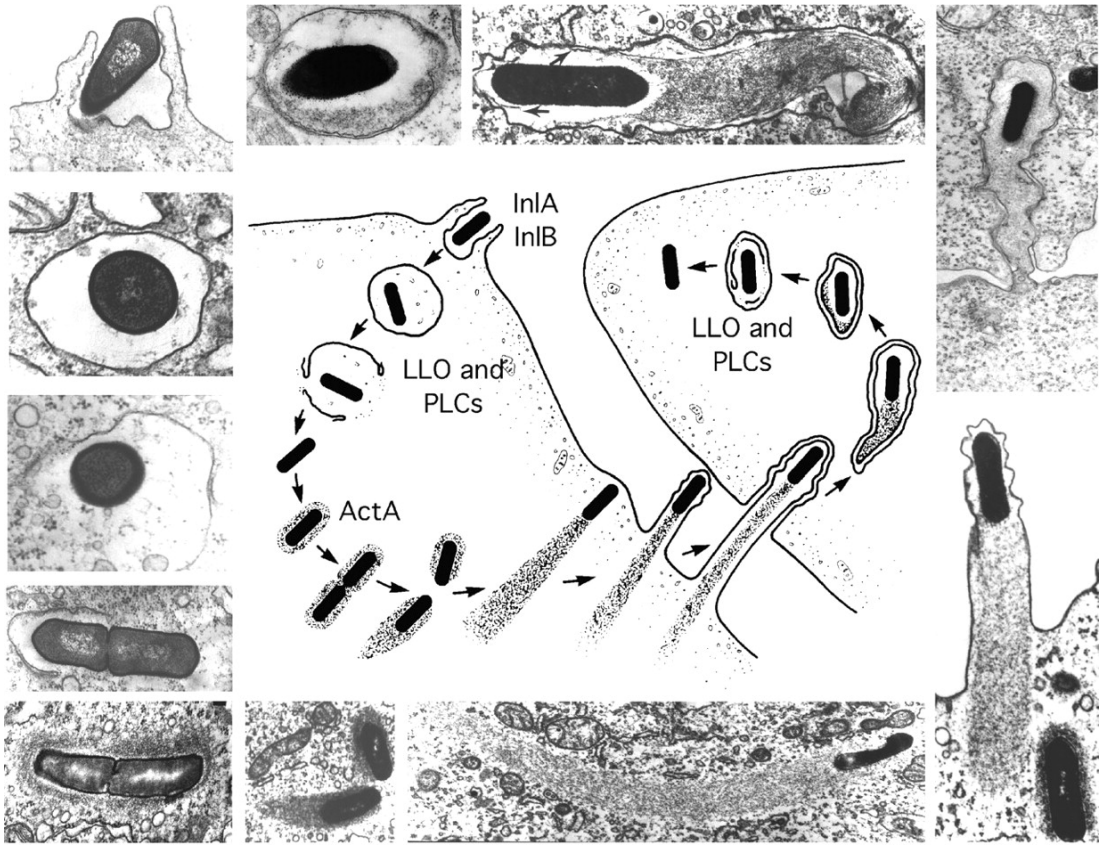

Figure 1.1. The intracellular *L. monocytogenes* life cycle.
L. monocytogenes possesses multiple virulence factors that allow it to enter cells and spread cell-to-cell. Figure from reference (3).

1.2 Isoprenoid precursor biosynthesis pathways in bacteria

The isoprenoid precursor molecules isopentenyl pyrophosphate and dimethylallyl pyrophosphate are essential in all cells (7). These precursors are the building blocks for isoprenoids, a diverse class of compounds containing more than 30,000 unique molecules. The vast majority of organisms produce these molecules using one of two pathways: the mevalonate pathway or the nonmevalonate pathway (also referred to as the DXP pathway). Mammals only have the mevalonate pathway (8), but it is of clinical significance because the rate-limiting enzyme of the mevalonate pathway is the target of statins, cholesterol drugs used by millions of people on a daily basis. In contrast to mammals, bacteria have both pathways in a fairly even distribution (9). Gram-negative bacteria have a slight bias towards the nonmevalonate pathway and Gram-positive bacteria have a slight bias towards the mevalonate pathway, but why this bias exists is not clearly understood.

L. monocytogenes is unique because it contains genes encoding for both the mevalonate and the nonmevalonate pathways (10). It is reported that the mevalonate pathway is essential, while the nonmevalonate pathway has little or no apparent function. We sought to understand why both pathways exist in *L. monocytogenes* if only the mevalonate pathway is used for growth. Furthermore, the nonpathogenic species *Listeria innocua* is believed to have evolved from *L. monocytogenes* (11), but has an incomplete nonmevalonate pathway. This raised the question of whether the nonmevalonate pathway has a role in *L. monocytogenes* pathogenesis, because it has maintained the pathway and was lost in *L. innocua*.

1.3 Bacterial small molecules and the innate immune system

The mechanisms by which *L. monocytogenes* invades a host cell, escapes a vacuole, and spreads cell-to-cell have been well-characterized (3). However, there are still unresolved questions about how a host cell recognizes *L. monocytogenes*, and the strategies *L. monocytogenes* uses to avoid host detection. Previous studies from the Portnoy lab showed that the small molecule cyclic-di-AMP is produced and secreted by *L. monocytogenes*, and is then recognized by the mammalian protein Stimulator of Interferon Genes (STING) (12,13). Activation of STING induces Type I interferons and seems to inhibit cell-mediated immunity against *L. monocytogenes* (14). This discovery, along with several others outside of the lab, raised questions about whether other nonpeptidic antigens were produced by bacteria and what impact they had on the host immune system (15). Indeed, studies on MAIT cells and their cognate activating ligand, an intermediate of bacterial riboflavin biosynthesis, have helped reveal the complex functions of innate-like cells in the immune system (16). Furthermore, a huge number of novel small molecules have recently been discovered (17), sparking excitement that bacterial small-molecule ligands may have important unrecognized functions in both bacterial physiology and the innate immune system.

1.4 (E)-4-hydroxy-3-methyl-but-2-enyl pyrophosphate and Vγ9Vδ2 T-cells

(E)-4-hydroxy-3-methyl-but-2-enyl pyrophosphate (HMBPP) is an intermediate molecule of the nonmevalonate pathway that potently activates innate-like Vγ9Vδ2 T-cells. Vγ9Vδ2 T-cells are a subset of γδ T-cells that exist in humans and nonhuman primates, along with a number of other organisms, but crucially, are not found in mice (18). In contrast to conventional T-cells, which recognize antigens using their T-cell receptor after the antigen is presented on an MHC molecule, Vγ9Vδ2 T-cells recognize conformational changes in the butyrophilin protein BTN3A1 (19,20). BTN3A1 is a transmembrane protein expressed on most professional and nonprofessional antigen presenting cells, and is activated by multiple natural ligands including HMBPP and the downstream isoprenoid precursors, IPP and DMAPP. However, it is estimated to be approximately 10,000 times more sensitive to HMBPP than IPP or DMAPP, likely because IPP and DMAPP are ligands naturally produced in host cells (10). HMBPP, IPP, DMAPP, and synthetic ligands that mimic HMBPP are chemically similar in their pyrophosphate group, and thus these compounds as a group are termed phosphoantigens. When BTN3A1 binds phosphoantigen molecules on the intracellular domain, a conformational change is induced extracellularly, which allows the Vγ9Vδ2 T-cell receptor to bind and for the cell to become activated (Fig. 1.2).

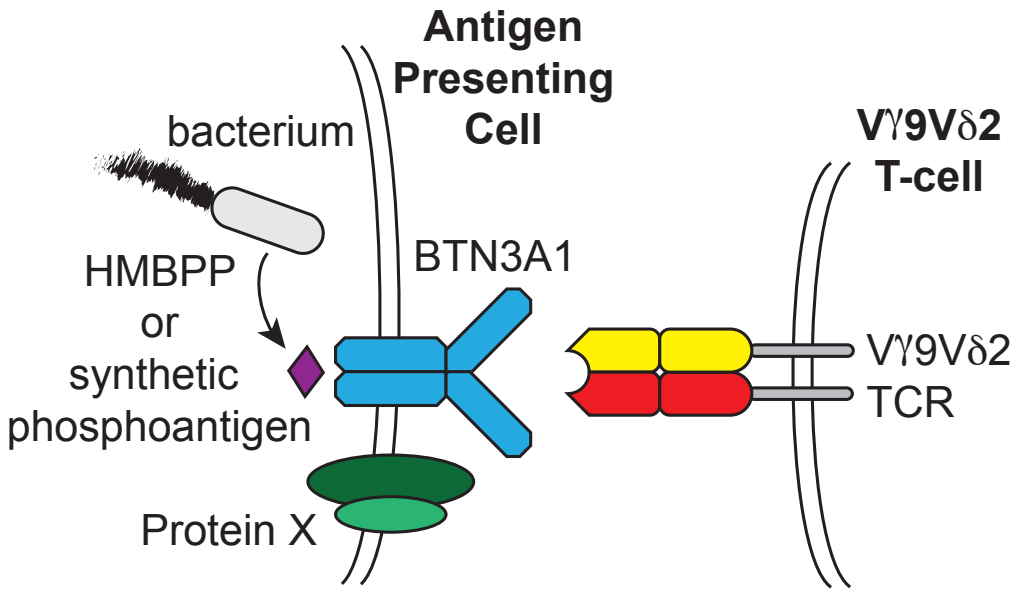

Figure 1.2. Simplified diagram of phosphoantigen-induced Vγ9Vδ2 T-cell activation.
Phosphoantigens produced by bacteria or transported into the cell bind the intracellular domain of BTN3A1. This causes an extracellular conformational change that, in combination with an unknown costimulatory Protein X, allows for Vγ9Vδ2 T-cell binding and activation.

Vγ9Vδ2 T-cells are activated by infection with HMBPP-producing microorganisms or synthetic ligands, at which point they proliferate and perform a wide variety of functions. They have been found to have direct cytotoxic activity against cells infected with bacterial pathogens, and are also capable of producing cytokines to alter the local immune microenvironment in response to infection (21–23). Human studies have observed that Vγ9Vδ2 T-cells can expand to constitute up to 50% of all T-cells in the peripheral blood during bacterial infections, and there are strong correlations between high Vγ9Vδ2 T-cell levels and positive outcomes in some types of cancers (24). Nonetheless, their precise role in immunity has been difficult to elucidate as their absence in mice or any other genetically tractable model organism has made it very challenging to use typical immunological approaches (25–27).

Despite the absence of easily tractable model systems, a remarkable series of studies have been conducted using nonhuman primates to examine Vγ9Vδ2 T-cell function during infection. These studies demonstrated that a strain of *L. monocytogenes* containing a constitutively activate mutation in the master virulence regulator PrfA (PrfA*) increases humoral and cellular immune responses in primates (28). They next showed that vaccination with an attenuated *L. monocytogenes* strain Δ*actA prfA** activates Vγ9Vδ2 T-cells *in vivo*. Furthermore, if the activated Vγ9Vδ2 T-cells are purified from peripheral blood, they are capable of specifically targeting and killing *L. monocytogenes*-infected cells *in vitro* (29). Vγ9Vδ2 T-cell activation was shown to be dependent on bacterial HMBPP production, because vaccination with a strain that does not produce HMBPP (Δ*actA prfA** Δ*gcpE*) activates fewer Vγ9Vδ2 T-cells than Δ*actA prfA** (30). Finally, they demonstrated that activated Vγ9Vδ2 T-cells reduced bacterial burdens in macaques infected with *M. tuberculosis*, both after *ex vivo* activation of Vγ9Vδ2 T-cells with purified HMBPP (31) or after the animals were vaccinated with an HMBPP-producing strain of *L. monocytogenes* (32).

This work showed that *L. monocytogenes* HMBPP production can increase control of *M. tuberculosis*, but we were curious whether it would be possible to manipulate the nonmevalonate pathway to produce even more HMBPP than is endogenously produced by *L. monocytogenes* 10403S. However, that question required a deeper understanding of the nonmevalonate pathway function in *L. monocytogenes*, which became the starting point for this work.

1.5 From model organism to cancer immunotherapy: bugs as drugs

L. monocytogenes is a model organism of bacterial pathogenesis, but is also known to induce a potent $CD8^+$ T-cell response against both bacterial antigens and artificial neoantigens expressed by virulent or attenuated strains (33). This discovery ultimately led to an effort to examine whether *L. monocytogenes* could be used as a cancer immunotherapy platform. Subsequent clinical trials provided a unique opportunity to gain insight into Vγ9Vδ2 T-cell responses after *L. monocytogenes* treatment. These studies observed that Vγ9Vδ2 T-cells proliferated after every administration of the *L. monocytogenes* vaccine, and unexpectedly, did not contract or express typical exhaustion markers despite repeated exposure to bacteria and HMBPP

(unpublished data, Aduro Biotech). Additionally, Vγ9Vδ2 T-cells were the only cell subset that significantly increased in response to treatment, while B cells, NK cells, and both $CD4^+$ and $CD8^+$ T-cells remained constant in all patients.

As a result, we were curious to better understand the function Vγ9Vδ2 T-cells in the human immune system and, at a more basic level, what role the nonmevalonate pathway has in *L. monocytogenes* bacterial physiology. In the context of human infections or therapies, how does HMBPP production and activation of Vγ9Vδ2 T-cells influence the outcome of primary infections and the development of adaptive immunity? Does a strong cytotoxic and innate-like response from Vγ9Vδ2 T-cells help control an infection, but does that come at the cost of long-term immunity? Answering these questions would have significant implications for all HMBPP-producing bacterial pathogens.

A second line of questioning is relevant for understanding *L. monocytogenes* metabolism and pathogenesis. *L. monocytogenes* infects a broad range of primates, ruminants, and lagomorphs, the vast majority of which are not known to have an HMBPP-responsive cell type. It seemed very unlikely that any growth advantage conferred by activating Vγ9Vδ2 T-cells in primates would exert a strong enough selective pressure to maintain the nonmevalonate pathway. Therefore, we wanted to understand if the nonmevalonate pathway functioned at all as a means of growth, and whether a non-immunological role for the pathway impacted bacterial pathogenesis.

Chapter 2

The nonmevalonate pathway of isoprenoid biosynthesis supports anaerobic growth of *Listeria monocytogenes*

Sections of this chapter were submitted for publication as:

Lee, E.D., Navas, K.I., Portnoy, D.A. (2019). The nonmevalonate pathway of isoprenoid biosynthesis supports anaerobic growth of *Listeria monocytogenes.*

2.1 Summary of results

Isoprenoids are an essential and diverse class of molecules present in all forms of life that are synthesized from an essential common precursor derived from either the mevalonate pathway or the nonmevalonate pathway. Most bacteria have one pathway or the other, but the Gram-positive, facultative intracellular pathogen *Listeria monocytogenes* is unusual because it encodes all the genes for both pathways. While the mevalonate pathway has previously been reported as essential, here we demonstrate that the nonmevalonate pathway can support growth of strains 10403S and EGD-e, but only anaerobically. *L. monocytogenes* lacking the gene *hmgR*, the rate-limiting enzyme of the mevalonate pathway, had a doubling time of four hours in anaerobic conditions in contrast to the 45-minute doubling time of WT. In contrast, deleting *hmgR* in two clinical isolates resulted in mutants that grew significantly faster, doubling in approximately two hours anaerobically, although they still failed to grow under aerobic conditions without mevalonate. The difference in anaerobic growth rate was traced to three amino acid changes in the nonmevalonate pathway enzyme GcpE, and these changes were sufficient to increase the growth rate of 10403S to the rate observed in the clinical isolates. Despite an increased growth rate, virulence was still dependent on the mevalonate pathway in 10403S strains expressing the more active GcpE allele.

2.2 Introduction

Isoprenoids represent the largest family of compounds present in all living organisms, used for a wide variety of processes including cell wall synthesis, electron transport, and maintaining membrane fluidity (7). Isoprenoids are derived from the essential isoprenoid precursor molecules isopentenyl pyrophosphate (IPP) or dimethylallyl pyrophosphate (DMAPP). These precursors are synthesized by two distinct pathways, the mevalonate pathway and the nonmevalonate pathway (Fig. 1A). While mammals all use the mevalonate pathway (8), bacteria usually encode genes for only one of the two pathways (9). In rare instances bacteria lack both pathways, such as the obligate intracellular bacteria *Rickettsia parkeri*, but these bacteria depend on the host cell as a source for isoprenoid precursors (34). *Listeria monocytogenes* is a Gram-positive, facultative intracellular pathogen that, unlike most bacteria, has the genes for both the mevalonate and the nonmevalonate pathways (10). Work from others reported that the rate-limiting enzyme of the mevalonate pathway, HmgR, is essential in *L. monocytogenes* EGD-e, as strains lacking *hmgR* cannot grow unless supplemented with mevalonate in the growth media (35,36). Deleting either of the last two enzymes in the nonmevalonate pathway, GcpE or LytB, had no impact on growth *in vitro* and a negligible effect on virulence (36).

While it is curious that *L. monocytogenes* has both isoprenoid precursor pathways, interest in these pathways also stems from observations that an intermediate molecule of the nonmevalonate pathway, (E)-4-hydroxy-3-methyl-but-2-enyl pyrophosphate (HMBPP), activates Vγ9Vδ2 T-cells, an innate-like T-cell subset found in humans and non-human primates, but not in mice (37). Upon activation by microorganisms with the nonmevalonate pathway or synthetic ligands, Vγ9Vδ2 T-cells proliferate, produce proinflammatory cytokines, and have cytotoxic activity against cells presenting HMBPP (20). Vγ9Vδ2 T-cells have a broad role communicating with innate

and adaptive immune cells to coordinate responses to bacterial infections, but it has been difficult to gain a mechanistic understanding of their functions due to the challenge of developing an appropriate model system (26,27).

L. monocytogenes is being developed as a cancer vaccine platform, using a live-attenuated recombinant bacterial strain to stimulate $CD8^+$ T-cell responses (33). Despite impressive results in mice, human clinical trials have shown promising, but limited responses to *L. monocytogenes*-based treatments. Given the potential role of $V\gamma9V\delta2$ T-cells in responses to HMBPP-producing *L. monocytogenes* in humans, we were interested in further understanding isoprenoid precursor pathways in strain 10403S, the bacterial strain used for these studies. Additionally, we were intrigued by the observation that *L. monocytogenes* contains both pathways, despite no reported function for the nonmevalonate pathway.

In this study, we further examined the role of the mevalonate and nonmevalonate pathways for *L. monocytogenes* growth and pathogenesis. Additionally, the nonmevalonate pathway was examined in two *L. monocytogenes* strains, FSL N1-017 which was isolated from trout brine (38) and HPB2262 Aureli 1997 (HPB2262) which was isolated from an outbreak of gastroenteritis (39). These isolates were chosen because they are in *L. monocytogenes* lineage I, which are far more prevalent in human listeriosis cases and are genetically distinct from 10403S and EGD-e, which are in lineage II (40). We found that the mevalonate pathway was not essential for growth when Δ*hmgR* mutants were cultured anaerobically, as strains with only the nonmevalonate pathway grew in the absence of mevalonate. Additionally, three amino acid differences found in the lineage I strains could significantly alter GcpE function in *L. monocytogenes* strain 10403S, resulting in improved anaerobic growth compared to WT *L. monocytogenes*. These results demonstrate that either the mevalonate pathway or the nonmevalonate pathway is sufficient for *L. monocytogenes* growth in anaerobic conditions.

2.3 Results

2.3.1 *L. monocytogenes* 10403S does not require the mevalonate pathway for anaerobic growth.

Consistent with previous reports (36), a 10403S strain lacking *hmgR* (10403S Δ*hmgR*) was unable to grow on BHI agar unless supplemented with mevalonate (Fig. 1B). In liquid media the growth of 10403S Δ*hmgR* was fully restored with 1 mM mevalonate or if *hmgR* was complemented on an integrating plasmid pPL2 (Fig. 1C).

The last two enzymes of the nonmevalonate pathway, GcpE and LytB, contain [4Fe-4S] iron-sulfur clusters (FeS clusters) (41,42). In the presence of oxygen, FeS clusters can be oxidized, leaving a catalytically inactive $[3Fe\text{-}4S]^{1+}$ FeS cluster (43). GcpE and LytB (also referred to as IspG and IspH, respectively) are particularly oxygen-labile in other organisms, since the FeS cluster is solvent-exposed (44–46). We hypothesized that *L. monocytogenes* growth using the nonmevalonate pathway might be promoted anaerobically, due to decreased oxidation of GcpE or LytB FeS clusters. Indeed, strains lacking *hmgR* grew in the absence of mevalonate, although they exhibited a severe increase in doubling time, increasing from 43 mins aerobically with mevalonate to approximately four hours anaerobically without mevalonate (Fig. 2A). Additionally, 10403S Δ*hmgR* formed a visible colony overnight on BHI agar supplemented with mevalonate, while it required four to five days to form similarly sized colonies anaerobically without mevalonate. Growth was dependent on the nonmevalonate pathway, as mutants in both pathways (10403S Δ*hmgR*Δ*gcpE* and 10403S Δ*hmgR*Δ*lytB*) lost viability over the course of the anaerobic experiment (Fig. 2A) and did not form colonies on BHI agar anaerobically without mevalonate.

To examine whether anaerobic growth was a result of acquired suppressor mutations, the plating efficiency of strains was examined in aerobic and anaerobic conditions after overnight cultures were plated with or without mevalonate or oxygen. Aerobically, no 10403S Δ*hmgR* colonies grew unless the media contained mevalonate. Anaerobically, equal numbers of bacteria were recovered without mevalonate, relative to media with mevalonate (Fig. 2B). Collectively, these data indicate that the nonmevalonate pathway supports growth in the absence of the mevalonate pathway.

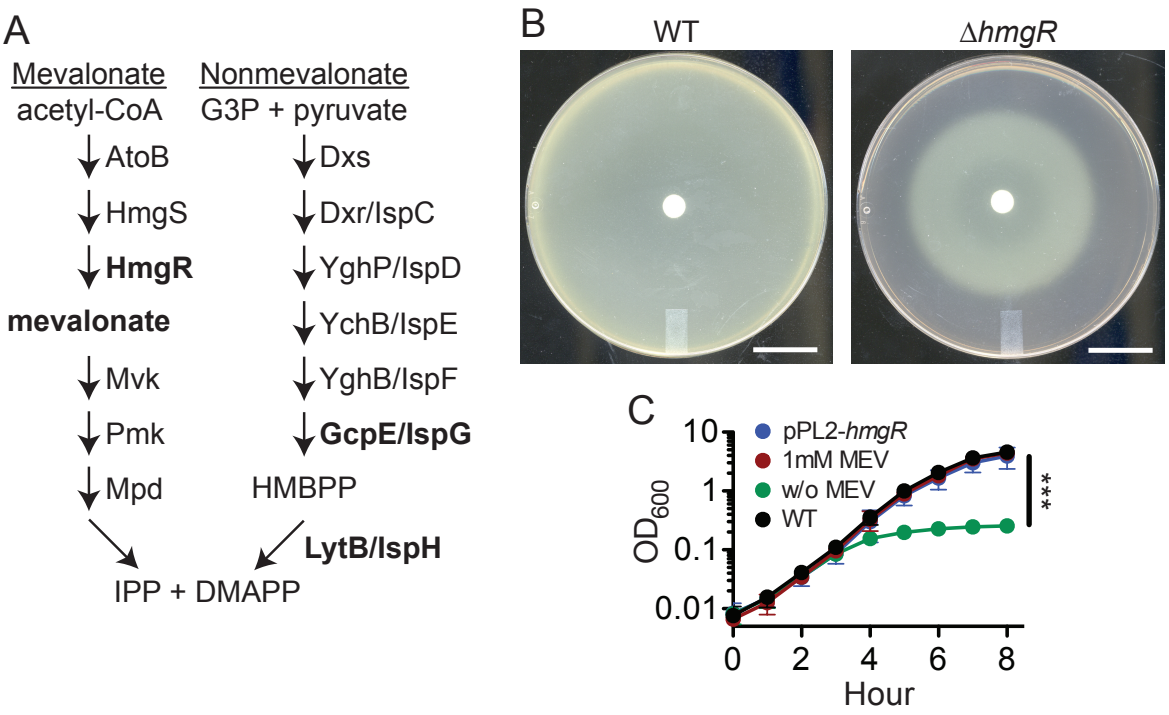

Figure 2.1. The mevalonate pathway is essential for aerobic growth.
A. Abbreviated diagram of *L. monocytogenes* isoprenoid precursor pathways. See reference (10) for full pathway. **B.** Disk diffusion assay using 10 µL of 1 M mevalonate on a BHI agar plate spread with WT or 10403S Δ*hmgR*, demonstrating mevalonate-dependent growth. White bar is 20 mm. **C.** Aerobic BHI growth curve of WT, 10403S Δ*hmgR*, and 10403S Δ*hmgR* with *hmgR* gene on the integrating plasmid pPL2. 10403S Δ*hmgR* was grown in BHI supplemented with the indicated concentrations of mevalonate.

2.3.2 Growth phenotype of mevalonate pathway mutants in other *L. monocytogenes* strains.

Previous work on *L. monocytogenes* isoprenoid precursor pathways was conducted using strain EGD-e, where the mevalonate pathway was found to be essential (36). However, the authors did not examine anaerobic growth of their mevalonate pathway mutant, so we were curious whether any strain-specific growth differences existed between EGD-e and 10403S. The mevalonate pathway was deleted in EGD-e (EGD-e Δ*hmgR*), and two lineage I strains, *L. monocytogenes* FSL N1-017 (FSL Δ*hmgR*) and *L. monocytogenes* HPB2262 (HPB Δ*hmgR*). Both lineage I strains doubled in approximately two hours when *hmgR* was deleted, which was significantly faster than 10403S Δ*hmgR* (Fig. 2C). EGD-e Δ*hmgR* grew on BHI agar anaerobically without mevalonate (Fig. S1), but did not grow in liquid culture, preventing the measurement of a doubling time.

To determine whether there was a genetically encoded basis for the observed differences in growth, we compared the 5' UTRs and coding sequences of 10403S, FSL N1-017, and HPB2262 for each gene in the nonmevalonate pathway. Three genes, *dxr*, *ispE*, and *ispF*, were identical among all three strains. The 5' UTR of *ispD* differed

between strains, but no growth differences were observed when the genes for *ispD* or *lytB* from the lineage I strain were introduced into 10403S Δ*hmgR*. However, strains complemented with *gcpE* from either FSL N1-017 or HPB2262 grew significantly faster than strains with 10403S *gcpE* (Fig. 2D).

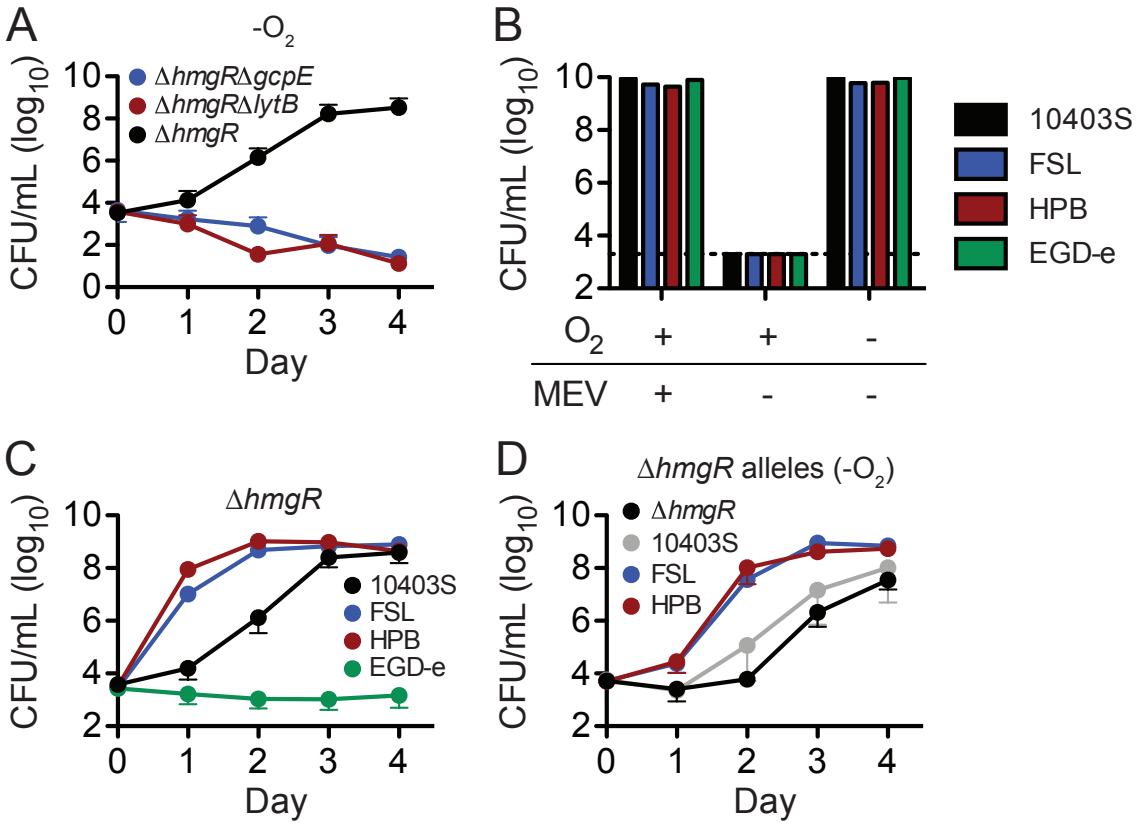

Figure 2.2. The nonmevalonate pathway is sufficient for anaerobic growth. **A.** Anaerobic BHI growth curve of 10403S Δ*hmgR* compared to mutants in both pathways (10403S Δ*hmgR*Δ*gcpE* and 10403S Δ*hmgR*Δ*lytB*). **B.** CFUs measured after plating aerobic 10403S Δ*hmgR* cultures in indicated oxygen or mevalonate conditions. **C.** Anaerobic growth of 10403S Δ*hmgR* compared to Δ*hmgR* mutants from indicated *L. monocytogenes* strains. **D.** Anaerobic growth of 10403S Δ*hmgR*Δ*gcpE* with *gcpE* from indicated strains on pPL2, compared to 10403S Δ*hmgR* with *gcpE* on the chromosome.

2.3.3 Three residues in GcpE account for differences in anaerobic growth.

gcpE chimeric proteins were constructed to more precisely identify the molecular origin of the growth differences between 10403S and the lineage I strains. First, the 5' UTRs and coding sequences from each strain were exchanged and introduced into 10403S Δ*hmgR*Δ*gcpE*. Only strains complemented with the protein coding sequence from either lineage I strain grew significantly faster, even if expressed downstream of the 10403S 5' UTR (Fig. 3A). Twelve amino acid differences exist in GcpE between 10403S and the lineage I strains. A chimeric protein was constructed containing the N-

terminal portion of 10403S and the C-terminal portion of the FSL N1-017 protein, from amino acid 251 (Fig. 3B). The C-terminal end was chosen because it contained all four residues involved with FeS cluster coordination and the majority of the catalytic residues. Strains complemented with the chimeric strain grew as well as strains with the entire FSL N1-017 gene (Fig. 3C).

The C-terminal end of GcpE has nine differences between the lineage I strains and 10403S, the majority of which are located in three distinct areas, therefore we focused on those changes. Two pairs of mutations, GcpE$^{I343V/D344E}$ and GcpE$^{F357Y/V359E}$, had no impact on anaerobic growth (Fig. 3D). Mutating three other residues in combination, GcpE$^{K291T/E293K/V294A}$ (GcpE*), significantly increased the growth rate of 10403S Δ*hmgR* Δ*gcpE* while the single mutants of either GcpE^{K291T} or GcpE^{V294A} were not sufficient to increase (Fig. 4A). Furthermore, when the same GcpE* mutations were made on the chromosome rather than on a plasmid, the resulting strain (10403S Δ*hmgR gcpE**) had an identical anaerobic growth rate as FSL Δ*hmgR* (Fig. 4B).

Given the distinct growth differences between 10403S Δ*hmgR* and 10403S Δ*hmgR gcpE**, we sought to understand how these mutations impacted protein function. The protein structure prediction program Phyre2 was used to generate a model of GcpE based on the crystal structure from *Aquifex aeolicus* (strain VF5). The predicted structure placed residues 291-294 in a loop distal from both the FeS cluster and the catalytic TIM barrel in the protein (Fig. 4C), providing little insight into the mechanism by which these mutations alter 10403S Δ*hmgR gcpE** anaerobic growth.

2.3.4 HMBPP quantification using high-performance liquid chromatography.

Liquid chromatography-triple quadrupole mass spectrometry was then used to directly measure HMBPP levels in strains grown anaerobically (Fig. 2.4D). Deleting *gcpE* modestly reduced HMBPP, while it significantly increased after deleting *lytB*. *L. monocytogenes* 10403S produced a similar amount of HMBPP as EGD-e, but both clinical isolates produced more. Despite the significantly different growth rates of Δ*hmgR* and Δ*hmgR gcpE**, the two strains produced similar amounts of HMBPP.

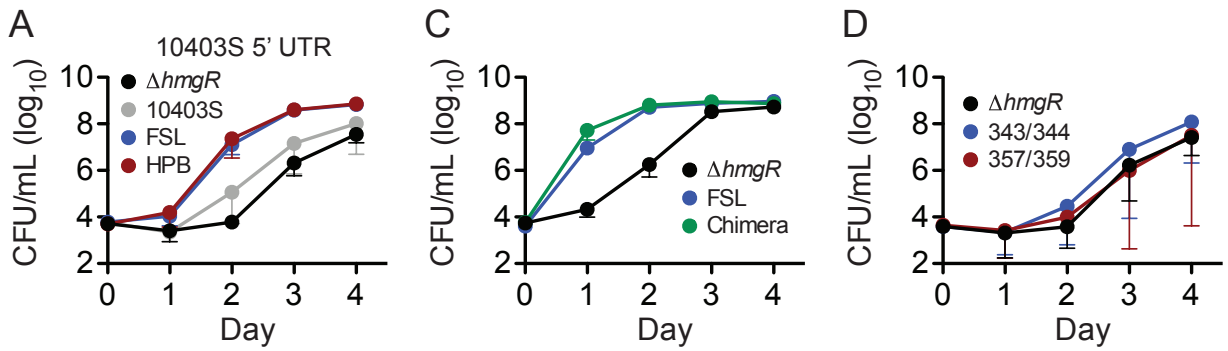

B

```
10403S       1 MNERIFRENTRPVQVGNLTIGGSEELTIQSMTTTKTHDVEATVAEIHRLEEAGCQIVRVACPDERAANALSAIKKKIHIP
EGD-e        1 ................................................................................
FSL N1-017   1 ........K.......................................V.......................R....
HPB2262      1 ........K.......................................V.......................R....

10403S      81 LVADIHFDYRLALKAIDAGVDKIRINPGNIGRRDRVEKVVNAAKAKNIPIRIGVNAGSLEKKIIQKYGYPTADGMVESAL
EGD-e       81 ................................................................................
FSL N1-017  81 ................................................................................E.......
HPB2262     81 ................................................................................E.......

10403S     161 AHIKILEDLDFYDIIVSLKASDVNLAIEAYDKASRAFNYPLHLGITESGTQFAGGIKSAAGLGAILSLGIGNTLRVSLSA
EGD-e      161 ................................................................................
FSL N1-017 161 ................................................................................
HPB2262    161 ................................................................................

10403S     241 DPVEEIKVAREVLKSFGFSSNAAMLISCPTCGRIEIDLIRIANEVENYIAKIEVPIKVAVLGCAVNGPGEAREADIGIAG
EGD-e      241 ................L...............................................................
FSL N1-017 241 ................L..............................T.KA..........................
HPB2262    241 ................L..............................T.KA..........................

10403S     321 SNGEGLLFRHGKIIRKVPEAIMIDELKKEIDILAEEFFVKKIDLESLR
EGD-e      321 ...................................................
FSL N1-017 321 ....................VE............Y.E..T......
HPB2262    321 ....................VE............Y.E..T......
```

Figure 2.3. Increased growth of lineage I strains is caused by changes in GcpE coding sequence.

A. Anaerobic growth of 10403S Δ*hmgR*Δ*gcpE* complemented with the *gcpE* coding sequence from different strains, all expressed from the 10403S 5' UTR. **B.** Sequence alignment of *L. monocytogenes* GcpE found in two lineage I strains and two laboratory strains. Listed residues indicate sequence differences relative to 10403S. **C.** Anaerobic growth of 10403S Δ*hmgR*, FSL N1-017 Δ*hmgR*, and 10403S Δ*hmgR*Δ*gcpE* complemented with a GcpE chimera containing the N-terminal domain (amino acids 1-250) from 10403S and the C-terminal domain from FSL N1-017 (amino acids 251-369). **D.** Anaerobic growth of 10403S Δ*hmgR*Δ*gcpE* complemented with point mutations GcpE$^{I343V/D344E}$ or GcpE$^{F357Y/V359E}$.

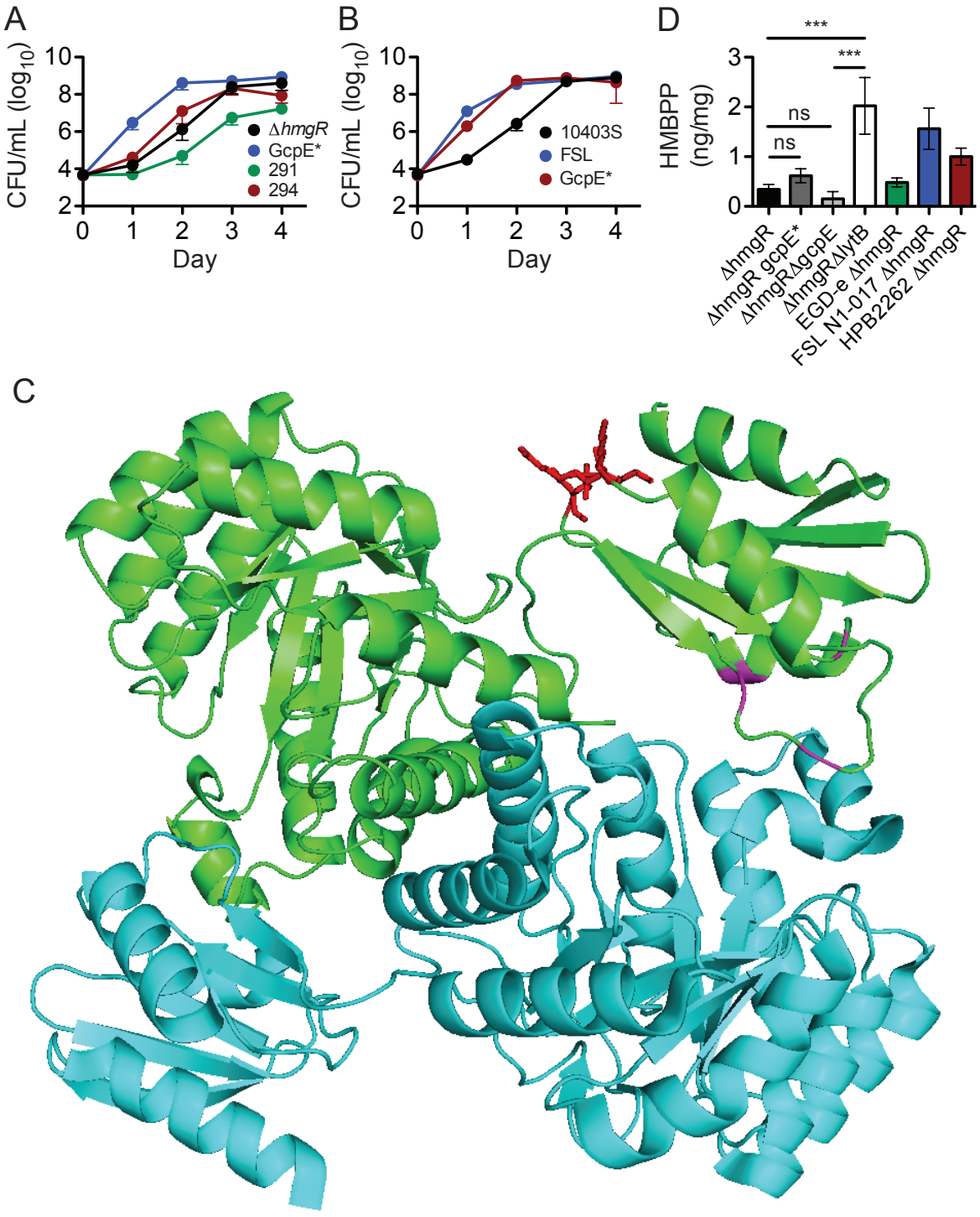

Figure 2.4. Point mutations fixing GcpE function increase anaerobic growth. **A.** Anaerobic growth of Δ*hmgR*Δ*gcpE* complemented with GcpE$^{K291T/E293K/V294A}$ or point mutations GcpE^{K291T} and GcpE^{V294A}. **B.** Anaerobic growth of 10403S Δ*hmgR*, FSL N1-017 Δ*hmgR*, and 10403S Δ*hmgR* with GcpE$^{K291T/E293K/V294A}$ mutation on the chromosome. **C.** Predicted GcpE structure generated with Phyre2 protein structure prediction software. Two GcpE dimers colored in green and cyan, with iron-sulfur cluster coordinating residues colored in purple and residues 291-294 colored in red.

2.3.5 Nonmevalonate pathway function does not alter *L. monocytogenes* virulence in mice.

Previous studies found minimal virulence defects when the nonmevalonate pathway was mutated in EGD-e (35,36,47), so we were curious whether 10403S had a similar phenotype. No significant virulence defects were observed in an IV infection (Fig. S2A) or a five-day oral infection (Fig. S2B) with nonmevalonate pathway mutants. Furthermore, there were no differences in virulence between 10403S Δ*hmgR* and 10403S Δ*hmgR gcpE** in an IV infection (Fig. 5A) and or infection model (Fig. 5B), as both had significant virulence defects, but were not different from each other.

We hypothesized that the nonmevalonate pathway may have a minor contribution to growth, and if so, differences might become apparent in a long-term oral infection model. During an oral infection, systemic bacterial dissemination adds an additional layer of complexity for understanding bacterial survival in the gut. Bacteria that spread from the gut can colonize the gallbladder and reseed the intestinal tract (48–50). This reservoir of bacteria is then the principal source of bacteria shed in the feces, rather than bacteria that have only survived in the anaerobic environment of the gut. Therefore, to prevent systemic dissemination and more closely examine long-term survival, a transposon (51) was used to disrupt the essential virulence factor listeriolysin O in our WT strain (10403S *hly::Tn917*), both nonmevalonate pathway deletions (10403S Δ*gcpE hly::Tn917* and 10403S Δ*lytB hly::Tn917*) and the fast-growing GcpE mutant (10403S *gcpE* hly::Tn917*). After oral infection, *L. monocytogenes* CFUs in the feces decreased over time, but mice continued to shed detectable amounts of bacteria 31 days post-infection (Fig. 5C). Previous studies show that mice stop shedding WT two weeks post infection in a streptomycin pretreatment model (52), so it was unexpected that all 10403S *hly::Tn917* strains continued to be shed four weeks post infection. While small differences in the median CFUs shed from mice were noted, these changes did not rise to the level of statistical significance. These data suggest that the increased *in vitro* anaerobic growth with a GcpE* mutation does not impact bacterial survival when the bacteria are confined to the gut of mice.

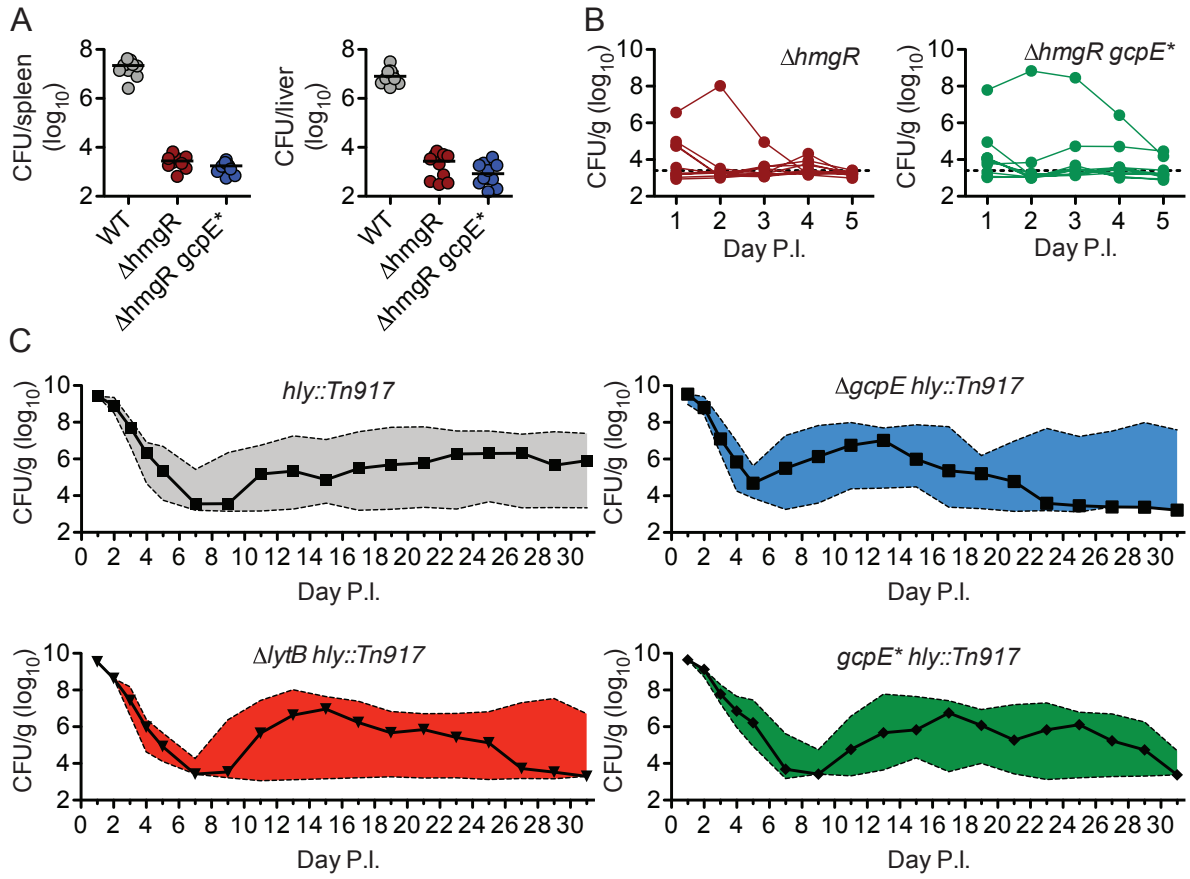

Figure 2.5. *L. monocytogenes* virulence in mice does not change with increased nonmevalonate pathway growth.

A. CFUs recovered from indicated organs one day after IV infection with indicated *L. monocytogenes* strains. Data show two independent experiments, with ten mice total for each strain, plotting medians and interquartile range. **B.** CFUs recovered from mice five days after oral infection with indicated *L. monocytogenes* strains. Data show two independent experiments, with ten mice total for each strain. **C.** CFUs recovered from pellets after oral infection with indicated *L. monocytogenes* strains. Plotted line is median CFUs from two independent experiments (10403S *hly::Tn917*, 10403S *gcpE* hly::Tn917*, n = 20; 10403S Δ*gcpE*, 10403S Δ*lytB*, n = 15) and shaded area is interquartile range.

2.4 Discussion

The results of this study show that the *L. monocytogenes* mevalonate pathway was essential for growth aerobically and supports growth anaerobically, while the nonmevalonate pathway was sufficient for growth only anaerobically. This growth phenotype was observed in four *L. monocytogenes* strains, although strains FSL N1-017 and HPB2262 lacking *hmgR* grew significantly faster than 10403S and EGD-e. Genetic approaches were used to identify three amino acid residues in the nonmevalonate pathway enzyme GcpE that were sufficient to eliminate differences in anaerobic growth between strains. A strain with $GcpE^{K291T/E293K/V294A}$ mutations grew more rapidly in pure culture, but did not have significantly altered growth phenotypes in mice.

As a facultative anaerobe, *L. monocytogenes* substantially reprograms its metabolism in the absence of oxygen (53). We show that the nonmevalonate pathway functions anaerobically, but note that *L. monocytogenes* still grows faster using the mevalonate pathway. This implies that there may be unidentified anaerobic growth conditions where the nonmevalonate pathway is required or beneficial for growth. Aerobically, *L. monocytogenes* uses oxygen as a terminal electron acceptor to maintain NAD+/NADH ratios while pyruvate is converted to a variety of reduced (lactate, ethanol) and oxidized fermentation products (acetate, acetoin). Anaerobically, pyruvate represents the primary electron acceptor and consequently, the reduced fermentation product lactate predominates (54). Reflecting these metabolic changes, pyruvate dehydrogenase is downregulated anaerobically and presumably, less acetyl-CoA is generated (53). The mevalonate and nonmevalonate pathways start with distinct molecules to generate isoprenoid precursors. The mevalonate pathway uses two molecules of acetyl-CoA, while the nonmevalonate pathway uses one molecule of pyruvate and one molecule of glyceraldehyde 3-phosphate. Under anaerobic conditions, the metabolic shift towards lactate fermentation may limit acetyl-CoA levels, or the acetyl-CoA that is present may need to be used for NAD+ regeneration. As a result, *L. monocytogenes* may use the nonmevalonate pathway anaerobically as an acetyl-CoA-independent means of producing isoprenoid precursors. However, under conditions used in this study the mevalonate pathway was sufficient.

We hypothesize that the nonmevalonate pathway fails to function aerobically in *L. monocytogenes* because GcpE and LytB are oxygen-labile, FeS cluster-containing enzymes. FeS clusters are essential metal cofactors in enzymes, but can be oxidized and lost in the presence of oxygen. As a result, organisms have developed mechanisms for protecting FeS clusters from oxidation, including multiple biosynthetic pathways to produce replacement FeS clusters for those damaged by oxidative stresses (55). Three distinct pathways for FeS cluster synthesis have been identified and designated as the Nif, Suf, and Isc systems (56). The Gram-negative bacteria *Escherichia coli* has both the Isc and Suf systems (57,58) while the Gram-positive model organism *Bacillus subtilis* and *L. monocytogenes* only have the Suf system. Isc and Suf genes are essential, but recent studies show that they are essential for synthesizing the FeS clusters in GcpE and LytB (59,60). *B. subtilis* only encodes the nonmevalonate pathway, but grows aerobically, which suggests that *L. monocytogenes* is fundamentally different from *B. subtilis* and may have a defect synthesizing FeS clusters which prevents it from using the nonmevalonate pathway anaerobically.

The crystal structure of *L. monocytogenes* GcpE has not been solved, but structures from other organisms point toward a mechanism by which mutations in GcpE may alter enzyme function (61–64). GcpE has two major domains, consisting of a catalytic TIM barrel at the N-terminal end, and an FeS cluster coordinated by three cysteine residues and one glutamic acid residue at the C-terminal end. The protein forms a homodimer consisting of two subunits aligned “head-to-tail.” This allows the FeS cluster of one subunit to catalyze reactions in the active site of the opposite subunit, but this mechanism requires the C-terminal domain to rotate significantly while “closing” on a ligand (63,65). We hypothesize that all three amino acid changes identified are necessary to alter enzyme kinetics and allow catalysis to proceed more quickly.

Dozens of preclinical studies and clinical trials have used *L. monocytogenes* 10403S as a vaccine vector for cancer immunotherapy (29,30,33,66–68). All the strains used in these studies produce HMBPP based on the observation that they stimulate Vγ9Vδ2 T-cells (30). Based on the results of this study, we predict that 10403S makes less HMBPP than the lineage I strains, although absolute HMBPP concentrations have not been directly measured. The role of Vγ9Vδ2 T-cells is still unclear, so it is difficult to determine whether cellular activation in response to HMBPP enhances or diminishes the efficacy of a *L. monocytogenes*-based vaccine in primates. However, characterizing HMBPP production in the presence of the mevalonate pathway and metabolically engineering 10403S to produce more HMBPP may be useful to improve our understanding of Vγ9Vδ2 T-cells and their role in vaccine development (69).

The two *L. monocytogenes* isolates used in this study raise interesting questions about the relationship between nonmevalonate pathway and *L. monocytogenes* pathogenesis in humans. HPB2262 was isolated from an outbreak of febrile gastroenteritis caused by contaminated corn salad (39), but the symptoms of the outbreak were unique because the disease was almost exclusively noninvasive. In contrast, FSL N1-017 was isolated from trout in brine and is not associated with any human outbreaks. However, it is closely related to strain FSL R2-503 which is a clinical isolate from a different outbreak of gastroenteritis (38,70). It is possible that having a functional nonmevalonate pathway provides *L. monocytogenes* with a selective growth advantage in the human gut. Alternatively, they may have a greater capacity to produce HMBPP and stimulate Vγ9Vδ2 T-cells, which may trigger an immune response that contributes to disease (71). Separating causative versus correlative factors related to Vγ9Vδ2 T-cells would be challenging though, given the absence of animal models and likelihood that other genes in lineage I *L. monocytogenes* strains influence pathogenesis.

A large number of clinically significant bacterial and protozoan pathogens such as *Vibrio cholerae*, *Pseudomonas aeruginosa*, *Clostridium difficile*, *Mycobacterium tuberculosis*, and *Plasmodium* species have the nonmevalonate pathway and produce HMBPP. However, the nonmevalonate pathway is essential for producing isoprenoid precursors in all of these organisms, making it extremely difficult to separate growth defects from virulence defects. In bacteria that encode both pathways, including *Mycobacterium marinum* (72) and several *Streptomyces* and *Nocardia* species (73), even less is known about isoprenoid pathways. By understanding the role of the nonmevalonate pathway in *L. monocytogenes*, it may be possible to metabolically

engineer other bacteria to intentionally manipulate Vγ9Vδ2 T-cell activation levels and improve adaptive immune responses to pathogens.

2.5 Materials and Methods

Construction of *L. monocytogenes* strains

The *L. monocytogenes* strains used in this study are all derived from wild-type 10403S (DP-L6253) unless otherwise noted and are listed in Table 1. Gene deletions were generated by allelic exchange using the plasmid pKSV7 (74). All *L. monocytogenes* strains were grown in brain heart infusion (BHI) broth supplemented with 5 g/L yeast extract, 1 g/L L-cysteine hydrochloride, and 0.001 g/L resazurin sodium salt, and media was supplemented with 1 mM mevalonate as needed to support the growth of auxotrophic Δ*hmgR* strains. Mevalonate was produced by hydrolyzing DL-mevalonolactone (Sigma-Aldrich CAS Number 674-26-0) with 1 N NaOH at 37 ºC for 1 hour, according to previously reported methods (35). Agar plates were incubated anaerobically using a BD GasPak EZ anaerobic pouch system (Cat no. 260683) and liquid cultures were incubated in an anaerobic chamber (Coy Laboratory Products) with an environment of 2% H_2 balanced with N_2.

E. coli strains used in this study are listed in Table 2. For vector construction, plasmids were introduced into TOP10 *E. coli* (Invitrogen) or XL1 Blue *E. coli* (Stratagene). Plasmids were then transformed into SM10 *E. coli* and conjugated into *L. monocytogenes*. PCR was performed with KAPA HiFi DNA polymerase (Kapa Biosystems) or Q5 DNA polymerase (NEB). Positive clones were identified by performing colony PCRs using SapphireAmp Fast PCR Master Mix (Takara Bio) and verified by Sanger sequencing.

Aerobic growth curves

Strains were grown overnight at 37 ºC in filter-sterilized BHI and were supplemented with 500 μM mevalonate as necessary. Bacteria were washed with PBS and diluted in 20 mL fresh BHI to an optical density at a wavelength of 600 nm (OD_{600}) = 0.01. Cells were cultured at 37 ºC with shaking and growth was measured spectrophotometrically hourly.

Anaerobic growth curves

Media was degassed overnight in an anaerobic chamber to allow residual oxygen to diffuse out of the media. Overnight cultures of cells were first grown aerobically and were back diluted into anaerobic media to a concentration of 10^3 CFUs/mL. Samples were removed from the chamber daily and plated by 10-fold serial dilutions to enumerate CFUs.

Structure prediction

The Phyre2 protein modeling web portal was used to generate a predicted model of *L. monocytogenes* 10403S GcpE (75).

Sample Preparation for Mass Spectrometry

L. monocytogenes cultures were grown aerobically and 250 µL of overnight culture were backdiluted into 10 mL anaerobic media, then incubated anaerobically for 2 days at 37 ºC. Cultures were removed from the anaerobic chamber and centrifuged at 4,300 RCF for 15 mins at 4 ºC. After centrifugation, the supernatant was aspirated and cell pellets were snap frozen in liquid nitrogen. Bacteria were resuspended in 1 mL sterile PBS, transferred to a tared 1.5 mL microcentrifuge tube with PBS, and pelleted again at 16,000 RCF for 1 min. The supernatant was aspirated and then snap frozen in liquid nitrogen again. Samples were stored at -80 ºC until HMBPP extraction step.

HMBPP Extraction from *L. monocytogenes*

500 µL of ice-cold acetonitrile/methanol/water (2:2:1, v/v/v) containing 0.1% ammonium hydroxide was added to bacterial pellet. 2-3 beads (3 mm) were added to microcentrifuge tube and tubes were vortexed for 10 mins in a Tissuelyser-48 (Shanghai Jingxin Industrial Development Co., Ltd). Lysates were centrifuged for 5 mins at 20,000 RCF in a microcentrifuge, and 450 µL of supernatant was transferred to a clean 1.5 mL microcentrifuge tube. The pellet was extracted with another 500 µL of extraction solvent as described above. The supernatants were combined, and the extract (approximately 900 µL) was evaporated under a stream of nitrogen gas at room temperature. The residue was dissolved in 100 µL of 10 mM ammonium acetate, adjusted to pH 9.0 with ammonium hydroxide, and 100 µL of chloroform was added to extract the hydrophobic compounds. The extract was then centrifuged for 5 mins at 20,000 RCF to facilitate fast phase separation. 50 µL of the aqueous phase was transferred to a new 1.5 mL microcentrifuge tube then 50 µL acetonitrile was added, and samples were centrifuged for 5 mins at 20,000 RCF to remove any precipitates. The supernatant was then analyzed by liquid chromatography-triple quadrupole mass spectrometry (LC-MS/MS) as described below.

HILIC Separation Conditions

An ACQUITY UPLC BEH HILIC Column (1.7 µm, 100×2.1 mm; Waters) was used for separation. Solvent A contained 20 mM ammonium acetate adjusted to pH 9.4 with LC–MS grade ammonium hydroxide. Solvent B contained 80% acetonitrile and 20 mM ammonium acetate adjusted to pH 9.4 with LC–MS grade ammonium hydroxide. The solvent gradient profile is described as follows: 0-5 mins, 100% solvent B gradually changed to 84%; 5-10 mins, elution with 84% solvent B; 10-11 mins, 16% solvent A gradually changed to 40%; 11-15 min, column wash with 40% solvent A; 15-30 mins, column equilibration with 100% solvent B. Separation was performed at 40 °C with a flow rate of 200 µL min^{-1} and 10 µL was injected.

MS Method and Data Processing

A Thermo Scientific™ Dionex™ UltiMate™ 3000 UHPLC system coupled with Q Exactive hybrid quadrupole-Orbitrap mass spectrometer, equipped with heated electrospray ion (HESI) source, was used for LC-MS measurements. For better specificity and sensitivity, full scan data were acquired at 70,000 resolving power (FWHM at m/z 200), and MS scan range was 75-400 m/z. High resolution accurate mass (HRAM) data was acquired in negative ion mode. Source conditions were as follows: the sheath gas flow rate was 35 arbitrary units, and auxiliary gas flow rate was

8 arbitrary units; the spray voltage was 3.5 kV, and the capillary temperature was 400°C; the AGC target was 10^6.

The Xcalibur platform was used for spectra visualization, qualitative and quantitative analysis. The peak area of EIC (Extracted Ion Chromatogram) was used for quantification. The m/z of standard HMBPP in negative mode was 260.9940, and the extract ion precision was 10 ppm. The concentration of HMBPP was calculated by an external standard and standard curves were linear over ranges of 0.02-1 ng/μL for HMBPP with r^2 greater than 0.996. Samples were normalized by initial pellet mass.

Intravenous infections

Intravenous (IV) infections were adapted from previously reported methods (76,77). Briefly, 8-week-old female CD-1 (Charles River) mice were infected IV with 10^5 CFUs in 200 μL of PBS, and organs were harvested 48 hrs post infection. When mice were infected with Δ*hmgR* mutants, the inoculum was increased to 10^6 CFUs and organs were harvested 24 hours post infection due to the growth defect of this strain. To measure organ CFUs, mice were euthanized and spleens, livers, and gallbladders were removed, homogenized in 5, 10, or 0.5 mL of 0.1% IGEPAL CA-630 (Sigma), respectively, and plated to enumerate bacteria.

Oral infections

Oral infections were adapted from previously reported methods (52,78,79). Briefly, 5 mg/mL of streptomycin sulfate was added to the drinking water of 8-week-old female CD-1 (Charles River) mice two days prior to infection. One day prior to infection, mice were transferred to clean cages and chow was removed to fast the mice overnight. Mice were fed a small piece of white bread inoculated with 10^7 CFUs of *L. monocytogenes* in 5 μL of PBS, and 3 μL of butter was overlaid on the bread. When mice were infected with Δ*hmgR* mutants, the inoculum was increased to 10^8 CFUs, due to the growth defect of this strain. After infection, mice were returned to cages with standard drinking water and chow. To measure infection burden, pellets were collected from each mouse, weighed, homogenized in 1 mL PBS, and plated by serial dilution to enumerate CFUs. Homogenates were plated on selective BHI agar supplemented with 6 g/L lithium chloride, 6 g/L glycine, 50 mg/L nalidixic acid, and 200 mg/L streptomycin (80). Pellets were collected daily for the first five days post-infection, and every two days for the remainder of the experiment. These studies were carried out in strict accordance with the recommendations in the Guide for the Care and Use of Laboratory Animals of the National Institutes of Health. All protocols were reviewed and approved by the Animal Care and Use Committee at the University of California, Berkeley (AUP-2016-05-8811).

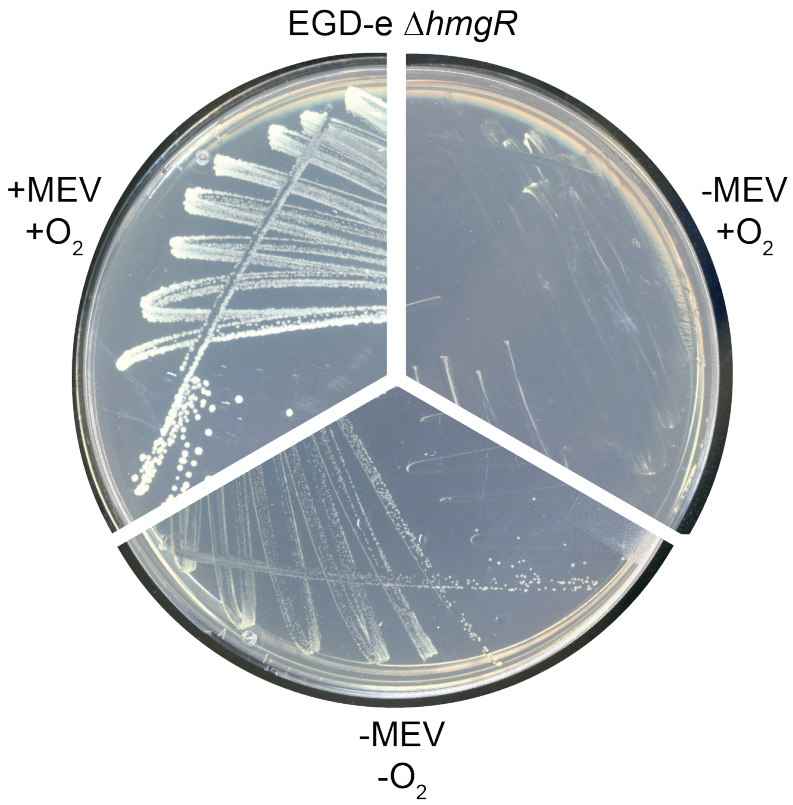

Supplemental Figure 2.1. EGD-e Δ*hmgR* grows on BHI agar without mevalonate. Clockwise from top left: plate images of EGD-e cultured aerobically with mevalonate, aerobically without mevalonate, and anaerobically without mevalonate.

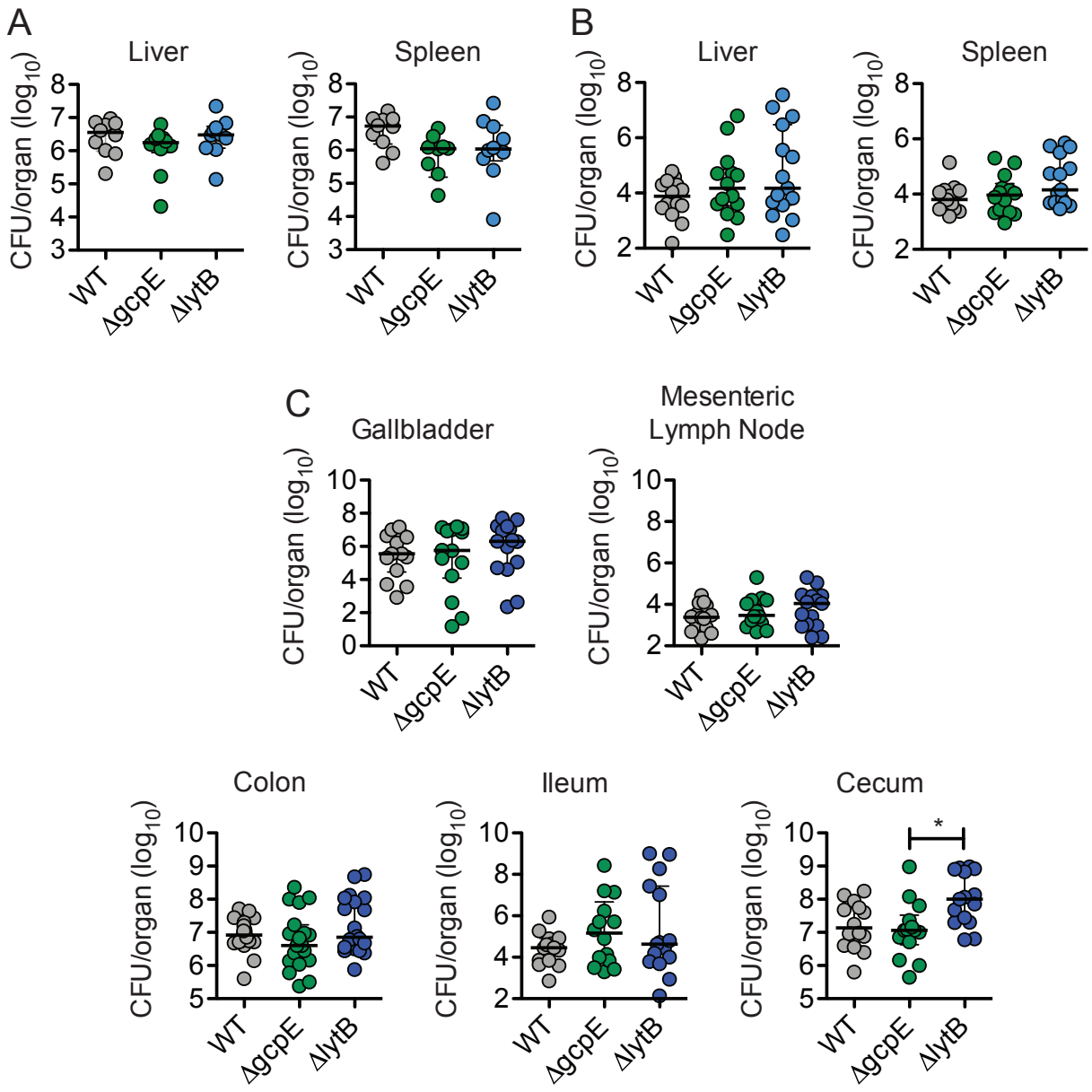

Supplemental Figure 2.2. Nonmevalonate pathway mutants do not have virulence defects.

A. CFUs recovered from CD-1 mice two days after IV infection with 10^5 CFUs of indicated *L. monocytogenes* strains. **B.** CFUs recovered from mice five days after oral infection with indicated *L. monocytogenes* strains. **C.** CFUs recovered from additional mouse organs, five days after oral infection with indicated *L. monocytogenes* strains.

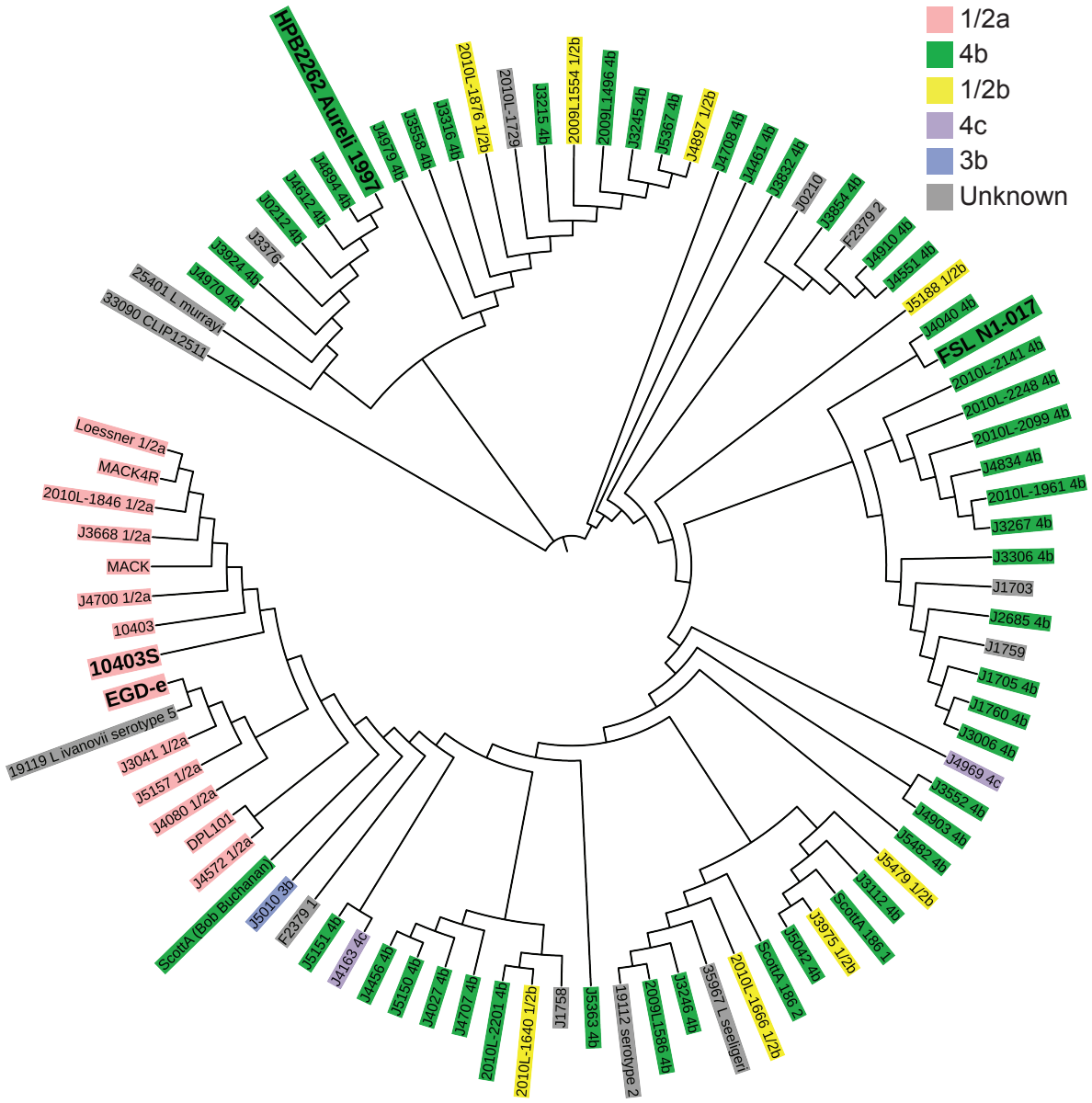

Supplemental Figure 2.3. Phylogenetic tree of *gcpE* genes from various *L. monocytogenes* laboratory strains and clinical isolates.
Strains are colored by serotype.

Supplemental Methods

Phylogenetic tree of *gcpE* alleles

PCRs were performed on laboratory strains and human placental isolates to amplify *gcpE* from each strain. Gel extractions were performed using QIAprep 2.0 spin columns (Cat No. 27115), according to manufacturer's instructions. Sequencing was performed using Sanger sequencing, and phylogenetic tree was constructed using Interactive Tree Of Life (iTOL) v4 (81).

Table 2.1: *L. monocytogenes* strains

Strain	Description	Reference
DP-L6253	10403S WT	(82)
DP-L6700	Δ*hmgR*	This study
DP-L6701	Δ*hmgR* + pPL2-*hmgR*	This study
DP-L197	EGD-e	(82)
DP-L6702	EGD-e Δ*hmgR*	This study
DP-L6703	FSL N1-017	(83)
DP-L6704	FSL N1-017 Δ*hmgR*	This study
DP-L6705	HPB2262 (Aureli 1997)	(39)
DP-L6706	HPB2262 Δ*hmgR*	This study
DP-L6707	Δ*hmgR* + pPL2-*ispD* (10403S)	This study
DP-L6708	Δ*hmgR* + pPL2-*ispD* (FSL N1-017)	This study
DP-L6709	Δ*hmgR* + pPL2-*ispD* (HPB2262)	This study
DP-L6710	Δ*hmgR* + pPL2-*gcpE* (10403S)	This study
DP-L6711	Δ*hmgR* + pPL2-*gcpE* (FSL N1-017)	This study
DP-L6712	Δ*hmgR* + pPL2-*gcpE* (HPB2262)	This study
DP-L6713	Δ*hmgR* + pPL2-*lytB* (10403S)	This study
DP-L6714	Δ*hmgR* + pPL2-*lytB* (FSL N1-017)	This study
DP-L6715	Δ*hmgR* + pPL2-*lytB* (HPB2262)	This study
DP-L6716	Δ*hmgR*Δ*gcpE*	This study
DP-L6717	Δ*hmgR*Δ*gcpE* + pPL2-*gcpE* (P_{10403S} 10403S)	This study
DP-L6718	Δ*hmgR*Δ*gcpE* + pPL2-*gcpE* (P_{10403S} FSL N1-017)	This study
DP-L6719	Δ*hmgR*Δ*gcpE* + pPL2-*gcpE* (P_{10403S} HPB2262)	This study
DP-L6720	Δ*hmgR*Δ*gcpE* + pPL2-*gcpE* (10403S$^{1-250}$/FSL N1-017$^{251-369}$)	This study
DP-L6721	Δ*hmgR*Δ*gcpE* + pPL2-*gcpE*$^{I343V/D344E}$	This study
DP-L6722	Δ*hmgR*Δ*gcpE* + pPL2-*gcpE*$^{F357Y/V359E}$	This study
DP-L6723	Δ*hmgR*Δ*gcpE* + pPL2-*gcpE*$^{K291T/E293K/V294A}$	This study
DP-L6724	Δ*hmgR*Δ*gcpE* + pPL2-*gcpE*^{K291T}	This study
DP-L6725	Δ*hmgR*Δ*gcpE* + pPL2-*gcpE*^{V294A}	This study
DP-L6726	Δ*hmgRgcpE*$^{K291T/E293K/V294A}$	This study
DP-L2209	*hly::Tn917*	(51)
DP-L6727	*gcpE*$^{K291T/E293K/V294A}$	This study
DP-L6728	*gcpE*$^{K291T/E293K/V294A}$ *hly::Tn917*	This study
DP-L6729	Δ*gcpE*	This study
DP-L6730	Δ*gcpE hly::Tn917*	This study
DP-L6731	Δ*lytB*	This study
DP-L6732	Δ*lytB hly::Tn917*	This study

Table 2.2: *E. coli* strains

Strain	Plasmid or genotype	Reference
XL1-Blue	Cloning; recA1 endA1 gyrA96 thi-1 hsdR17 supE44 relA1 lac [F´proAB $lacI^q$ ZΔM15 Tn10 (Tet^r)]	Stratagene
TOP10	Cloning; F- *mcrA* Δ(*mrr-hsd*RMS-*mcr*BC) Φ80*lac*ZΔM15 Δ *lac*X74 *rec*A1 *ara*D139 Δ(*araleu*)7697 *gal*U *gal*K *rps*L (StrR) *end*A1 *nup*G	Invitrogen
SM10	Conjugation; thi-1 thr-1 leuB6 tonA21 lacY1 supE44 recA λ^- integrated [RP4-2-Tcr::Mu] $aphA^+$ (Km^r) Tra^+	(84)
DP-E6324	pKSV7-oriT	(85)
DP-E6733	pKSV7-Δ*hmgR* (10403S/FSL N1-017)	This study
DP-E6734	pKSV7-Δ*hmgR* (EGD-e)	This study
DP-E6735	pKSV7-Δ*hmgR* (HPB2262)	This study
DP-E6736	pKSV7-Δ*gcpE*	This study
DP-E6737	pKSV7-Δ*lytB*	This study
DP-E6738	pKSV7-*gcpE*$^{K291T/E293K/V294A}$	This study
DP-E6333	pPL2t	(86)
DP-E6739	pPL2-*ispD* (10403S)	This study
DP-E6740	pPL2-*ispD* (FSL N1-017)	This study
DP-E6741	pPL2-*ispD* (HPB2262)	This study
DP-E6742	pPL2-*gcpE* (10403S)	This study
DP-E6743	pPL2-*gcpE* (FSL N1-017)	This study
DP-E6744	pPL2-*gcpE* (HPB2262)	This study
DP-E6745	pPL2-*lytB* (10403S)	This study
DP-E6746	pPL2-*lytB* (FSL N1-017)	This study
DP-E6747	pPL2-*lytB* (HPB2262)	This study
DP-E6748	pPL2-*gcpE* (P_{10403S} FSL N1-017)	This study
DP-E6749	pPL2-*gcpE* (P_{10403S} HPB2262)	This study
DP-E6750	pPL2-*gcpE* (10403S$^{1-250}$/FSL N1-017$^{251-369}$)	This study
DP-E6751	pPL2-*gcpE*$^{I343V/D344E}$	This study
DP-E6752	pPL2-*gcpE*$^{F357Y/V359E}$	This study
DP-E6753	pPL2-*gcpE*$^{K291T/E293K/V294A}$	This study
DP-E6754	pPL2-*gcpE*^{K291T}	This study
DP-E6755	pPL2-*gcpE*^{V294A}	This study
DP-E6756	pPL2-*hmgR*	This study

Chapter 3

Activation of the two-component system LisRK increases *L. monocytogenes* growth using the nonmevalonate pathway of isoprenoid biosynthesis

3.1 Summary of results

The nonmevalonate pathway of isoprenoid precursor biosynthesis was recently found to be sufficient for *L. monocytogenes* growth in anaerobic conditions. We showed that lineage II strains and lineage I *L. monocytogenes* strains encoded different alleles of the nonmevalonate pathway enzyme GcpE, which led to distinct differences in anaerobic growth rates between strains. This observation demonstrated that nonmevalonate pathway growth could be altered with mutations in the pathway itself, but left the question of whether any other proteins also helped regulate the nonmevalonate pathway. We anaerobically passaged a mutant in the nonmevalonate pathway, Δ*hmgR*, and used whole genome sequencing to identify suppressor mutations that allowed this mutant to grow faster using the nonmevalonate pathway. Three unique point mutations were identified in the histidine kinase LisK, which is part of the two-component regulatory system LisRK. A frameshift mutation was also identified in the protease ClpC, but was not studied further. Deleting *lisK* from Δ*hmgR* caused bacteria to lyse in the absence of mevalonate, suggesting that the suppressor mutations activated or altered LisRK signaling. However, we were unable to identify any genes whose expression obviously changed in different LisRK mutant strains. This study suggests that the nonmevalonate pathway can be activated in response to environmental signals, but further studies are needed to better define the LisRK regulon in strain 10403S.

3.2 Introduction

Isoprenoid precursor biosynthesis is an essential process in all cells. Isoprenoid precursor molecules, isopentenyl pyrophosphate (IPP) and dimethyl-allyl pyrophosphate (DMAPP) can be produced by two unique biosynthetic pathways in bacteria, called the mevalonate pathway and the nonmevalonate pathway (7). Most bacteria have one pathway or the other, but *Listeria monocytogenes* is unique in that it has genes for both pathways (9,10). Work from previous authors report that the mevalonate pathway is essential for *L. monocytogenes* growth, but recently we demonstrated that the nonmevalonate pathway was sufficient for anaerobic growth, even if the rate limiting gene of the mevalonate pathway was deleted.

Furthermore, we observed that different strains of (39) *L. monocytogenes* had substantially different growth phenotypes when *hmgR* was deleted (Δ*hmgR*) and the bacteria were cultured anaerobically. One environmental and one clinical isolate, FSL N1-017 (70) and HPB2262 Aureli 1997 (39), grew significantly faster on the nonmevalonate pathway than two commonly used laboratory strains, 10403S and EGD-e. Three amino acid changes in the nonmevalonate pathway enzyme GcpE were sufficient to increase 10403S growth rates to the same rate as the lineage I strains. All three changes, K291T, E293K, and V294A, needed to be present to alter *L. monocytogenes* growth, and any single mutation did not alter growth rates.

We were curious whether we could better understand the regulatory network controlling the nonmevalonate pathway, by identifying other suppressor mutations that also increased the growth rate of 10403S Δ*hmgR*. Suppressor mutations were identified by utilizing the severe anaerobic growth defect of 10403S Δ*hmgR*, which made it possible to isolate mutants that grew faster anaerobically. Specific mutations were identified using whole genome sequencing and were further characterized with

molecular genetics. The results of this study demonstrate that several unique point mutations in the histidine kinase LisK significantly increased Δ*hmgR* anaerobic growth rates. The precise mechanism of these mutations was not identified, but the data suggest that these mutations activate or increase signaling in the two-component system LisRK, rather than disrupting signaling.

3.3 Results

3.3.1 Identification of suppressor mutations that alter *L. monocytogenes* growth using the nonmevalonate pathway

Fast growing suppressor mutants were isolated by sequentially passaging Δ*hmgR* anaerobically in BHI broth. We reasoned that any Δ*hmgR* mutants that grew faster anaerobically would have a competitive advantage in broth culture, which would allow the fast-growing suppressor mutants to outcompete parental Δ*hmgR* bacteria over the course of several passages. Six cultures were started from unique colonies on plates and each was grown anaerobically for five passages. No changes in growth were observed for the first two passages and each culture required four to five days to grow to turbidity (OD ≈ 1.0). Growth rate increased from the third passage onward, as each passage required two days to reach stationary phase anaerobically. Aliquots from the fifth passage were frozen, thawed to confirm that the fast growth was maintained, before genomic DNA was prepared and sent for whole genome sequencing.

Suppressor mutations were mapped to five different genes (Table 3.1). Mutations in identified in culture 2 were not fully penetrant, likely as a result of the method used to isolate suppressor mutations. Five out of the six cultures had mutations in the histidine kinase LisK and one of the cultures also had another mutation in the response regulator LisR. As a result, we focused on these genes for further characterization. A transposon in the gene *lmo1389* (*lmo1389::himar1*) was used to transduce the suppressor mutations from cultures 1, 3, and 4, into a clean Δ*hmgR* background, and Sanger sequencing was used to confirm that the LisK mutations had been transduced. These rederived LisK* mutants (Δ*hmgR lisK** 1, Δ*hmgR lisK** 3, and Δ*hmgR lisK** 4) were the strains used for all subsequent analyses. Anaerobic growth curves confirmed that the resulting strains had a similar fast growing phenotype in broth cultures (Fig. 3.1A).

Table 3.1: Suppressor mutations identified from Δ*hmgR* anaerobic cultures

Culture	*lisK* (lmo1378)	*lisR* (lmo1377)	multidrug ABC transporter ATP-binding protein (lmo1505)	ATP-dependent Clp protease ATP-binding subunit ClpC (lmo0232)	glycosidase (lmo2444)
1	Glu276Lys				
2	Val84Gly Arg172Trp 1302A>G	435C>T (-243 of lisR)			Ala46fs
3	Phe260Val				
4	Ile36Val				
5	Arg176Leu			Asn25fs	
6			Asp24fs		

Table 3.1: Suppressor mutations identified in Δ*hmgR* cultures.
DNA and amino acid mutations identified by Illumina HiSeq whole genome sequencing of fast-growing Δ*hmgR* suppressor mutants. Amino acid mutations are listed, and base pairs are indicated if a change resulted in a silent mutation at the amino acid level. Frame-shift mutations are indicated by "fs."

3.3.2 Deleting the histidine kinase LisK severely impairs ΔhmgR growth aerobically and anaerobically

LisR and LisK form a bacterial signaling network called a two-component system. Two-component systems (TCSs) are multi-protein signaling networks that help bacteria sense extracellular environmental changes and transcriptionally alter genetic programs that help them survive in that new environment (87). At their simplest, TCSs have a transmembrane histidine kinase that, in response to its activating signal, forms a homodimer that autophosphorylates a histidine residue located in the kinase domain of the protein. This activated histidine kinase then interacts with its cognate response regulator and transfers the activated phosphate group to an aspartate residue on the response regulator. The phosphorylated response regulator can then act as either a transcriptional activator or repressor for the genes in its regulon.

LisRK is one of sixteen known TCSs in *L. monocytogenes* and has been implicated in tolerance of osmotic stress and cell membrane stress (88–91). However, neither its activating signal nor its DNA binding sequence motif have been identified. To examine the effect of the suppressor mutations on LisK signaling, *lisK* was deleted from Δ*hmgR* (Δ*hmgR*Δ*lisK*). Unexpectedly, Δ*hmgR*Δ*lisK* had a significantly different growth phenotype than Δ*hmgR* when grown aerobically in BHI broth (Fig. 3.1B). In high mevalonate concentrations, Δ*hmgR* had no growth defect relative to WT, but Δ*hmgR*Δ*lisK* took slightly longer to reach stationary phase. Furthermore, Δ*hmgR* grew slightly without mevalonate, eventually reaching a stationary phase after approximately four hours of growth. In contrast, Δ*hmgR*Δ*lisK* growth stopped at approximately the same time, but the OD decreased over the time course until it was undetectable 24 hours post inoculation. Live microscopy was used to observe bacterial growth as Δ*hmgR* and Δ*hmgR*Δ*lisK* reached stationary phase (Fig. 3.2). Upon inoculation, Δ*hmgR* divided several times, but stopped dividing after approximately four hours. In contrast,

Δ*hmgR*Δ*lisK* bacteria continued growing and formed very elongated cells shapes. As time passed, bacteria eventually disappeared from the field of view, which suggested that bacteria were lysing.

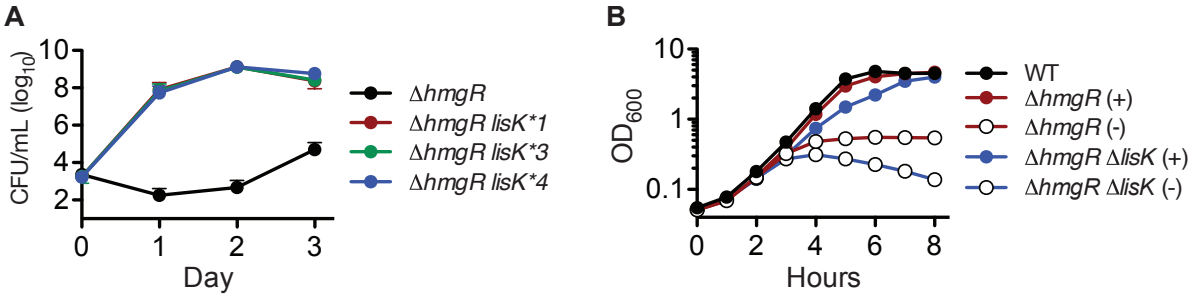

Figure 3.1. Suppressor mutations in *lisK* increase anaerobic growth of Δ*hmgR*. **A.** Anaerobic BHI growth curve of Δ*hmgR* and Δ*hmgR* suppressors with *lisK* mutations. **B.** Aerobic BHI growth curve of WT, Δ*hmgR*, and Δ*hmgR*Δ*lisK*. Δ*hmgR* and Δ*hmgR*Δ*lisK* were grown in BHI with (+) or without (-) 2.5 mM mevalonate.

3.3.3 Mutations in LisRK do not impact growth or virulence

Due to the significant *in vitro* growth phenotypes observed in Δ*hmgR*Δ*lisK*, we were curious whether mutating the LisRK TCS alone impacted growth or pathogenesis of 10403S. Neither a *lisK* mutant (Δ*lisK*) or *lisR* mutant (Δ*lisR*) had a growth defect in bone marrow derived macrophages (Fig. 3.3A), but Δ*lisK* infection of macrophages caused slightly higher levels of host cell death in a lactate dehydrogenase assay (Fig. 3.3B). After a 48 hour intravenous infection, there was no significant change in virulence (Fig. 3.3C). This is in contrast to Δ*hmgR*Δ*lisK* infections, because recoverable CFUs in macrophases rapidly decreased to below the limit of detection by the final eight-hour time point (Fig. 3.3D).

These observations suggested that the suppressor mutations in LisK were not disrupting or blocking LisRK signaling, but were instead constitutively activating signaling. As a result, we further characterized the Δ*hmgR lisK** mutants in the same assays to determine whether the suppressor mutations had different impacts on bacterial than a *lisK* deletion. All three Δ*hmgR lisK** mutants grew significantly more in bone marrow derived macrophages relative to the original Δ*hmgR* strain (Fig. 3.3E). They also caused significantly less host cell death than Δ*hmgR*, which is likely the reason more CFUs were recovered eight hours post infection. These data were consistent with the hypothesis that LisK suppressor mutations were activating rather than inhibitory, so we sought to directly link LisRK signaling and the nonmevalonate pathway.

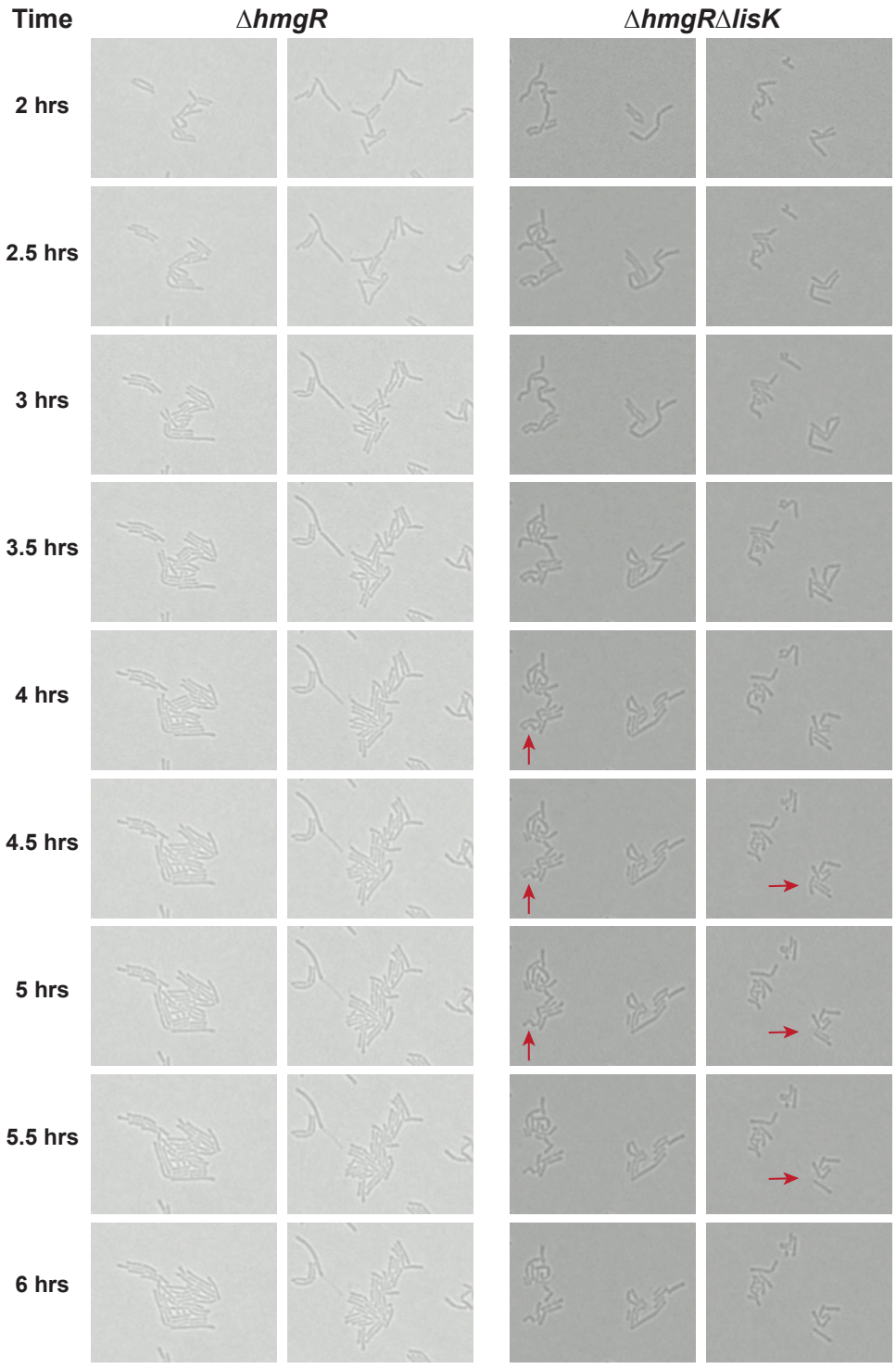

Figure 3.2. Live microscopy of Δ*hmgR* and Δ*hmgR*Δ*lisK*.
Two representative fields of view from Δ*hmgR* and Δ*hmgR*Δ*lisK* growth on a BHI agar pad without mevalonate. Δ*hmgR* divides several times, but stops growing at approximately 4 hours post inoculation. Individual Δ*hmgR*Δ*lisK* cells begin disappearing from the field of view at approximately 4 hours post inoculation.

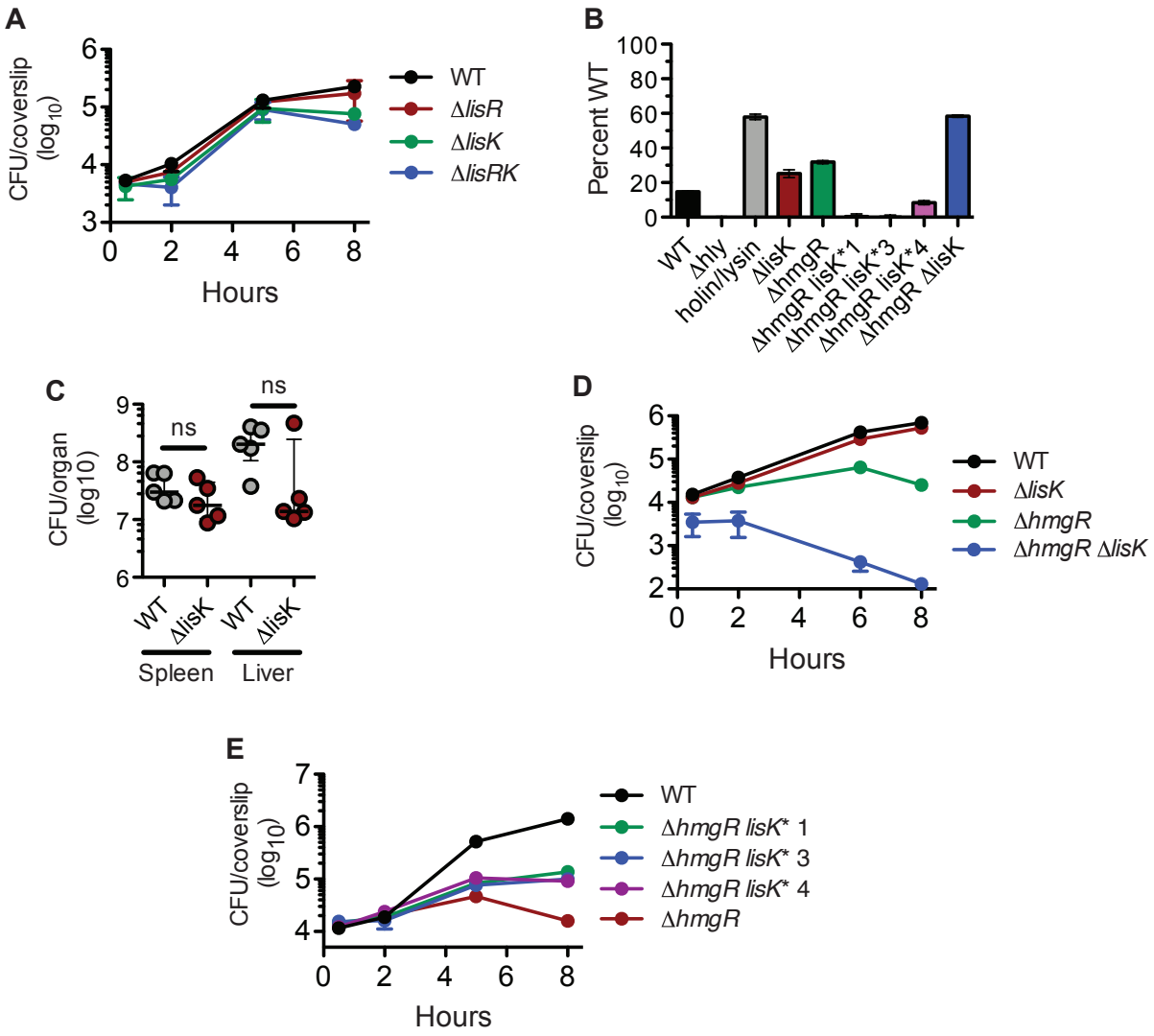

Figure 3.3. LisRK mutations dramatically impair growth in combination with Δ*hmgR*, but do not impact virulence on their own.
A. Bone marrow-derived macrophage growth curve of LisRK mutants. Neither Δ*lisK*, Δ*lisR*, or Δ*lisRK* have virulence defects in bone marrow-derived macrophages. **B.** Lactate dehydrogenase release assay of Δ*hmgR lisK** strains. Δ*hmgR lisK** mutants induce significantly less cell death than Δ*hmgR*, while Δ*hmgR* Δ*lisK* induces significantly more cell death. **C.** CFUs recovered from indicated organs one day after IV infection with WT or Δ*lisK L. monocytogenes*. Δ*lisK* does not have a significant growth defect compared to WT. **D.** Bone marrow-derived macrophage growth curve of Δ*hmgR* Δ*lisK* mutant. Δ*hmgR* Δ*lisK* has a severe growth defect and does not survive in cells over the course of an eight hour growth curve. **E.** Bone marrow-derived macrophage growth curve of WT, Δ*hmgR*, and three Δ*hmgR lisK** suppressor mutants.

3.3.4 GcpE and LytB expression levels do not change anaerobically

Based on our prior work with the lineage I strains FSL N1-017 and HPB2262 we were curious whether strain-specific differences existed that could contribute to growth on the nonmevalonate pathway. To examine whether regulatory factors in each strain could alter growth, both *gcpE* and *lytB* were deleted from FSL N1-017 (FSL Δ*gcpE* and FSL Δ*lytB*), HPB2262 (HPB Δ*gcpE* and HPB Δ*lytB*), and EGD-e (EGD-e Δ*gcpE* and EGD-e Δ*lytB*). Next, 6xHis-tagged copies of 10403S *gcpE* and 10403S *lytB* were complemented into their respective deletion strains, so that each strain expressed *gcpE* or *lytB* from 10403S. These genes were chosen because they are the rate-limiting steps in the nonmevalonate pathway, and we previously observed that minor changes to the GcpE coding sequence significantly impacted *L. monocytogenes* anaerobic growth using the nonmevalonate pathway. We then asked whether protein levels of GcpE or LytB changed in any of these strains, under aerobic or anaerobic conditions. No changes in either GcpE (Fig. 3.4A) or LytB (Fig. 3.4B) were detected in any of the strains by Western Blot. The loading control varied significantly in the first blot, but when it was repeated with select strains, we observed similar results (Fig. 3.4C, 3.4D).

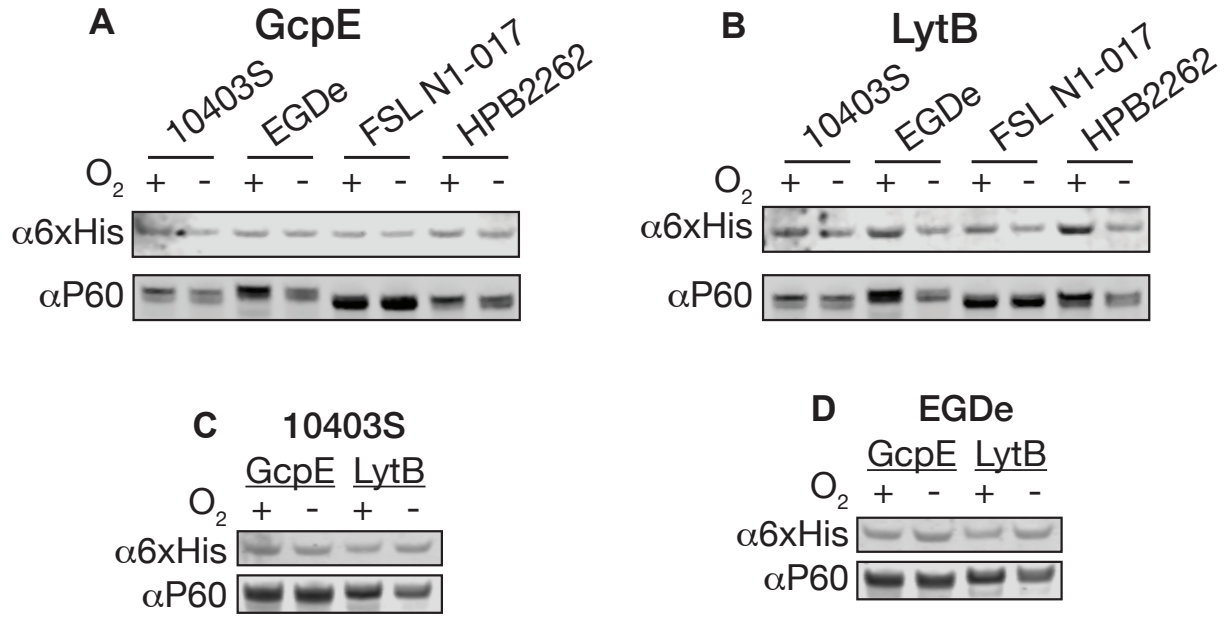

Figure 3.4. Western blot for GcpE and LytB in aerobic and anaerobic conditions **A**. Western blot for 6xHis-GcpE in indicated *L. monocytogenes* strains, when cultured aerobically and anaerobically. **B.** Western blot for 6xHis-LytB in indicated *L. monocytogenes* strains, when cultured aerobically and anaerobically. **C.** Replicate of previous Western blots using 10403S strains. **D.** Replicate of previous Western blots using EGD-e strains.

3.3.5 Genes in the nonmevalonate pathway are not part of the LisRK regulon

Several studies have attempted to define the LisRK regulon in *L. monocytogenes.* One study showed that deleting *lisK* increased sensitivity to sodium chloride (89), while another used the more generalized approach of comparing microarray data between WT and Δ*lisR* in response to cefuroxime, a ß-lactam antibiotic that targets cell wall synthesis (90). Both studies used the strain LO28, which is a serotype 1/2c strain, in comparison to the more-commonly used strains 10403S and EGD-e, both of which are serotype 1/2a. The second study showed that the gene encoding undecaprenyl diphosphate synthase, *lmo1315*, is upregulated in response to cefuroxime in WT, but not in Δ*lisR* (90). UPP synthase is downstream of both isoprenoid precursor pathways, but is an essential step in the undecaprenol biosynthesis pathway. The *lmo1315* operon also contains *dxr*, which is the second committed step of the nonmevalonate pathway. We hypothesized that the LisK* suppressor mutations could constitutively upregulate this operon, thereby increasing anaerobic growth using the nonmevalonate pathway.

Quantitative real-time PCR (qRT-PCR) was performed on bacteria to examine whether expression levels of any putative LisRK-regulated genes changed with oxygen levels. We used *qoxA* (*lmo0013*) as a positive control, because it is known to be significantly downregulated anaerobically in *L. monocytogenes*. Anaerobically, *qoxA* mRNA levels decreased almost 5-fold in all strains (Fig. 3.5A), relative to aerobic conditions. *dxr* expression was measured in the same samples, but there were no obvious trends in *dxr* expression between Δ*lisRK* and *lisK** mutants, either with or without oxygen (Fig. 3.5B). As a result, other reportedly LisRK-regulated genes were examined.

Lmo0292 is an HtrA-like protein, a class of heat shock proteins necessary for bacterial survival at high temperatures. *Lmo0292* was found to be positively regulated by LisRK, because *lmo0292* RNA levels at stationary phase decreased significantly when *lisK* was deleted from EGD-e (92). In 10403S Δ*lisRK* we observed that *lmo0292* expression increased both aerobically and anaerobically relative to WT (Fig. 3.5C), and LisK* mutants also had increased RNA levels. Since similar results were observed in both Δ*lisRK* and LisK* strains, it did not help elucidate the mechanism by which the suppressor mutations altered Δ*hmgR* anaerobic growth.

LisRK is reported to regulate a family of sRNAs, LhrC1-5, in the strain LO28 (93). They found that stress activates LisR, which upregulates LhrC1-5. These in turn suppress several genes, including a heme oxygenase-like protein *lmo0484*. Even though their data showed only a modest increase in *lmo0484* expression in a Δ*lhrC1-5* strain one hour after cefuroxime exposure, we still chose to measure *lmo0484* expression by qPCR in our LisK* mutants. We observed no significant changes in *lmo0484* expression level between mutants, including Δ*lisR*, Δ*lisRK*, and the LisK* mutants (Fig. 3.5D).

One confounding factor of this study was potential variation between anaerobic sample prep, and a failure to confirm that previous results, such as LisRK activation in response to cefuroxime stress, repeated in 10403S. Future studies would benefit from a more “omics-based” approach, using a combination of LisRK knockouts and suppressor mutants to define the LisRK regulon and its relationship with the nonmevalonate pathway.

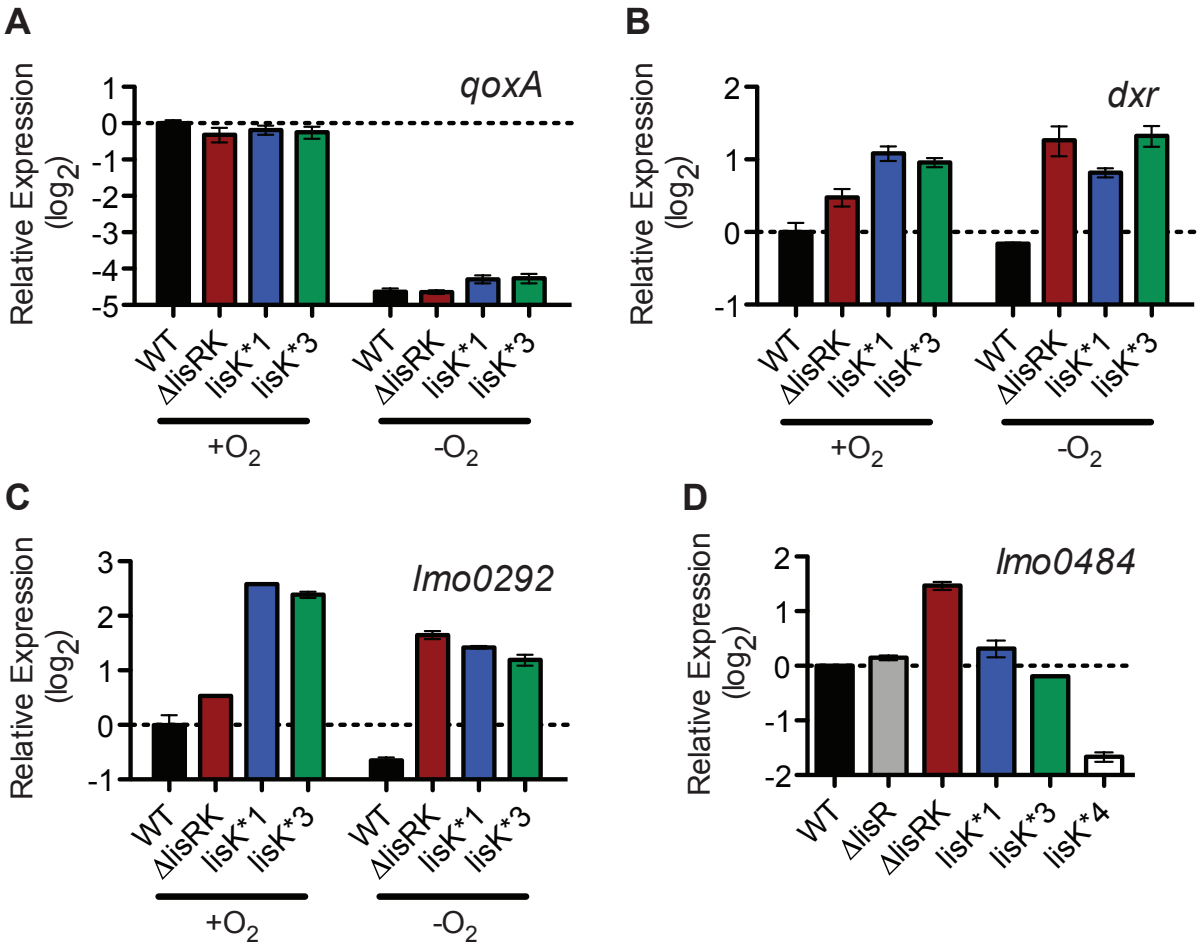

Figure 3.5. qRT-PCR of potential LisRK-regulated genes in aerobic and anaerobic conditions.

A. Relative expression levels of *qoxA* in *L. monocytogenes* strains grown aerobically and anaerobically. **B.** Relative expression levels of *dxr* in *L. monocytogenes* strains grown aerobically and anaerobically. **C.** Relative expression levels of *lmo0292* in *L. monocytogenes* strains grown aerobically and anaerobically. **D.** Relative expression levels of *lmo0484* in *L. monocytogenes* strains grown aerobically.

3.4 Discussion

Previous work demonstrated that genetic differences in the nonmevalonate pathway enzyme GcpE significantly increased 10403S Δ*hmgR* growth anaerobically. In this work, we examined whether suppressor mutations in 10403S Δ*hmgR* could also increase anaerobic growth rates, to gain a better understanding of how the nonmevalonate pathway is regulated in *L. monocytogenes*. We isolated mutations in Δ*hmgR* that increased growth using the nonmevalonate pathway by sequentially passaging cultures anaerobically and performing whole genome sequencing to identify mutations.

Multiple mutations in the two-component system LisRK arose in fast-growing strains. All of the mutations caused point mutations rather than frameshift mutations, which was curious because it is statistically far more likely for a frameshift mutation to occur. This suggested that the mutations maintained LisRK signaling instead of causing a loss-of-function mutation. Indeed, we observed that Δ*hmgR*Δ*lisK* lysed in broth without mevalonate, which supported the hypothesis that our suppressor mutations altered, rather than disrupted, LisRK signaling. Work from other authors had identified one gene involved with isoprenoid biosynthesis, *lmo1315*, as being transcriptionally regulated by LisR in the *L. monocytogenes* strain LO28. However, in 10403S neither *lmo1315* nor *dxr* expression levels changed in the presence or absence of LisR or LisK, when comparing aerobic or anaerobic conditions. These observations do not exclude the possibility that the operon is upregulated in response to cefuroxime stress, but this condition was not tested.

Several questions will likely need to be answered in order to gain a better understanding of the relationship between LisRK and the nonmevalonate pathway. A putative LisRK DNA binding sequence was recently identified, and it would be interesting to perform a more complete bioinformatics analysis to define the LisRK regulon (94). Additionally, identifying the specific activating signal may reveal conditions in which the nonmevalonate pathway is activated, and provide more insight into why *L. monocytogenes* has two isoprenoid pathways. To this end, it would be useful to translationally fuse a LisRK regulated 5' UTR to a reporter gene such as ß-galactosidase or ß-glucaronidase, which would be a means of easily screening conditions in which the two-component system is activated.

Ultimately, we failed to clearly define a connection between the nonmevalonate pathway and LisRK, but there are several interesting possibilities that may warrant further investigation. LisR regulates a set of small regulatory RNAs, *lhrC1-5*, in a heme-dependent manner, with *lhrC1-5* downregulating their target genes in response to heme stress (93). Among the *lhrC1-5* regulated genes is *lmo0484*, a heme-monooxygenase that helps maintain iron homeostasis. Even though no consistent changes in *lmo0484* mRNA levels were observed, two enzymes in the nonmevalonate pathway, GcpE and LytB, contain iron-sulfur clusters and have been shown to be the only essential iron-sulfur cluster containing enzymes in *Escherichia coli* and *Bacillus subtilis* (59,60). Thus, it may be worth examining whether there is any connection between LisRK activation, *lhrC1-5* regulation, and iron-sulfur cluster biosynthesis in *L. monocytogenes*.

One of the significant challenges with this study was simply that two-component systems are not well characterized outside of a few model organisms. Additionally, our previous work demonstrated that there are significant strain-specific differences in

nonmevalonate pathway genes that can alter the pathway's function. All previous LisRK studies in *L. monocytogenes* used EGD-e or LO28, which may have impacted our ability to replicate previously published results. Furthermore, those studies varied in whether they examined histidine kinase deletions, response regulator deletions, or deletions that remove the entire two component system. As a result, it is difficult to rule out the possibility that cross-talk between unrelated two-component systems with LisR or LisK was responsible for the inconsistencies between studies (87).

One entirely unaddressed question is how the frameshift mutation identified in ClpC impacts anaerobic growth on the nonmevalonate pathway. ClpC is the protease responsible for degrading MurA, a key peptidoglycan hydrolase involved with peptidoglycan biosynthesis in *B. subtilis* and *L. monocytogenes* (95–97). ClpC disruption leads to MurA accumulation, which can in turn increase the production of UDP-N-acetylglucosamine (UDP-GlcNAc) and stimulate cell wall biosynthesis. Curiously, a ClpC transposon (DP-L5647) was previously identified in a screen for hyperhemolytic mutants in 10403S, which may also would be useful for further examining this hypothesis. Presently, we believe that the slow growth observed in 10403S is due to a metabolic bottleneck within the nonmevalonate pathway, and mutations in GcpE relieve this bottleneck. Further analysis of a ClpC mutant and UDP-GlcNAc accumulation may reveal another metabolic bottleneck that influences Δ*hmgR* growth, outside of the nonmevalonate pathway enzymes.

Our previous study found that mutations in GcpE, which increased the growth rate of Δ*hmgR*, did not significantly increase HMBPP production. The suppressor mutations identified in this study may provide an alternative means of manipulating HMBPP production, which may prove useful as we gain a better understanding of Vγ9Vδ2 T-cells. These suppressor mutations in LisRK also suggest that the nonmevalonate pathway may be activated in response to particular environmental cues, so it would be exciting to search for the exact activating stimulus.

3.5 Materials and Methods

Construction of L. monocytogenes strains

The *L. monocytogenes* strains used in this study are all derived from wild-type 10403S (DP-L6253) unless otherwise noted and are listed in Table 3.2. Gene deletions were generated by allelic exchange using the plasmid pKSV7 (74). All *L. monocytogenes* strains were grown in brain heart infusion (BHI) broth and media was supplemented with 1 mM mevalonate as needed to support the growth of auxotrophic Δ*hmgR* strains. Mevalonate was produced by hydrolyzing DL-mevalonolactone (Sigma-Aldrich CAS Number 674-26-0) with 1 N NaOH at 37 ºC for 1 hour, according to previously reported methods (35). Strains were cultured anaerobically using a BD GasPak EZ anaerobic pouch system (Cat no. 260683).

E. coli strains used in this study are listed in Table 3.3. For vector construction, plasmids were introduced into TOP10 *E. coli* (Invitrogen) or XL1 Blue *E. coli* (Stratagene). Plasmids were then transformed into SM10 *E. coli* and conjugated into *L. monocytogenes*. PCR was performed with KAPA HiFi DNA polymerase (Kapa

Biosystems). Positive clones were identified by performing colony PCRs using SapphireAmp Fast PCR Master Mix (Takara Bio) and verified by Sanger sequencing.

Generation of Δ*hmgR* suppressor mutations

Methods for generating suppressor mutations were adapted from previously published protocols (86). Six independent Δ*hmgR* cultures were incubated anaerobically without mevalonate for five days until they reached stationary phase. Cultures were then backdiluted in fresh BHI and grown anaerobically again until they reached stationary phase. This process was repeated four times in total, at which point the cultures grew to stationary phase within two days. Each culture was then frozen down, thawed, and anaerobic growth phenotype was confirmed before genomic DNA was prepared.

Whole Genome Sequencing

Genomic DNA was prepared from a 5 mL overnight culture of bacteria using a MasterPure Gram Positive DNA Purifiation Kit (Epicentre, MGP04100) according to manufacturer's instructions. DNA was submitted for library preparation and was sequenced using single-read 50 Illumina sequencing at the Vincent J. Coates Genomics Sequencing Laboratory at UC Berkeley, supported by NIH S10 OD018174 Instrumentation Grant. Data was assembled and aligned to the 10403S reference genome (GenBank: GCA_000168695.2) and SNP/InDel/structural variation of strains was determined using CLC Genomics Workbench (QIAGEN Bioinformatics).

Phage transduction

Generalized transduction was performed as previously described (98) using the U153 phage (99). Briefly, phage were propagated in *L. monocytogenes* MACK (DP-L861) at 30 ºC. To generate a transducing lysate, approximately 10^9 CFUs of donor strain was combined with ~10^7 plaque forming units (PFUs) of U153 and immobilized in 0.7% LB agar with 10 mM $MgSO_4$ and 10 mM $CaCl_2$ overnight at 30 ºC. Recovered phage could be used for generalized transduction by lysogenizing 10^8 CFUs of recipient *L. monocytogenes* with ~10^7 PFU of transducing lysate in LB broth with 10 mM $MgSO_4$ and 10 mM $CaCl_2$, incubating for 30 mins at room temperature, and selecting for erythromycin on selective BHI agar at 37 ºC.

Aerobic growth curves

Strains were grown overnight at 37 ºC in filter-sterilized BHI and were supplemented with 500 μM mevalonate as necessary. Cells were washed with PBS and diluted in 20 mL fresh BHI. Cells were cultured at 37 ºC with shaking and growth was measured spectrophotometrically by optical density at a wavelength of 600 nm (OD_{600}).

Anaerobic growth curves

Media was degassed overnight anaerobically to allow residual oxygen to diffuse out of the media. Overnight cultures of cells were first grown aerobically and were back diluted into anaerobic media to a concentration of 10^3 CFUs/mL. Samples were removed from the glovebox daily and plated by 10-fold serial dilutions to enumerate CFUs.

Intravenous infections

Intravenous (IV) infections were adapted from previously reported methods (76,77). Briefly, 8-week-old female CD-1 (Charles River) mice were infected IV with 10^5 CFUs in 200 µL of PBS, and organs were harvested 48 hrs post infection. To collect organs, mice were euthanized and spleens and livers were removed, homogenized in 5 or 10 mL of 0.1% IGEPAL CA-630 (Sigma), respectively, and plated to enumerate bacterial burdens.

Lactate Dehydrogenase Assay

L. monocytogenes strains were grown overnight at 30 ºC in BHI without shaking. Bone marrow-derived macrophages were plated at 5 x 10^5 cells per well in a 24-well plate, in standard media supplemented with PAM3CSK. Cells were infected with a multiplicity of infection (MOI) of 2 and lactate dehydrogenase release assay was performed according to previously published methods (100).

Intracellular Macrophage Growth Curve

Bone marrow-derived macrophages were harvested as described previously (101). Briefly, 3 x 10^6 cells were plated in 60 mm non-TC treated petri dishes. Cells were infected with a multiplicity of infection (MOI) of 0.1 and growth curves were performed as described previously (102).

Immunoblots for GcpE and LytB

All immunoblotting was performed as previously described (103). Briefly, overnight cultures were diluted 1:10 into aerobic or anaerobic BHI, incubated for five hours at 37 °C, then bacteria were pelleted by centrifugation. Bacterial pellet was washed with 1 mL of PBS, then pelleted for 1 min at 13,000 RPM and supernatant was removed. The pellet was resuspended in 100 µL of 0.1% IGEPAL CA-630 (Sigma) and 0.1 mM phenylmethylsulfonyl fluoride (PMSF), then 0.1 mm silica/zirconium beads were used to bead beat bacteria for 15 minutes. Bacterial lysates were centrifuged for 15 mins at 13,000 RPM, then 90 µL of supernatant was transferred to a new tube and 30 µL of 4x LDS Buffer (Invitrogen) containing 5% ß-mercaptoethanol was added. Samples were boiled for 20 minutes, and proteins were separated by SDS-PAGE.

Primary antibody against the 6x-His tag was used at a dilution of 1:2,000 and a mouse monoclonal antibody against P60 (Adipogen) was used at a dilution of 1:5,000. P60 is a constitutively expressed bacterial protein used as a loading control (104). Goat α-mouse secondary antibody was used at a dilution of 1:5,000 and donkey α-rabbit antibody was used at a dilution of 1:10,000. All immunoblots were visualized and quantified using Odyssey Imager, according to the manufacturer's instructions.

Quantitative Real-time PCR (qPCR) of Bacterial Transcripts

Overnight cultures of bacteria were backdiluted to OD_{600}=0.01 into 5 mL BHI and grown in indicated conditions until they reached an OD_{600}=1.0. An equal volume of RNAprotect Bacteria Reagent (Qiagen) was added to the culture to stop growth, and bacteria were harvested by centrifugation and flash frozen in liquid nitrogen prior to RNA extraction. Bacteria were lysed in phenol:chloroform containing 1% SDS by

vortexing with 0.1 mm silica/zirconium beads (BioSpec Products Inc.). Nucleic acids were precipitated from the aqueous fraction overnight at −80 °C in ethanol containing 150 mM sodium acetate (pH 5.2). Precipitated nucleic acids were washed with ethanol and treated with TURBO DNase per manufacturer's instructions (Life Technologies Corporation). RNA was again precipitated overnight and then washed in ethanol. RT–PCR was performed with iScript Reverse Transcriptase (Bio-Rad) and quantitative PCR (qPCR) of resulting cDNA was performed with KAPA SYBR Fast using the manufacturer's recommended cycling parameters (Kapa Biosystems). For each gene, two pairs of primers were designed using Primer3Plus, but only one primer pair was used, based on their melting curves. Primers for qPCR are listed in Table 3.4.

Table 3.2: *L. monocytogenes* strains

Strain	Description	Reference
DP-L6253	10403S WT	(82)
DP-L6700	Δ*hmgR*	(Lee, ED *et al*. 2019)
DP-L6729	Δ*gcpE*	(Lee, ED *et al*. 2019)
DP-L6731	Δ*lytB*	(Lee, ED *et al*. 2019)
DP-L6770	EGD-e Δ*gcpE*	(Lee, ED *et al*. 2019)
DP-L6771	EGD-e Δ*lytB*	(Lee, ED *et al*. 2019)
DP-L6772	FSL N1-017 Δ*gcpE*	(Lee, ED *et al*. 2019)
DP-L6773	FSL N1-017 Δ*lytB*	(Lee, ED *et al*. 2019)
DP-L6774	HPB2262 Δ*gcpE*	(Lee, ED *et al*. 2019)
DP-L6775	HPB2262 Δ*lytB*	(Lee, ED *et al*. 2019)
DP-L6776	Δ*hmgR* Δ*lisK*	This study
DP-L6777	Δ*hmgR* Δ*lisR*	This study
DP-L6778	Δ*lisK*	This study
DP-L6779	Δ*lisR*	This study
DP-L6780	Δ*lisRK*	This study
DP-L6781	Δ*hmgR lisK*1 lmo1389::himar1*	This study
DP-L6782	Δ*hmgR lisK*3 lmo1389::himar1*	This study
DP-L6783	Δ*hmgR lisK*4 lmo1389::himar1*	This study
DP-L6784	Δ*hmgR* (Suppressor #1)	This study
DP-L6785	Δ*hmgR* (Suppressor #2)	This study
DP-L6786	Δ*hmgR* (Suppressor #3)	This study
DP-L6787	Δ*hmgR* (Suppressor #4)	This study
DP-L6788	Δ*hmgR* (Suppressor #5)	This study
DP-L6789	Δ*hmgR* (Suppressor #6)	This study
DP-L6790	Δ*hmgR clpC::himar1*	This study
DP-L6791	Δ*gcpE* + pPL2-*gcpE-6xHis* (10403S)	This study
DP-L6792	Δ*lytB* + pPL2-*lytB-6xHis* (10403S)	This study
DP-L6793	FSL N1-017 Δ*gcpE* + pPL2-*gcpE-6xHis* (10403S)	This study
DP-L6794	FSL N1-017 Δ*lytB* + pPL2-*lytB-6xHis* (10403S)	This study
DP-L6795	HPB2262 Δ*gcpE* + pPL2-*gcpE-6xHis* (10403S)	This study
DP-L6796	HPB2262 Δ*lytB* + pPL2-*lytB-6xHis* (10403S)	This study
DP-L6797	EGD-e Δ*gcpE* + pPL2-*gcpE-6xHis* (10403S)	This study
DP-L6798	EGD-e Δ*lytB* + pPL2-*lytB-6xHis* (10403S)	This study

Table 3.3: *E. coli* strains

Strain	Description	Reference
DP-L6799	pKSV7x-*gcpE* (EGD-e)	This study
DP-L6800	pKSV7x-*lytB* (EGD-e)	This study
DP-L6801	pKSV7x-*gcpE* (FSL N1-017)	This study
DP-L6802	pKSV7x-*lytB* (FSL N1-017)	This study
DP-L6803	pKSV7x-*gcpE* (HPB2262)	This study
DP-L6804	pKSV7x-*lytB* (HPB2262)	This study
DP-L6805	pPL2-*gcpE-6xHis* (10403S)	This study
DP-L6806	pPL2-*lytB-6xHis* (10403S)	This study

Table 3.4: Primers used for qPCR

Primer	Sequence	Description
oEDL142	gggagcgttggactacttcc	F qPCR primer for *dxr*
oEDL143	cttttctttcgccgaacgca	R qPCR primer for *dxr*
oEDL177	ctaatgatggacgcgctgga	F qPCR primer for *lisR*
oEDL178	ttgtttcacttggcgcacac	R qPCR primer for *lisR*
oEDL179	caagcttttgggttccgcaa	F qPCR primer for *qoxA*
oEDL180	cgccgttgaagtttgcgtta	R qPCR primer for *qoxA*
oEDL188	ttacatacaccggagagcgc	F qPCR primer for *lmo0292*
oEDL189	tttgtagaactcgcctcggc	R qPCR primer for *lmo0292*
oEDL369	cacacggcagaacaaaagacac	F qPCR primer for *lmo0484*
oEDL370	gattgcatttcctacgatgcctttc	R qPCR primer for *lmo0484*

Chapter 4

Concluding Remarks and Future Directions

4.1 Summary of results

In this study, we demonstrate that the nonmevalonate pathway is sufficient for anaerobic growth in *L. monocytogenes*. We confirmed previous work showing that the mevalonate pathway is essential aerobically, but found that anaerobic conditions allowed a knockout in the mevalonate pathway to grow, albeit with a severe growth defect. Additionally, multiple mechanisms were identified by which the slow anaerobic growth in Δ*hmgR* could be increased, using both targeted genetic approaches and unbiased suppressor mutation analysis.

In the targeted approach, multiple lineage I *L. monocytogenes* strains were found to grow significantly faster using the nonmevalonate pathway than 10403S. This growth difference was due to three point mutations in the nonmevalonate pathway enzyme GcpE that are present in the clinical isolates, but not 10403S: K291T, E293K, and V294A. Single point mutants did not increase growth, suggesting that all three mutations in GcpE needed to occur in tandem to have an effect. When these mutations were made in a 10403S Δ*hmgR* strain, its growth rate increased to the same as the clinical isolates, but the amount of HMBPP produced did not significantly change. These observations demonstrate that HMBPP concentration is not directly proportional to anaerobic growth rate and suggest that further work is needed to fully understand metabolism using the nonmevalonate pathway in *L. monocytogenes*.

In addition to examining the specific nonmevalonate pathway genes, we asked whether other mutations could impact growth by sequentially passaging Δ*hmgR* to isolate fast-growing suppressor mutants. The highest frequency mutations were in the protein LisK, a sensor histidine kinase that, in combination with the response regulator LisR, forms the two-component system LisRK. Deleting *lisK* from Δ*hmgR* resulted in an extremely growth-impaired strain, which suggests that the point mutations increase or alter, rather than disrupt, LisRK signaling. We were unable to identify specific changes in LisRK-regulated genes that could impact the nonmevalonate pathway, but more intentionally examining the LisRK regulon may be an interesting area of further study, and could help reveal other methods by which growth on the nonmevalonate pathway could be improved.

4.2 Remaining questions

4.2.1 The role of the nonmevalonate pathway in *L. monocytogenes* biology

At the beginning of this work, we set out to answer two major questions about isoprenoid precursor biosynthesis pathways in *L. monocytogenes*. First, can *L. monocytogenes* use the nonmevalonate pathway for growth? We demonstrated that the nonmevalonate pathway is sufficient for growth anaerobically. The precise reasons why *L. monocytogenes* needs to be cultured anaerobically for the nonmevalonate pathway to function are not clear, but it may stem from a faulty iron-sulfur cluster biosynthesis pathway, an inability to keep the bacterial cytosol reduced, or metabolic changes anaerobically that require reallocation of pathway precursors like acetyl-CoA. However, answering this question about isoprenoid precursor pathways in *L. monocytogenes* will contribute to our broader understanding of isoprenoid metabolism in bacteria. The vast majority of bacteria have one of the two pathways, but there has only been speculation as to why one pathway might be favored or beneficial over the other in a bacterial species. If we understand the conditions or signals that lead to greater flux through the nonmevalonate pathway, that may point towards more generalizable conditions that other bacteria experience.

The second, and seemingly more important question, is still unanswered: why does *L. monocytogenes* maintain two pathways, when a single pathway is sufficient for the vast majority of cells? Is it simply that *L. monocytogenes* is in the process of losing both pathways and we examined it during this transitional period? Our assumption has been that it would be extremely unlikely for humans, nonhuman primates, or other Vγ9Vδ2 T-cell producing organisms to have a strong enough selective pressure to maintain the nonmevalonate pathway and HMBPP production, but this may be a possibility. Getting a mechanistic understanding of why the nonmevalonate pathway functions anaerobically may point towards the pathway's broader role for *L. monocytogenes* biology. Alternatively, while mice do not have BTN3A1 or the Vγ9Vδ2 T-cell receptor, there is still a possibility that different receptors and cell types could work in a functionally analogous manner to recognize bacterial phosphoantigens.

4.2.2 The nonmevalonate pathway and biosynthesis of iron-sulfur clusters

We found that the nonmevalonate pathway functions anaerobically, but have been unable to determine why it does not work aerobically and have been unable to isolate any suppressor mutants that grow aerobically. We hypothesize that the nonmevalonate pathway may be limited the fact that GcpE and LytB contain iron sulfur clusters, metal cofactors in proteins, which are sensitive to oxygen in purified proteins. However, many organisms exclusively have the nonmevalonate pathway and grow in the presence of oxygen, which suggests that the oxygen sensitive nature of iron-sulfur clusters can change in a cell. Other circumstantial evidence also suggests that *L. monocytogenes* may be a unique organism in terms of iron-sulfur clusters. A large number of bacterial pathogens have iron-sulfur cluster containing virulence factors and use them to sense the iron and oxygen concentration changes that occur during infection (105). Despite the apparent practicality of iron-sulfur clusters for sensing the environment, no iron-sulfur cluster containing virulence factors have been identified in *L. monocytogenes* to date.

Three different iron-sulfur biosynthesis pathways have been identified in bacteria, termed Isc, Suf, and Nif. All of these multi-gene pathways can synthesize iron-sulfur clusters, but in organisms that encode more than one pathway, the Isc system is considered to be the housekeeping pathway while the Suf system operates better under stress conditions. *E. coli* encode both the Isc and Suf system, but *Bacillus subtilis* and *L. monocytogenes* only have a single Suf-like system. A series of exciting genetic studies in *E. coli* and *B. subtilis* showed that iron-sulfur biosynthesis pathways are only essential for the nonmevalonate pathway (59,60). *E. coli* and *B. subtilis* mutants lacking the capability to synthesize iron-sulfur clusters had growth defects, but these data show that the iron-sulfur clusters found in GcpE (also called IspG) and LytB (also IspH) are the only truly essential iron-sulfur clusters in each bacteria,. Considering the wide distribution of iron-sulfur cluster containing enzymes across all cellular processes, this is a remarkable discovery that emphasizes the central importance of isoprenoid precursor pathways (106).

To explore whether *L. monocytogenes* has a deficiency synthesizing iron-sulfur clusters, we complemented the iron-sulfur cluster biosynthesis operons from both *E. coli* and *B. subtilis* into Δ*hmgR* and expressed the operons under both their native 5' UTR and a constitutively active 5' UTR. Preliminary data indicate that constitutive expression of the *B. subtilis* SUF-like system may increase Δ*hmgR* growth rate anaerobically (Kathleen Navas, unpublished data), but further work needs to be done to better characterize iron-sulfur cluster biosynthesis in *L. monocytogenes*.

4.2.3 The role of Vγ9Vδ2 T-cells in bacterial infections and adaptive immunity

Peripheral to this study has been the question of how Vγ9Vδ2 T-cell activation influences the outcome of primary infections, as well as the development of adaptive immunity against a pathogen. Activated Vγ9Vδ2 T-cells can have cytotoxic activity against HMBPP-presenting cells, which conceivably helps limit the spread of bacterial infections. However, it is not clear whether a rapid, innate-like response sacrifices stronger adaptive immunity by limiting antigen production or inhibiting the development of memory T-cells. In a handful of primate studies using *L. monocytogenes* as a vaccine platform, they have observed that reducing HMBPP production by deleting *gcpE* improves protection against *M. tuberculosis.* These studies were conducted using 10403S, and our data suggest that there is a very modest difference in HMBPP production between WT and Δ*gcpE*. Using the discoveries presented here, it would be intriguing to engineer a 10403S strain that produces HMBPP at similar or greater levels as the lineage I strains and examine whether that strain is less effective at inducing immunity than WT 10403S.

Metabolically engineering HMBPP production in *L. monocytogenes* and conducting the necessary studies in primate models would be both technically challenging and expensive. However, in the absence of a reliable humanized mouse model or other model organism with Vγ9Vδ2 T-cells, there are distinct limits on how much we can learn about these cells. Immunologists continue to use mouse models to understand the immune system and they continue to learn greater and greater details about how the mouse immune system works. One wonders though, how the absence of entire cell types will impact our ability to translate basic research discoveries into practical therapies in the future.

4.2.4 Engineering isoprenoid precursor pathways in other bacterial pathogens

In terms of infectious disease prevention, vaccines are the gold standard for both cost efficiency and long-term efficacy. Unfortunately, the past several decades of research have largely failed to yield progress in this area, with the exception of the pneumococcal vaccine. While some of this may be traced to decreased interest or investment in vaccine development, I would question whether our models need to advance to make progress. Decades of work and countless dollars have been spent trying to develop vaccines against *Chlamydia trachomatis* and *Mycobacterium tuberculosis*, without success. Intriguingly, both pathogens have the nonmevalonate pathway, they latently infect a host, and positive results in mice have not translated well into clinical trials.

At the same time as we use *L. monocytogenes* to advance our understanding of Vγ9Vδ2 T-cells, it would be interesting to begin engineering these pathogens so that they do not produce HMBPP. If Vγ9Vδ2 T-cell activation reduces the initial disease severity, but inhibits adaptive immunity, would replacing the nonmevalonate pathway with the mevalonate pathway increase vaccine efficacy? In particular, *M. marinum* is one of the few organisms other than *L. monocytogenes* that has both isoprenoid precursor pathways, so it is conceivable that the mevalonate pathway could be cloned into *M. tuberculosis* or the vaccine strain, Bacillus Calmette-Guérin. This line of questioning also encounters the challenge of adequately modeling Vγ9Vδ2 T-cell functions in the immune system, but the potential benefits derived from improving the *M. tuberculosis* vaccine can hardly be understated.

4.3 Concluding thoughts

There are several broad aspects of the *L. monocytogenes* field that I hope will advance during the next generation of graduate students. Since 2015, an assortment of students and postdocs have made a half-hearted effort to develop CRISPR-based genetic tools in *Listeria*, but no one has ever invested enough time to really get it to work. In addition to the "we should have it because Jennifer Doudna is at Berkeley" angle, it would be a leap forward from our current cloning genetic tools. Not only would CRISPR allow us to perform genetic screens more rapidly, but there are entire categories of genetic mutants that simply cannot be made with allelic exchange. Any strain that has a growth defect is rapidly outcompeted during the cloning process, which makes it very challenging to create mutants that have any sort of a growth defect. In the same vein, it would be extremely valuable to develop transposon sequencing (TnSeq) in *L. monocytogenes*. The value of transposon sequencing is obvious, but similar to our efforts with CRISPR, several lab members have briefly attempted to make it work, without fully committing to the tool-building endeavor.

For this work in particular, I hope that the discoveries presented here will contribute to the broader scientific endeavor. I envisioned 'solving' the mevalonate and nonmevalonate pathway question during my first two years, identifying an HMBPP-responsive cell type in mice the following year, and then spending the rest of my time engineering isoprenoid precursor pathways in *Mycobacterium marinum* and *Mycobacterium tuberculosis* to make a better vaccine strain. This did not happen, but so goes science.

Prior to every lab retreat, Dan has suggested that we play a game of sorts, asking us to envision what our science will look like five, ten, or twenty years into the future. We never have, inevitably sliding into the finest idle chatter over beers on his back patio, so here seems as good a place as any to speculate about the future of this science. Five years from now, in 2024, we will have completely solved the nonmevalonate pathway in *L. monocytogenes*. Whether it requires point mutations in other enzymes, activation of additional regulatory proteins, the bug's inability to synthesize iron-sulfur clusters, or some presently unknown factor, I believe that we will understand *why L. monocytogenes* has both pathways. Ten years from now, in 2029, we will have completed a study using rationally designed bacterial strains in nonhuman primates. The possibility that one of these strains should be tested in primates has been raised from the very beginning of this work, but limited model systems and the sheer cost of nonhuman primate work mean that any study requires a highly coordinated effort to succeed. The study won't necessarily use a *L. monocytogenes* strain, as there is and presumably still will be, far more incentive to improve the BCG vaccine rather than develop a *L. monocytogenes* vaccine from scratch. Twenty years from now, in 2039, what's old is now new. Despite the attempt, and failure, to use *L. monocytogenes* as a personalized immunotherapy platform, aberrant Vγ9Vδ2 T-cell stimulation is the real reason it failed in clinical trials. Having resolved that issue, personalized immunotherapies have become commonplace. Other technological advances mean that a cancer can be sequenced, artificial intelligence identifies a collection of

immunostimulatory epitopes, and an antigen-containing plasmid can be printed, all in the span of a week with little to no human intervention.

In many ways it seems like there are two major categories of scientific projects: ones that pick up a thread and ones that continue pulling on a thread. The Portnoy Lab has been pulling on the thread of *L. monocytogenes* virulence factors for decades, developing tools to understand virulence and revealing the deepest minutiae of ActA and LLO. As scientists in the lab have picked up new threads, it has oftentimes required someone new to follow up on an initial discovery before reaching a major breakthrough. One could argue that the discovery of multidrug resistance transporters (107) was a key piece to help with the identification of c-di-AMP (12), the discovery of STING (108), and much more work on *L. monocytogenes* metabolism (86,109). Similarly, significant effort was required to find that PrfA is activated in a reducing environment (76). The broad conclusion, that *L. monocytogenes* is redox sensitive, was again fundamental to the discovery of a completely novel extracellular electron transport chain in *L. monocytogenes* (79). believe that this work on isoprenoid precursors falls into the first category, as it built upon no more than a handful of published papers. It would be wrong to assume that this work will have a fraction of the impact as the studies mentioned above, but I hope that it will. At last however, my time in the lab is done, so the demonstration of this work's significance will be left as an exercise for the reader.

References

1. Nguyen BN, Peterson BN, Portnoy DA. 2019. Listeriolysin O: A phagosome-specific cytolysin revisited. Cell Microbiol 21, 1–12.
2. Tilney LG, Portnoy DA. 1989. Actin Filaments and the Growth, Movement, and Spread of the Intracellular Bacterial Parsite *Listeria monocytogenes*. J Cell Biol 109, 1597–1608.
3. Portnoy DA, Auerbuch V, Glomski IJ. 2002. The cell biology of *Listeria monocytogenes* infection: The intersection of bacterial pathogenesis and cell-mediated immunity. J Cell Biol 158, 409–414.
4. Vance RE, Isberg RR, Portnoy DA. 2009. Patterns of Pathogenesis: Discrimination of Pathogenic and Nonpathogenic Microbes by the Innate Immune System. Cell Host Microbe 6, 10–21.
5. Portnoy DA, Chen C, Mitchell G. 2016. Strategies Used by Bacteria to Grow in Macrophages. Microbiol Spectr 4, 1–22.
6. Vance RE, Eichberg MJ, Portnoy DA, Raulet DH. 2017. Listening to each other: Infectious disease and cancer immunology. Sci Immunol 2, 1–6.
7. Lombard J, Moreira D. 2011. Origins and early evolution of the mevalonate pathway of isoprenoid biosynthesis in the three domains of life. Mol Biol Evol 28, 87–99.
8. Rohmer M. 2008. From molecular fossils of bacterial hopanoids to the formation of isoprene units: discovery and elucidation of the methylerythritol phosphate pathway. Lipids 43, 1095–1107.
9. Kuzuyama T, Seto H. 2012. Two distinct pathways for essential metabolic precursors for isoprenoid biosynthesis. Proc Japan Acad Ser B 88, 41–52.
10. Heuston S, Begley M, Gahan CGM, Hill C. 2012. Isoprenoid biosynthesis in bacterial pathogens. Microbiology 158, 1389–1401.
11. Ragon M, Wirth T, Hollandt F, Lavenir R, Lecuit M, Monnier A Le, Brisse S. 2008. A new perspective on *Listeria monocytogenes* evolution. PLoS Pathog 4,
12. Woodward JJ, Iavarone AT, Portnoy DA. 2010. c-di-AMP secreted by intracellular *Listeria monocytogenes* activates a host type I interferon response. Science (80-) 328, 1703–1705.
13. Sauer JD, Sotelo-Troha K, Von Moltke J, Monroe KM, Rae CS, Brubaker SW, Hyodo M, Hayakawa Y, Woodward JJ, Portnoy DA, Vance RE. 2011. The N-ethyl-N-nitrosourea-induced Goldenticket mouse mutant reveals an essential function of sting in the in vivo interferon response to *Listeria monocytogenes* and cyclic dinucleotides. Infect Immun 79, 688–694.
14. Archer KA, Durack J, Portnoy DA. 2014. STING-Dependent Type I IFN Production Inhibits Cell-Mediated Immunity to *Listeria monocytogenes*. PLoS Pathog 10, 1–14.
15. Vance RE, Isberg RR, Portnoy DA. 2010. Pathogenic Microbes By the Innate Immune System. Cell 6, 10–21.
16. Godfrey DI, Koay H-F, McCluskey J, Gherardin NA. 2019. The biology and functional importance of MAIT cells. Nat Immunol 20, 1110–1128.
17. Whiteley AT, Eaglesham JB, de Oliveira Mann CC, Morehouse BR, Lowey B, Nieminen EA, Danilchanka O, King DS, Lee ASY, Mekalanos JJ, Kranzusch PJ. 2019. Bacterial cGAS-like enzymes synthesize diverse nucleotide signals. Nature

567, 194–199.
18. Kazen AR, Adams EJ. 2011. Evolution of the V, D, and J gene segments used in the primate gammadelta T-cell receptor reveals a dichotomy of conservation and diversity. Proc Natl Acad Sci 108, E332-40.
19. Sandstrom A, Peigné CM, Léger A, Crooks J, Konczak F, Gesnel MC, Breathnach R, Bonneville M, Scotet E, Adams EJ. 2014. The intracellular B30.2 domain of butyrophilin 3A1 binds phosphoantigens to mediate activation of human Vγ9Vδ2T Cells. Immunity 40, 490–500.
20. Gu S, Nawrocka W, Adams EJ. 2015. Sensing of pyrophosphate metabolites by Vγ9Vγ2 T cells. Front Immunol 6, 1–10.
21. Hayday AC. 2009. γδ T Cells and the Lymphoid Stress-Surveillance Response. Immunity 31, 184–196.
22. Bonneville M, O'Brien RL, Born WK. 2010. Gammadelta T cell effector functions: a blend of innate programming and acquired plasticity. Nat Rev Immunol 10, 467–78.
23. Adams EJ, Gu S, Luoma AM. 2015. Human gamma delta T cells: Evolution and ligand recognition. Cell Immunol 296, 31–40.
24. Gentles AJ, Newman AM, Liu CL, Bratman S V., Feng W, Kim D, Nair VS, Xu Y, Khuong A, Hoang CD, Diehn M, West RB, Plevritis SK, Alizadeh AA. 2015. The prognostic landscape of genes and infiltrating immune cells across human cancers. Nat Med 21, 938–945.
25. Karunakaran MM, Herrmann T. 2014. The Vγ9Vδ2 T cell antigen receptor and butyrophilin-3 A1: Models of interaction, the possibility of co-evolution, and the case of dendritic epidermal T cells. Front Immunol 5, 1–13.
26. Tyler CJ, Doherty DG, Moser B, Eberl M. 2015. Human Vγ9/Vδ2 T cells: Innate adaptors of the immune system. Cell Immunol 296, 10–21.
27. Willcox BE, Willcox CR. 2019. γδ TCR ligands: the quest to solve a 500-million-year-old mystery. Nat Immunol 20, 121–128.
28. Yan L, Qiu J, Chen J, Ryan-Payseur B, Huang D, Wang Y, Rong L, Melton-Witt JA, Freitag NE, Chen ZW. 2008. Selected *prfA** mutations in recombinant attenuated *Listeria monocytogenes* strains augment expression of foreign immunogens and enhance vaccine-elicited humoral and cellular immune responses. Infect Immun 76, 3439–3450.
29. Ryan-Payseur B, Frencher J, Shen L, Chen CY, Huang D, Chen ZW. 2012. Multieffector-Functional Immune Responses of HMBPP-Specific Vγ2Vδ2 T Cells in Nonhuman Primates Inoculated with *Listeria monocytogenes ΔactA prfA**. J Immunol 189, 1285–1293.
30. Frencher JT, Shen H, Yan L, Wilson JO, Freitag NE, Rizzo N, Chen CY, Chen ZW, Rizzo AN, Chen CY, Chen ZW. 2014. HMBPP-deficient *Listeria* mutant immunization alters pulmonary/systemic responses, effector functions, and memory polarization of Vγ2Vδ2 T cells. J Leukoc Biol 96, 957–967.
31. Qaqish A, Huang D, Chen CY, Zhang Z, Wang R, Yang E, Yang L, Larsen MH, Jr WRJ, Qian L, Frencher J, Shen L, Chen ZW. 2017. Adoptive transfer of phosphoantigen-specific γδ T-cell subset attenuates *Mycobacterium tuberculosis* infection in nonhuman primates. J Immunol 198, 4753–4763.
32. Shen L, Frencher J, Huang D, Wang W, Yang E, Chen CY, Zhang Z. 2019.

Immunization of Vγ2Vδ2 T cells programs sustained effector memory responses that control tuberculosis in nonhuman primates. 116, 1–8.
33. Flickinger J, Rodeck U, Snook A. 2018. *Listeria monocytogenes* as a Vector for Cancer Immunotherapy: Current Understanding and Progress. Vaccines 6, 48.
34. Ahyong V, Berdan CA, Nomura DK, Welch MD. 2019. A metabolic dependency for host isoprenoids in the obligate intracellular pathogen *Rickettsia parkeri* underlies a sensitivity for the statin class of host-targeted therapeutics. BioRxiv Available from: https://doi.org/10.1101/528018.
35. Begley M, Bron PA, Heuston S, Casey PG, Englert N, Wiesner J, Jomaa H, Gahan CGM, Hill C. 2008. Analysis of the isoprenoid biosynthesis pathways in *Listeria monocytogenes* reveals a role for the alternative 2-C-methyl-D-erythritol 4-phosphate pathway in murine infection. Infect Immun 76, 5392–5401.
36. Heuston S, Begley M, Davey MS, Eberl M, Casey PG, Hill C, Gahan CGM. 2012. HmgR, a key enzyme in the mevalonate pathway for isoprenoid biosynthesis, is essential for growth of *Listeria monocytogenes* EGDe. Microbiology 158, 1684–93.
37. Boutin L, Scotet E. 2018. Towards deciphering the hidden mechanisms that contribute to the antigenic activation process of human Vγ9Vδ2 T cells. Front Immunol 9, 1–9.
38. den Bakker HC, Desjardins CA, Griggs AD, Peters JE, Zeng Q, Young SK, Kodira CD, Yandava C, Hepburn TA, Haas BJ, Birren BW, Wiedmann M. 2013. Evolutionary Dynamics of the Accessory Genome of *Listeria monocytogenes*. 8,
39. Aureli P, Fiorucci GC, Caroli D, Marchiaro G, Novara O, Leone L, Salmaso S. 2000. An outbreak of febrile gastroenteritis associated with corn contaminated by *Listeria monocytogenes*. N Engl J Med 342, 1236–41.
40. Maury MM, Tsai YH, Charlier C, Touchon M, Chenal-Francisque V, Leclercq A, Criscuolo A, Gaultier C, Roussel S, Brisabois A, Disson O, Rocha EPC, Brisse S, Lecuit M. 2016. Uncovering *Listeria monocytogenes* hypervirulence by harnessing its biodiversity. Nat Genet 48, 308–313.
41. Adam P, Hecht S, Eisenreich W, Kaiser J, Grawert T, Arigoni D, Bacher A, Rohdich F. 2002. Biosynthesis of terpenes: studies on 1-hydroxy-2-methyl-2-(E)-butenyl 4-diphosphate reductase. Proc Natl Acad Sci U S A 99, 12108–12113.
42. Wolff M, Seemann M, Grosdemange-Billiard C, Tritsch D, Campos N, Rodríguez-Concepción M, Boronat A, Rohmer M. 2002. Isoprenoid biosynthesis via the methylerythritol phosphate pathway. (E)-4-Hydroxy-3-methylbut-2-enyl diphosphate: chemical synthesis and formation from methylerythritol cyclodiphosphate by a cell-free system from *Escherichia coli*. Tetrahedron Lett 43, 2555–2559.
43. Flint DH, Tuminello JF, Emptage MH. 1993. The inactivation of Fe-S cluster containing hydro-lyases by superoxide. J Biol Chem 268, 22369–22376.
44. Rivasseau C, Seemann M, Boisson A-M, Streb P, Gout E, Douce R, Rohmer M, Bligny R. 2009. Accumulation of 2-C-methyl-D-erythritol 2,4-cyclodiphosphate in illuminated plant leaves at supraoptimal temperatures reveals a bottleneck of the prokaryotic methylerythritol 4-phosphate pathway of isoprenoid biosynthesis. Plant Cell Environ 32, 82–92.
45. Artsatbanov VY, Vostroknutova GN, Shleeva MO, Goncharenko A V, Zinin AI,

Ostrovsky DN, Kapreliants AS. 2012. Influence of oxidative and nitrosative stress on accumulation of diphosphate intermediates of the non-mevalonate pathway of isoprenoid biosynthesis in corynebacteria and mycobacteria. Biochem 77, 362–371.
46. Martien JI, Hebert AS, Stevenson DM, Regner MR, Khana DB, Coon JJ, Amador-Noguez D. 2019. Systems-Level Analysis of Oxygen Exposure in *Zymomonas mobilis*: Implications for Isoprenoid Production. mSystems 4, 1–23.
47. Begley M, Gahan CGM, Kollas AK, Hintz M, Hill C, Jomaa H, Eberl M. 2004. The interplay between classical and alternative isoprenoid biosynthesis controls γδ T cell bioactivity of *Listeria monocytogenes*. FEBS Lett 561, 99–104.
48. Hardy J, Margolis JJ, Contag CH. 2006. Induced biliary excretion of *Listeria monocytogenes*. Infect Immun 74, 1819–1827.
49. Melton-Witt JA, Rafelski SM, Portnoy DA, Bakardjiev AI. 2012. Oral infection with signature-tagged *Listeria monocytogenes* reveals organ-specific growth and dissemination routes in guinea pigs. Infect Immun 80, 720–732.
50. Zhang T, Abel S, Abel zur Wiesch P, Sasabe J, Davis BM, Higgins DE, Waldor MK. 2017. Deciphering the landscape of host barriers to *Listeria monocytogenes* infection. Proc Natl Acad Sci 114, 6334–6339.
51. Camilli A, Portnoy DA, Youngman P. 1990. Insertional Mutagenesis of *Listeria monocytogenes* with a Novel Tn*917* Derivative That Allows Direct Cloning of DNA Flanking Transposon Insertions. J Bacteriol 172, 3738–3744.
52. Becattini S, Littmann ER, Carter RA, Kim SG, Morjaria SM, Ling L, Gyaltshen Y, Fontana E, Taur Y, Leiner IM, Pamer EG. 2017. Commensal microbes provide first line defense against *Listeria monocytogenes* infection. J Exp Med 214, 1973–1989.
53. Müller-Herbst S, Wüstner S, Mühlig A, Eder D, M Fuchs T, Held C, Ehrenreich A, Scherer S, Fuchs TM, Held C, Ehrenreich A, Scherer S. 2014. Identification of genes essential for anaerobic growth of *Listeria monocytogenes*. Microbiology 160, 752–765.
54. Romick TL, Fleming HP, McFeeters RF. 1996. Aerobic and anaerobic metabolism of *Listeria monocytogenes* in defined glucose medium. Appl Environ Microbiol 62, 304–307.
55. Imlay JA. 2006. Iron-sulphur clusters and the problem with oxygen. Mol Microbiol 59, 1073–1082.
56. Johnson DC, Dean DR, Smith AD, Johnson MK. 2005. Structure, Function, and Formation of Biological Iron-Sulfur Clusters. Annu Rev Biochem 74, 247–281.
57. Jang S, Imlay JA. 2010. Hydrogen peroxide inactivates the *Escherichia coli* Isc iron-sulphur assembly system, and OxyR induces the Suf system to compensate. Mol Microbiol 78, 1448–1467.
58. Outten FW, Djaman O, Storz G. 2004. A suf operon requirement for Fe-S cluster assembly during iron starvation in *Escherichia coli*. Mol Microbiol 52, 861–872.
59. Tanaka N, Kanazawa M, Tonosaki K, Yokoyama N, Kuzuyama T, Takahashi Y. 2016. Novel features of the ISC machinery revealed by characterization of *Escherichia coli* mutants that survive without iron-sulfur clusters. Mol Microbiol 99, 835–848.
60. Yokoyama N, Nonaka C, Ohashi Y, Shioda M, Terahata T, Chen W, Sakamoto K,

Maruyama C, Saito T, Yuda E, Tanaka N, Fujishiro T, Kuzuyama T, Asai K, Takahashi Y. 2018. Distinct roles for U-type proteins in iron–sulfur cluster biosynthesis revealed by genetic analysis of the *Bacillus subtilis sufCDSUB* operon. Mol Microbiol 107, 688–703.
61. Lee M, Gräwert T, Quitterer F, Rohdich F, Eppinger J, Eisenreich W, Bacher A, Groll M. 2010. Biosynthesis of isoprenoids: crystal structure of the [4Fe-4S] cluster protein IspG. J Mol Biol 404, 600–610.
62. Quitterer F, Frank A, Wang K, Rao G, O'Dowd B, Li J, Guerra F, Abdel-Azeim S, Bacher A, Eppinger J, Oldfield E, Groll M. 2015. Atomic-Resolution Structures of Discrete Stages on the Reaction Coordinate of the [Fe4S4] Enzyme IspG (GcpE). J Mol Biol 427, 2220–2228.
63. Rekittke I, Jomaa H, Ermler U. 2012. Structure of the GcpE (IspG)-MEcPP complex from *Thermus thermophilus*. FEBS Lett 586, 3452–3457.
64. Rekittke I, Nonaka T, Wiesner J, Demmer U, Warkentin E, Jomaa H, Ermler U. 2011. Structure of the E-1-hydroxy-2-methyl-but-2-enyl-4-diphosphate synthase (GcpE) from *Thermus thermophilus*. FEBS Lett 585, 447–451.
65. Zhao L, Chang W-C, Xiao Y, Liu H-W, Liu P. 2013. Methylerythritol phosphate pathway of isoprenoid biosynthesis. Annu Rev Biochem 82, 497–530.
66. Qiu J, Yan L, Chen J, Chen CY, Shen L, Letvin NL, Haynes BF, Freitag N, Rong L, Frencher JT, Huang D, Wang X, Chen ZW. 2011. Intranasal vaccination with the recombinant *Listeria monocytogenes ΔactA prfA** mutant elicits robust systemic and pulmonary cellular responses and secretory mucosal IgA. Clin Vaccine Immunol 18, 640–646.
67. Shen H, Wang Y, Chen CY, Frencher J, Huang D, Yang E, Ryan-Payseur B, Chen ZW. 2015. Th17-related cytokines contribute to recall-like expansion/effector function of HMBPP-specific Vγ2Vδ2 T cells after *Mycobacterium tuberculosis* infection or vaccination. Eur J Immunol 45, 442–451.
68. Shen L, Frencher J, Huang D, Wang W, Yang E, Chen CY, Zhang Z, Wang R, Qaqish A, Larsen MH, Shen H, Porcelli SA, Jacobs WR, Chen ZW. 2019. Immunization of Vγ2Vδ2 T cells programs sustained effector memory responses that control tuberculosis in nonhuman primates. Proc Natl Acad Sci 116, 6371–6378.
69. Hoeres T, Smetak M, Pretscher D, Wilhelm M. 2018. Improving the efficiency of Vγ9Vδ2 T-cell immunotherapy in cancer. Front Immunol 9, 1–18.
70. Gray MJ, Zadoks RN, Fortes ED, Dogan B, Cai S, Chen Y, Scott VN, Gombas DE, Boor KJ, Wiedmann M. 2004. *Listeria monocytogenes* Isolates from Foods and Humans Form Distinct but Overlapping Populations. 70, 5833–5841.
71. McCarthy NE, Eberl M. 2018. Human γδ T-cell control of mucosal immunity and inflammation. Front Immunol 9, 985.
72. Stinear TP *et al.* 2008. Insights from the complete genome sequence of *Mycobacterium marinum* on the evolution of *Mycobacterium tuberculosis*. Genome Res 18, 729–741.
73. Dairi T. 2005. Studies on biosynthetic genes and enzymes of isoprenoids produced by actinomycetes. Jpn J Antibiot 58, 87–98.
74. Smith K, Youngman P. 1992. Use of a new integrational vector to investigate compartment-specific expression of the *Bacillus subtilis spollM* gene. Biochimie

74, 705–711.
75. Kelley LA, Mezulis S, Yates CM, Wass MN, Sternberg MJE. 2015. The Phyre2 web portal for protein modeling, prediction and analysis. Nat Protoc 10, 845–858.
76. Portman JL, Dubensky SB, Peterson BN, Whiteley AT, Portnoy DA. 2017. Activation of the *Listeria monocytogenes* Virulence Program by a Reducing Environment. MBio 8, e01595-17.
77. Auerbuch V, Lenz LL, Portnoy DA. 2001. Development of a competitive index assay to evaluate the virulence of *Listeria monocytogenes actA* mutants during primary and secondary infection of mice. Infect Immun 69, 5953–5957.
78. Bou Ghanem EN, Jones GS, Myers-Morales T, Patil PD, Hidayatullah AN, D'Orazio SEF. 2012. InlA promotes dissemination of *Listeria monocytogenes* to the mesenteric lymph nodes during food borne infection of mice. PLoS Pathog 8, e1003015.
79. Light SH, Su L, Rivera-Lugo R, Cornejo JA, Louie A, Iavarone AT, Ajo-Franklin CM, Portnoy DA. 2018. A flavin-based extracellular electron transfer mechanism in diverse Gram-positive bacteria. Nature 562, 140–144.
80. Lachica R V. 1990. Selective plating medium for quantitative recovery of food-borne *Listeria monocytogenes*. Appl Environ Microbiol 56, 167–169.
81. Letunic I, Bork P. 2019. Interactive Tree Of Life (iTOL) v4: recent updates and new developments. Nucleic Acids Res 47, W256–W259.
82. Bécavin C *et al.* 2014. Comparison of widely used *Listeria monocytogenes* strains EGD, 10403S, and EGD-e highlights genomic variations underlying differences in pathogenicity. MBio 5, e00969-14.
83. Den Bakker HC, Desjardins CA, Griggs AD, Peters JE, Zeng Q, Young SK, Kodira CD, Yandava C, Hepburn TA, Haas BJ, Birren BW, Wiedmann M. 2013. Evolutionary Dynamics of the Accessory Genome of *Listeria monocytogenes*. PLoS One 8, e67511.
84. Simon R, Priefer U, Pühler A. 1983. A Broad Host Range Mobilization System for In Vivo Genetic Engineering: Transposon Mutagenesis in Gram Negative Bacteria. Biotechnology 1, 784–791.
85. Camilli A, Tilney LG, Portnoy DA. 1993. Dual roles of *plcA* in *Listeria monocytogenes* pathogenesis. Mol Microbiol 8, 143–157.
86. Whiteley AT, Pollock AJ, Portnoy DA, Whiteley AT, Pollock AJ, Portnoy DA. 2015. The PAMP c-di-AMP Is Essential for *Listeria monocytogenes* Growth in Rich but Not Minimal Media due to a Toxic Increase in (p)ppGpp. Cell Host Microbe 17, 788–798.
87. Laub MT, Goulian M. 2007. Specificity in Two-Component Signal Transduction Pathways. Annu Rev Genet 41, 121–145.
88. Cotter PD, Emerson N, Gahan CG, Hill C. 1999. Identification and Disruption of lisRK, a Genetic Locus Encoding a Two-Component Signal Transduction System Involved in Stress Tolerance and Virulence in *Listeria monocytogenes*. J Bacteriol 181, 6840.
89. Sleator RD, Hill C. 2005. A novel role for the LisRK two-component regulatory system in listerial osmotolerance. Clin Microbiol Infect 11, 599–601.
90. Nielsen PK, Andersen AZ, Mols M, van der Veen S, Abee T, Kallipolitis BH. 2012. Genome-wide transcriptional profiling of the cell envelope stress response and

the role of LisRK and CesRK in *Listeria monocytogenes*. Microbiology 158, 963–974.
91. Glaser P *et al.* 2001. Comparative genomics of *Listeria* species. Science (80-) 294, 849–852.
92. Stack HM, Sleator RD, Bowers M, Hill C, Gahan CGM. 2005. Role for HtrA in stress induction and virulence potential in *Listeria monocytogenes*. Appl Environ Microbiol 71, 4241–4247.
93. dos Santos PT, Menendez-Gil P, Sabharwal D, Christensen JH, Brunhede MZ, Lillebæk EMS, Kallipolitis BH. 2018. The small regulatory RNAs LhrC1-5 contribute to the response of *Listeria monocytogenes* to heme toxicity. Front Microbiol 9, 1–16.
94. Sievers S, Lillebaek EMS, Jacobsen K, Lund A, Mollerup MS, Nielsen PK, Kallipolitis BH. 2014. A multicopy sRNA of *Listeria monocytogenes* regulates expression of the virulence adhesin LapB. Nucleic Acids Res 42, 9383–9398.
95. Kock H, Gerth U, Hecker M. 2004. MurAA, catalysing the first committed step in peptidoglycan biosynthesis, is a target of Clp-dependent proteolysis in *Bacillus subtilis*. Mol Microbiol 51, 1087–1102.
96. Rismondo J, Bender JK, Halbedel S. 2017. Suppressor Mutations Linking gpsB with the First Committed Step of Peptidoglycan Biosynthesis in *Listeria monocytogenes*. 199, 1–16.
97. Carroll SA, Josep SW, Hain T, Technow U, Darji A, Pashalidis P, Chakraborty T. 2003. Identification and Characterization of a Peptidoglycan Hydrolase, MurA, of *Listeria monocytogenes*, a Muramidase Needed for Cell Separation. J Bacteriol 185, 6801–6808.
98. Zemansky J, Kline BC, Woodward JJ, Leber JH, Marquis HH, Portnoy DA. 2009. Development of a mariner-based transposon and identification of *Listeria monocytogenes* determinants, including the peptidyl-prolyl isomerase PrsA2, that contribute to its hemolytic phenotype. J Bacteriol 191, 3950–3964.
99. Hodgson DA. 2000. Generalized transduction of serotype 1/2 and serotype 4b strains of *Listeria monocytogenes*. Mol Microbiol 35, 312–323.
100. Sauer JD, Witte CE, Zemansky J, Hanson B, Lauer P, Portnoy DA. 2010. *Listeria monocytogenes* triggers AIM2-mediated pyroptosis upon infrequent bacteriolysis in the macrophage cytosol. Cell Host Microbe 7, 412–419.
101. Sauer J, Pereyre S, Archer K, Burke T, Hanson B, Lauer P, Portnoy D. 2011. *Listeria monocytogenes* engineered to activate the Nlrc4 inflammasome are severely attenuated and are poor inducers of protective immunity. Proc Natl Acad Sci U S A 108, 12419–12424.
102. Portnoy DA, Jacks PS, Hinrichs DJ. 1988. Role of hemolysin for the intracellular growth of *Listeria monocytogenes*. J Exp Med 167, 1459–1471.
103. Reniere ML, Whiteley AT, Hamilton KL, John SM, Lauer P, Brennan RG, Portnoy DA. 2015. Glutathione activates virulence gene expression of an intracellular pathogen. Nature 517, 170–173.
104. Kohler S, Bubert A, Vogel M, Goebel W. 1991. Expression of the *iap* gene coding for protein p60 of *Listeria monocytogenes* is controlled on the posttranscriptional level. J Bacteriol 173, 4668–4674.
105. Miller HK, Auerbuch V. 2015. Bacterial iron-sulfur cluster sensors in mammalian

pathogens. Metallomics 7, 943–956.
106. Rocha AG, Dancis A. 2016. Life without Fe-S clusters. Mol Microbiol 99, 821–826.
107. Crimmins GT, Herskovits AA, Rehder K, Sivick KE, Lauer P, Dubensky Jr. TW, Portnoy DA. 2008. *Listeria monocytogenes* multidrug resistance transporters activate a cytosolic surveillance pathway of innate immunity. Proc Natl Acad Sci U S A 105, 10191–10196.
108. Burdette DL, Monroe KM, Sotelo-Troha K, Iwig JS, Eckert B, Hyodo M, Hayakawa Y, Vance RE. 2011. STING is a direct innate immune sensor of cyclic di-GMP. Nature 478, 515–518.
109. Whiteley AT, Garelis NE, Peterson BN, Choi PH, Tong L, Woodward JJ, Portnoy DA. 2017. c-di-AMP modulates *Listeria monocytogenes* central metabolism to regulate growth, antibiotic resistance and osmoregulation. Mol Microbiol 104, 212–233.

Supplemental Materials

Supplementary Table 1: Full strain catalog

	Organism	Genomic Alteration	Plasmid Details	Plasmid Backbone	Notes
EDL001	L. monocytogenes	WT 10403S			WT strain obtained from AW (probably AW106, DP-L6253)
EDL002	L. monocytogenes	ΔactAΔinlBΔlytB			Obtained from Aduro
EDL003	E. coli (XL1 Blue)	pKSV7oriT-lytB	pKSV7, unaltered	pKSV7	Obtained from Aduro (pBHE3404), plated on Lb-Carb?
EDL004	E. coli (XL1 Blue)	pKSV7oriT-gcpE	pKSV7, unaltered	pKSV7	Obtained from Aduro (pBHE3379), plated on Lb-Carb?
EDL005	L. monocytogenes	ΔactAΔinlBΔgcpE			Obtained from Aduro
EDL006	L. monocytogenes	ΔactAΔinlB			Lab stock: DP-L6054
EDL007	E. coli (SM10)	pKSV7oriT	pKSV7, unaltered	pKSV7	
EDL008	E. coli (SM10)	pKSV7oriT-ΔlytB	pKSV7, unaltered	pKSV7	In-frame, allelic exchange
EDL009	E. coli (SM10)	pKSV7oriT-ΔgcpE	pKSV7, unaltered	pKSV7	In-frame, allelic exchange
EDL010	E. coli (SM10)	pKSV7oriT-ΔhmgR	pKSV7, unaltered	pKSV7	In-frame, allelic exchange
EDL011	L. monocytogenes	ΔgcpE			
EDL012	L. monocytogenes	ΔlytB			
EDL013	L. monocytogenes	ΔhmgR			Add 250 µM /1 mM mevalonate to media
EDL014	L. monocytogenes	ΔactAΔlytB			
EDL015	L. monocytogenes	ΔactAΔgcpE			
EDL016	L. monocytogenes	ΔactAΔhmgR			Add 250 µM /1 mM mevalonate to media
EDL017	L. monocytogenes	ΔhmgRΔgcpE			Add 250 µM /1 mM mevalonate to media
EDL018	L. monocytogenes	ΔhmgRΔlytB			Add 250 µM /1 mM mevalonate to media
EDL019	L. monocytogenes	None		Unknown	DP-L3903, JP075
EDL020	L. monocytogenes	ΔhmgR		pPL2x	
EDL021	E. coli (SM10)	pPL2x-MEVk	Lmo0010-0012	pPL2x	Contains Lmo0010-Lmo0012
EDL022	E. coli (SM10)	pKSV7-MEVk	Lmo0010-0012	pKSV7	Contains Lmo0010-Lmo0012
EDL023	E. Coli (XL1 Blue)			pPL2x	Use EDL032 for Toxin/Antitoxin in plasmid
EDL024	E. coli (SM10)	pPL2x-hmgR	hmgR	pPL2x	Complements ΔhmgR/lmo0825
EDL025	L. monocytogenes (clinical isolate)				Clinical isolate FSL N1-017, PL300 from Pete
EDL026	L. monocytogenes (clinical isolate)				Clinical isolate HPB2262, PL309/Aureli 1997 from Pete
EDL027	L. monocytogenes	ΔprfA			Obtained from MLR
EDL028	L. monocytogenes	prfA*			Obtained from MLR
EDL029	L. monocytogenes	prfA*ΔhmgR			Add 250 µM /1 mM mevalonate to media
EDL030	L. monocytogenes	ΔprfAΔhmgR	None	None	Add 250 µM /1 mM mevalonate to media
EDL031	L. monocytogenes	ΔhmgR	pPL2x-hmgR	pPL2x	ΔhmgR complemented with pPL2x
EDL032	E. coli (DB3.1)	None	None	pPL2x	AW616
EDL033	E. coli (DB3.1)	None	None	pKSV7x	AW644
EDL034	E. coli (SM10)	pPL2x-lytB (B. subtilis)		pPL2x	lytB from B. subtilis to complement nonmevalonate pathway
EDL035	L. monocytogenes	ΔhmgRΔlytB	pPL2x-lytB (B. subtilis)	pPL2x	lytB from B. subtilis to complement nonmevalonate pathway
EDL036	B. subtilis 168				From AW373, dies at 4ºC
EDL037	L. monocytogenes	ΔactA			
EDL038	L. monocytogenes	ΔhmgR (FSL N1-017)			Clinical isolate FSL N1-017 with hmgR deleted, not Strep resistant
EDL039	L. monocytogenes	C484A (LLO)			DP-L4351 from JP11

EDL040	L. monocytogenes	L461T (LLO)			DP-L4017
EDL041	L. monocytogenes	ΔhlyΔ			DP-L2161
EDL042	L. monocytogenes	ΔhlyΔplcAΔplcB			DP-L2319
EDL043	L. monocytogenes	ΔactA L461T (LLO)			DP-L4038
EDL044	L. monocytogenes	holin/lysin			DP-L5750
EDL045	L. monocytogenes	ΔhmgR			Suppressor #1 selected in anaerobic BHI broth, AW002A; lisK* 826G>A
EDL046	L. monocytogenes	ΔhmgR			Suppressor #2 selected in anaerobic BHI broth, AW002B
EDL047	L. monocytogenes	ΔhmgR			Suppressor #3 selected in anaerobic BHI broth, AW002C; lisK* 778T>G
EDL048	L. monocytogenes	ΔhmgR			Suppressor #4 selected in anaerobic BHI broth, AW002D; lisK* 106A>G
EDL049	L. monocytogenes	ΔhmgR			Suppressor #5 selected in anaerobic BHI broth, AW002E
EDL050	L. monocytogenes	ΔhmgR			Suppressor #6 selected in anaerobic BHI broth, AW002F, frameshift in lmo1505
EDL051	E. coli (SM10)	pPL2x-lytB (FSL)		pPL2x	lytB from clinical isolate FSL N1-017
EDL052	L. monocytogenes	ΔhmgRΔlytB	pPL2x-lytB (FSL)		lytB from clinical isolate FSL N1-017
EDL053	L. monocytogenes WSLC 1001	None			Potentially phage P40 sensitive, DP-L3671
EDL054	L. ivanovii WSLC 3009	None			Potentially phage P40 sensitive, DP-L393
EDL055	E. coli (XL1 Blue?)	None	None	pJZ037	Adapted from pKSV7 and contains a transposase for generating *Lmo* transposon libraries
EDL056	L. monocytogenes	ErmR::Tn917			Erm Resistance transposon, DP-L3903
EDL057	L. monocytogenes				Mack (derived from EGD), DP-L861
EDL058	L. monocytogenes	WT_pTBL1 menB::himar1			JP126, WT_pTBL1 Mutant with Himar1 in lmo1673 (Raw Screen Hit)(Seq JPS555)
EDL059	L. monocytogenes	WT_pTBL1 cydA::himar1			JP127, WT_pTBL1 Mutant with Himar1 in lmo2718 (Raw Screen Hit)(Seq JPS556)
EDL060	L. monocytogenes	WT_pTBL1 lmo1930::himar1			JP128, WT_pTBL1 Mutant with Himar1 in lmo1930 (Raw Screen Hit)(Seq JPS557)
EDL061	L. monocytogenes	WT_pTBL1 cydB::himar1			JP129, WT_pTBL1 Mutant with Himar1 in lmo2717 (Raw Screen Hit)(Seq JPS558)
EDL062	L. monocytogenes	WT_pTBL1 mutS::himar1			JP130, WT_pTBL1 Mutant with Himar1 in lmo1403 (Raw Screen Hit)(Seq JPS560)
EDL063	L. monocytogenes	WT_pTBL1 hemL::himar1			JP131, WT_pTBL1 Mutant with Himar1 in lmo1553 (Raw Screen Hit)(Seq JPS564)
EDL064	E. coli (SM10)	pKSV7-lisK			Two component system hit with suppressor analysis in ΔhmgR; 6 starting, 6 ending amino acids
EDL065	L. monocytogenes	ΔgcpE, ErmR::Tn917			Erm resistant transposon from DP-L3903
EDL066	L. monocytogenes	ΔlytB, ErmR::Tn917			Erm resistant transposon from DP-L3903
EDL067	L. monocytogenes	ΔhmgR, ErmR::Tn917			Erm resistant transposon from DP-L3903
EDL068	E. coli (SM10)				KanR cassette replacing hmgR
EDL069	L. monocytogenes				DP-L5480
EDL070	L. monocytogenes				DP-L5481
EDL071	L. monocytogenes				DP-L5482
EDL072	L. monocytogenes				DP-L5483
EDL073	L. monocytogenes				DP-L5484
EDL074	L. monocytogenes	ΔlisK			6 starting + 6 ending amino acids, gene mutated in ΔhmgR suppressors

EDL075	L. monocytogenes	ΔhmgR ΔlisK			In-frame deletion of *hmgR* and *lisK* using pKSV7
EDL076	L. monocytogenes	ΔhmgR::KanR			In-frame replacement of *hmgR* with a Kanamycin resistance cassette
EDL077	L. monocytogenes	ΔmdrT			DP-L5446
EDL078	L. monocytogenes	ΔhmgR			Contains 826G>A in lisK and himar1 transposon at lmo1389 from TAP47 (phage lysate generated from RelAPQ background)
EDL079	L. monocytogenes	ΔhmgR			Contains 778T>G in lisK and himar1 transposon at lmo1389 from TAP47 (phage lysate generated from RelAPQ background)
EDL080	L. monocytogenes	ΔhmgR			Contains 106A>G in lisK and himar1 transposon at lmo1389 from TAP47 (phage lysate generated from RelAPQ background)
EDL081	L. monocytogenes	ΔhmgR ΔlisK	pPL3-mCherry		mCherry driven by pHyper on pPL2
EDL082	L. monocytogenes	None	pPL3-mCherry		mCherry driven by pHyper on pPL2
EDL083	L. monocytogenes	ΔhmgR lisK*1			Rederived lisK 826G>A mutation using lysate from EDL078, ΔhmgR lisK*1
EDL084	L. monocytogenes	ΔhmgR lisK*2			Rederived lisK 778T>G mutation using lysate from EDL079, ΔhmgR lisK*3
EDL085	L. monocytogenes	ΔhmgR lisK*3			Rederived lisK 106A>G mutation using lysate from EDL080, ΔhmgR lisk*4
EDL086	E. coli		pJZ037		MISLABELED IN STRAIN BOX, use for making transposon libraries in L. monocytogenes
EDL087	L. monocytogenes	ΔhmgR, LacZ-Tn917			ΔhmgR parent strain containing Tn917 containing LacZ gene, use to screen for WT mutants that don't complement hmgR growth
EDL088	E. coli (SM10)		pPL2x-Phyper-lisK		pPL2x containing lisK and Phyper promoter
EDL089	L. monocytogenes	ΔhmgR ΔlisK	pPL2x-Phyper-lisK		Complemented without the upstream RBS or downstream terminator, does not look like complementation by anaerobic growth
EDL090	E. coli (SM10)		pKSV7x-lisRK		Deletes both components of LisRK
EDL091	E. coli (SM10)		pPL2x-lisRK		Complements lisRK with the upstream RBS and downstream terminator
EDL092	L. monocytogenes	ΔhmgR ΔlisK	pPL2x-lisRK		lisRK complemented with the upstream RBS and downstream terminator, in a Δ*hmgR*Δ*lisK* background (should redo in Δ*lisRK*)
EDL093	L. monocytogenes	ΔlisRK			In-frame deletion of TCS lisRK using allelic exchange
EDL094	L. monocytogenes	ΔhmgR clpC::himar1			Transposon obtained from SL reducing agent screen using himar1
EDL095	E. coli (SM10)		pPL2x-Phyper-lisR	pPL2x	Overexpresses lisR to (hopefully) phenocopy constitutive activation of lisK
EDL096	L. monocytogenes		pPL2x-Phyper-lisR	pPL2x	Overexpresses lisR to (hopefully) phenocopy constitutive activation of lisK
EDL097	L. monocytogenes	ΔhmgR	pPL2x-Phyper-lisR	pPL2x	Overexpresses lisR to (hopefully) phenocopy constitutive activation of lisK
EDL098	E. coli (SM10)		pKSV7x-dxr-His	pKSV7x	Includes dxr gene, His tag, 1000bp after gene
EDL099	L. monocytogenes	lmo0013::himar1			quinol oxidase polypeptide II, rederived transposon (1-34) from screen hit done by VED, overexpressed in 4b serotypes extracellularly
EDL100	L. monocytogenes	lmo2529::himar1			ATPsynthase F1 beta subunit, rederived transposon (2-37?) from screen hit done by VED, growth defect in BHI
EDL101	L. monocytogenes	lmo0014::himar1			cytochrome aa3 quinol oxidase subunit I, rederived transposon (2-49) from screen hit done by VED

EDL102	L. monocytogenes	lmo0031::himar1			LacI family transcriptional regulator, rederived transposon (2-33) from screen hit done by VED
EDL103	L. monocytogenes	lmo1293::himar1			glycerol-3-phosphate dehydrogenase, rederived transposon (2-39) from screen hit done by VED
EDL104	L. monocytogenes	lmo2532::himar1			ATP synthase F1 subunit delta, rederived transposon (2-47) from screen hit done by VED, growth defect in BHI
EDL105	L. monocytogenes	lmo0401::himar1			alpha-mannosidase, rederived transposon (2-69) from screen hit done by VED
EDL106	L. monocytogenes	lmo0015::himar1			cytochrome aa3 quinol oxidase subunit III, rederived transposon (2-41) from screen hit done by VED
EDL107	L. monocytogenes	lmo1389::himar1			Contains himar1 transposon at lmo1389 from TAP47 (phage lysate generated from EDL083 background)
EDL108	L. monocytogenes	lisK 826G>A, lmo1389::himar1			Contains 826G>A in lisK and himar1 transposon at lmo1389 from TAP47 (phage lysate generated from EDL083 background)
EDL109	L. monocytogenes	lisK 778T>G, lmo1389::himar1			Contains 778T>G in lisK and himar1 transposon at lmo1389 from TAP47 (phage lysate generated from EDL084 background)
EDL110	L. monocytogenes	lisK 106A>G, lmo1389::himar1			Contains 106A>G in lisK and himar1 transposon at lmo1389 from TAP47 (phage lysate generated from EDL085 background)
EDL111	E. coli (SM10)		pPL2x-Phyper-dxr	pPL2x	"Overexpresses" dxr (lmo1317) driven by pHyper promoter, but contains 100bp from gene itself
EDL112	L. monocytogenes	ΔhmgR			Δ*hmgR* suppressor #1 selected in anaerobic BHI broth, second round
EDL113	L. monocytogenes	ΔhmgR			Δ*hmgR* suppressor #2 selected in anaerobic BHI broth, second round (no lisK suppressor)
EDL114	L. monocytogenes	ΔhmgR			Δ*hmgR* suppressor #3 selected in anaerobic BHI broth, second round (no lisK suppressor)
EDL115	L. monocytogenes	ΔhmgR			Δ*hmgR* suppressor #4 selected in anaerobic BHI broth, second round (no lisK suppressor)
EDL116	L. monocytogenes	ΔhmgR			Δ*hmgR* suppressor #5 selected in anaerobic BHI broth, second round (no lisK suppressor)
EDL117	L. monocytogenes	ΔhmgR			Δ*hmgR* suppressor #6 selected in anaerobic BHI broth, second round (no lisK suppressor)
EDL118	L. monocytogenes	ΔhmgR			Δ*hmgR* suppressor #7 selected in anaerobic BHI broth, second round (lisK 826G>A)
EDL119	L. monocytogenes	ΔhmgR			Δ*hmgR* suppressor #8 selected in anaerobic BHI broth, second round (bad F sequencing)
EDL120	L. monocytogenes	ΔhmgR			Δ*hmgR* suppressor #9 selected in anaerobic BHI broth, second round (mixed population at 522?)
EDL121	L. monocytogenes	ΔhmgR			ΔhmgR suppressor #10 selected in anaerobic BHI broth, second round (no lisK suppressor)
EDL122	L. monocytogenes	ΔhmgR			Δ*hmgR* suppressor #11 selected in anaerobic BHI broth, second round (no lisK suppressor)
EDL123	L. monocytogenes	WT	pPL2x-Phyper-dxr	pPL2x	BAD PLASMID
EDL124	L. monocytogenes	ΔlisRK	pPL2x-Phyper-dxr	pPL2x	BAD PLASMID
EDL125	L. monocytogenes	ΔhmgR	pPL2x-Phyper-dxr	pPL2x	BAD PLASMID
EDL126	L. monocytogenes	ΔhmgR ΔlisK	pPL2x-Phyper-dxr	pPL2x	BAD PLASMID
EDL127	E. coli (SM10)		pPL2x-Phyper-dxr	pPL2x	Overexpresses dxr (lmo1317) driven by pHyper promoter
EDL128	L. monocytogenes	WT	pPL2x-Phyper-dxr	pPL2x	Overexpresses dxr (lmo1317) driven by pHyper promoter

EDL129	L. monocytogenes	ΔhmgR	pPL2x-Phyper-dxr	pPL2x	Overexpresses dxr (lmo1317) driven by pHyper promoter
EDL130	L. monocytogenes	WT	pPL2x-Phyper-uppS	pPL2x	Overexpresses uppS (lmo1315) driven by pHyper promoter
EDL131	L. monocytogenes	ΔhmgR	pPL2x-Phyper-uppS	pPL2x	Overexpresses uppS (lmo1315) driven by pHyper promoter
EDL132	E. coli (SM10)		pPL2x-Phyper-uppS+dxr	pPL2x	Overexpresses uppS (lmo1315) and dxr (lmo1317) driven by pHyper promoter
EDL133	E. coli (SM10)		pPL2x-PactA-hmgR		hmgR under control of an ActA promoter (promoter copied from PactA-cre construct)
EDL134	L. monocytogenes	ΔactA ΔinlB			LADD strain constructed by Pete Lauer and Bill Hanson (probably DP-L6053)
EDL135	L. monocytogenes	ΔhmgR	pPL2x-PactA-hmgR		hmgR under control of an ActA promoter (promoter copied from PactA-cre construct)
EDL136	L. monocytogenes	ΔhmgR ΔlisK	pPL2x-PactA-hmgR		hmgR under control of an ActA promoter (promoter copied from PactA-cre construct)
EDL137	L. monocytogenes	ΔhmgR	pPL2x-Phyper-uppS+dxr		Overexpresses uppS (lmo1315) and dxr (lmo1317) driven by pHyper promoter, No increased growth rate anaerobically
EDL138	E. coli (SM10)		pPL2e-PactA-cre		DP-E6233, pPL2e-PactA-cre
EDL139	E. coli (SM10)		pPL2e-Phyper-T1 terminator-hmgR	pPL2e	hmgR under control of an ActA promoter but contains T1 terminator IN FRONT of gene
EDL140	E. coli (SM10)		pKSV7x-hmgR (HPB2262)		Knocks out hmgR (6 AA at start and end) in strain HPB2262
EDL141	E. coli (SM10)		pKSV7x-gcpE (FSL N1-017)		Knocks out gcpE (6 AA at start and end) in strain FSL N1-017
EDL142	E. coli (SM10)		pKSV7x-lytB (FSL N1-017)		Knocks out lytB (6 AA at start and end) in strain FSL N1-017
EDL143	L. monocytogenes (HPB2262)	ΔhmgR			
EDL144	L. monocytogenes (FSL N1-017)	ΔgcpE			
EDL145	L. monocytogenes (FSL N1-017)	ΔlytB			
EDL146	E. coli (SM10)		pPL2e-Pmpl-hmgR		hmgR under control of mpl promoter, built in pPL2e
EDL147	E. coli (SM10)		pPL2e-PinlA-hmgR		hmgR under control of inlA promoter, built in pPL2e
EDL148	L. monocytogenes	ΔhmgR ΔlisK			Non-lysing suppressor #2, generated by plating anaerobically -MEV
EDL149	L. monocytogenes	ΔhmgR ΔlisK			Non-lysing suppressor #1, generated by plating anaerobically -MEV
EDL150	L. monocytogenes	ΔhmgR ΔlisK			Non-lysing suppressor #3, generated by plating anaerobically -MEV
EDL151	L. monocytogenes	ΔhmgR ΔlisK			Non-lysing suppressor #4, generated by plating anaerobically -MEV
EDL152	L. monocytogenes	ΔhmgR ΔlisK			Non-lysing suppressor 1D, generated by plating anaerobically -MEV, grew up in 2 days
EDL153	E. coli (SM10)		NONE		Original strain obtained from Rich Calendar, used to remake competent cells from the Berkeley QB3
EDL154	L. monocytogenes (HPB2262)				Strep resistant clinical isolate, no other genetic mutations
EDL155	L. monocytogenes (FSL N1-017)				Strep resistant clinical isolate, no other genetic mutations
EDL156	L. monocytogenes	ΔhmgR ΔlisK			Non-lysing suppressor 2A, generated by plating anaerobically -MEV

EDL157	L. monocytogenes	ΔhmgR ΔlisK			Non-lysing suppressor 2B, generated by plating anaerobically -MEV
EDL158	L. monocytogenes	ΔhmgR ΔlisK			Non-lysing suppressor 2C, generated by plating anaerobically -MEV
EDL159	L. monocytogenes	ΔhmgR ΔlisK			Non-lysing suppressor 3A, generated by plating anaerobically -MEV
EDL160	L. monocytogenes	ΔhmgR ΔlisK			Non-lysing suppressor 3B, generated by plating anaerobically -MEV
EDL161	L. monocytogenes	ΔhmgR ΔlisK			Non-lysing suppressor 3C, generated by plating anaerobically -MEV
EDL162	E. coli (SM10)		pKSV7x-hmgR::ErmR	pKSV7x	Replacing hmgR gene with Erm resistance cassette from pPL2e
EDL163	E. coli (SM10)		pKSV7x-gcpE (HPB2262)	pKSV7x	Deletes gcpE from clinical isolate HPB2262, 6 AA at front and end (APL)
EDL164	E. coli (SM10)		pKSV7x-lytB (HPB2262)	pKSV7x	Deletes lytB from clinical isolate HPB2262, 6 AA at front and end (APL)
EDL165	L. monocytogenes (EGDe)				DP-L197
EDL166	E. coli (SM10)		pKSV7x-gcpE (EGDe)	pKSV7x	Deletes gcpE from EGDe, 6 AA at front and end
EDL167	E. coli (SM10)		pKSV7x-lytB (EGDe)	pKSV7x	Deletes lytB from EGDe, 6 AA at front and end
EDL168	E. coli (SM10)		pKSV7x-hmgR (EGDe)	pKSV7x	Deletes hmgR from EGDe, 6 AA at front and end
EDL169	L. monocytogenes	hmgR::ErmR			Replacing hmgR gene with Erm resistance cassette from pPL2e
EDL170	E. coli (SM10)		pPL2x-pNative-gcpE-6xHis (10403S)	pPL2x	Complements gcpE from 10403S on pPL2x using native promoter (200bp from TSS), allows for translation of His and Strep tags
EDL171	E. coli (SM10)		pPL2x-pNative-lytB-6xHis (10403S)	pPL2x	Complements lytB from 10403S on pPL2x using native promoter (200bp from TSS), allows for translation of His and Strep tags
EDL172	L. monocytogenes	ΔgcpE	pPL2x-pNative-gcpE (10403S)	pPL2x	Complements gcpE from 10403S on pPL2x using native promoter (200bp from TSS), allows for translation of His and Strep tags
EDL173	L. monocytogenes	ΔlytB	pPL2x-pNative-lytB (10403S)	pPL2x	Complements lytB from 10403S on pPL2x using native promoter (200bp from TSS), allows for translation of His and Strep tags
EDL174	L. monocytogenes (EGDe)	ΔhmgR			Deletes hmgR from EGDe, 6 AA at front and end
EDL175	L. monocytogenes (FSL N1-017)	ΔgcpE	pPL2x-pNative-gcpE (10403S)	pPL2x	Complements gcpE from 10403S on pPL2x using native promoter (200bp from TSS), allows for translation of His and Strep tags
EDL176	L. monocytogenes (FSL N1-017)	ΔlytB	pPL2x-pNative-lytB (10403S)	pPL2x	Complements lytB from 10403S on pPL2x using native promoter (200bp from TSS), allows for translation of His and Strep tags
EDL177	L. monocytogenes (EGDe)	ΔgcpE			Deletes gcpE from EGDe, 6 AA at front and end (APL)
EDL178	L. monocytogenes (EGDe)	ΔlytB			Deletes lytB from EGDe, 6 AA at front and end (APL)
EDL179	E. coli (SM10)		pKSV7x-pHyper-hmgR::ErmR	pKSV7x	Replacing hmgR gene with Erm resistance cassette from pPL2e, driven by pHyper promoter
EDL180	L. monocytogenes (EGDe)	ΔgcpE	pPL2x-pNative-gcpE (10403S)	pPL2x	Complements gcpE from 10403S on pPL2x using native promoter (200bp from TSS), allows for translation of His and Strep tags
EDL181	L. monocytogenes (EGDe)	ΔlytB	pPL2x-pNative-lytB (10403S)	pPL2x	Complements lytB from 10403S on pPL2x using native promoter (200bp from TSS), allows for translation of His and Strep tags

EDL182	L. monocytogenes (HPB2262)	ΔgcpE			Deletes gcpE from HPB2262, 6 AA at front and end
EDL183	L. monocytogenes (HPB2262)	ΔlytB			Deletes lytB from HPB2262, 6 AA at front and end
EDL184	L. monocytogenes (HPB2262)	ΔgcpE	pPL2x-pNative-gcpE (10403S)	pPL2x	Complements gcpE from 10403S on pPL2x using native promoter (200bp from TSS), allows for translation of His and Strep tags
EDL185	L. monocytogenes (HPB2262)	ΔlytB	pPL2x-pNative-lytB (10403S)	pPL2x	Complements lytB from 10403S on pPL2x using native promoter (200bp from TSS), allows for translation of His and Strep tags
EDL186	E. coli (XL1 Blue)		None	pJZ037	Adapted from pKSV7 and contains a transposase for generating *Lmo* transposon libraries
EDL187	E. coli (DB3.1)			pLIVCC	
EDL188	L. monocytogenes	hly::Tn917			Contains transposon in hly using lysate from DP-L2209, parental strain is EDL001
EDL189	L. monocytogenes	ΔgcpE hly::Tn917			Contains transposon in hly using lysate from DP-L2209, parental strain is EDL011
EDL190	L. monocytogenes	ΔlytB hly::Tn917			Contains transposon in hly using lysate from DP-L2209, parental strain is EDL012
EDL191	E. coli (SM10)		pPL2x-pNative-lisK*1	pPL2x	Complements lisK from EDL083 on pPL2x using native promoter (200bp from TSS)
EDL192	E. coli (SM10)		pPL2x-pNative-lisK*2	pPL2x	Complements lisK from EDL084 on pPL2x using native promoter (200bp from TSS)
EDL193	E. coli (SM10)		pPL2x-pNative-lisK*3	pPL2x	Complements lisK from EDL085 on pPL2x using native promoter (200bp from TSS)
EDL194	L. monocytogenes	ΔhmgR	pPL2x-pNative-lisK*1	pPL2x	Complements lisK from EDL083 on pPL2x using native promoter (200bp from TSS)
EDL195	L. monocytogenes	ΔhmgR	pPL2x-pNative-lisK*2	pPL2x	Complements lisK from EDL084 on pPL2x using native promoter (200bp from TSS)
EDL196	L. monocytogenes	ΔhmgR	pPL2x-pNative-lisK*3	pPL2x	Complements lisK from EDL085 on pPL2x using native promoter (200bp from TSS)
EDL197	E. coli (PPY)				PPY strain from Rob Nichols
EDL198	L. monocytogenes (HPB2262)	Himar1			Tn library prepared using pJZ037. Probably fairly poor coverage.
EDL199	L. monocytogenes (HPB2262)	Himar1			Tn library prepared using pJZ037. Probably fairly poor coverage.
EDL200	E. coli (SM10)		pKSV7x-lisR	pKSV7x	Deletes lisR from 10403S, 6 AA at front and end
EDL201	E. coli (SM10)		pKSV7x-hmgS	pKSV7x	Deletes hmgS from 10403S, 6 AA at front and end
EDL202	L. monocytogenes	ΔlisR			LisR deleted from 10403S, 6 AA at front and end
EDL203	L. monocytogenes	ΔhmgS			HmgS deleted from 10403S, 6 AA at front and end
EDL204	L. monocytogenes	ΔhmgS ΔhmgR			HmgS and HmgR deleted from 10403S, 6 AA at front and end
EDL205	L. monocytogenes	ΔhmgR ΔlisR			HmgR and LisR deleted from 10403S, 6 AA at front and end
EDL206	L. monocytogenes	WT			Contains a Tn917- LTV3 insertion that leads to constitutive expression of lacZ gene
EDL207	L. monocytogenes	ΔhmgR			Contains a Tn917- LTV3 insertion that leads to constitutive expression of lacZ gene
EDL208	L. monocytogenes	ΔhmgS			Contains a Tn917- LTV3 insertion that leads to constitutive expression of lacZ gene
EDL209	L. monocytogenes	ΔhmgR ΔlisK			Refreeze of EDL075 since old stock has decreased viability
EDL210	L. monocytogenes	ΔhmgR ΔlisR			Contains a Tn917- LTV3 insertion that leads to constitutive expression of lacZ gene

EDL211	L. monocytogenes	ΔhmgR ΔlisK			Contains a Tn917- LTV3 insertion that leads to constitutive expression of lacZ gene
EDL212	E. coli (SM10)		pKSV7x-lisRK::ErmR	pKSV7x	(should) Replace lisRK with ErmR cassette from pPL2e
EDL213	Enterococcus faecalis CG110		Tn916		DP-E205, Strain used to conjugate Tn916 into L. monocytogenes from Enterococcus (http://www.pnas.org/content/pnas/86/14/5522.full.pdf)
EDL214	E. coli (SM10)	Δlmo0061	pKSV7x-lmo0061	pKSV7x	pKSV7 to delete lmo0061 from 10403S, 6 AA at front and end
EDL215	L. monocytogenes	lisRK::ErmR			Replaces lisRK with ErmR cassette from pPL2e
EDL216	L. monocytogenes				Alex Louie WT Listeria
EDL217	E. coli (DH5-alpha)				DH5-alpha derivative expressing recombinase (from Chen)
EDL218	E. coli (DH5-alpha)				DH5-alpha expressing RegIII-gamma (from Freddy)
EDL219	L. monocytogenes	Δlmo0061			Lmo0061 deleted from 10403S, 6 AA at front and end (From Alex Louie WT, EDL216)
EDL220	L. monocytogenes	Δhly ΔgcpE			Knockout of gcpE derived from DP-L2161 Δhly background
EDL222	L. monocytogenes (HPB2262, StrepR)	ΔgcpE			Knockout of gcpE derived from EDL154
EDL223	L. monocytogenes (HPB2262, StrepR)	ΔlytB			Knockout of lytB derived from EDL154
EDL224	E. coli (DB3.1)		None		ccdB resistant E. coli with no plasmid
EDL225	E. coli (Top10)		None		ccdB sensitive E. coli with no plasmid, obtained from manufacturer
EDL226	E. coli (DB3.1)		pPL2-ccdB	pPL2x	Removed some parts of MCS, keeps ccdB toxin intact
EDL227	E. coli (Top10)		FSL N1-017 ΔhmgR Library 1	pPL2-ccdB	Approximately 500 colonies frozen down
EDL228	E. coli (Top10)		HPB2262 ΔhmgR Library 1	pPL2-ccdB	Approximately 500 colonies frozen down
EDL229	E. coli (SM10)		FSL N1-017 ΔhmgR Library 1	pPL2-ccdB	>2000 colonies frozen down
EDL230	E. coli (SM10)		HPB2262 ΔhmgR Library 1	pPL2-ccdB	>2000 colonies frozen down
EDL231	E. coli (Top10)		FSL N1-017 ΔhmgR Library 2	pPL2-ccdB	Approximately 700 colonies frozen down
EDL232	E. coli (Top10)		HPB2262 ΔhmgR Library 2	pPL2-ccdB	Approximately 700 colonies frozen down
EDL233	E. coli (SM10)		pPL2-ispD (10403S)	pPL2x	ispD from 10403S complemented with ~200 bp upstream promoter
EDL234	E. coli (SM10)		pPL2-ispD (FSL)	pPL2x	ispD from FSL N1-017 complemented with ~200 bp upstream promoter
EDL235	E. coli (SM10)		pPL2-ispD (HPB)	pPL2x	ispD from HPB2262 complemented with ~200 bp upstream promoter
EDL236	E. coli (SM10)		pPL2-ispD (Phyper)	pPL2x	ispD from 10403S complemented with Phyper promoter
EDL237	E. coli (SM10)		pPL2-gcpE (10403S)	pPL2x	gcpE from 10403S complemented with ~200 bp upstream promoter
EDL238	E. coli (SM10)		pPL2-gcpE (FSL)	pPL2x	gcpE from FSL N1-017 complemented with ~200 bp upstream promoter
EDL239	E. coli (SM10)		pPL2-gcpE (HPB)	pPL2x	gcpE from HPB2262 complemented with ~200 bp upstream promoter

EDL240	E. coli (SM10)		pPL2-gcpE (Phyper-HPB)	pPL2x	gcpE from HPB2262 complemented with Phyper promoter
EDL241	E. coli (SM10)		pPL2-lytB (10403S)	pPL2x	lytB from 10403S complemented with ~200 bp upstream promoter
EDL242	E. coli (SM10)		pPL2-lytB (FSL)	pPL2x	lytB from FSL N1-017 complemented with ~200 bp upstream promoter
EDL243	E. coli (SM10)		pPL2-lytB (HPB)	pPL2x	lytB from HPB2262 complemented with ~200 bp upstream promoter
EDL244	E. coli (SM10)		pPL2-lytB (Phyper-10403S)	pPL2x	lytB from 10403S complemented with Phyper promoter
EDL245	E. coli (SM10)		pPL2-lytB (Phyper-FSL,HPB)	pPL2x	lytB from FSL N1-017 complemented with Phyper promoter
EDL246	E. coli (DB3.1)		pPL2gg	pPL2x	pPL2x modified to have Golden Gate BbsI cut sites
EDL247	L. monocytogenes	ΔhmgR	pPL2-ispD (10403S)	pPL2x	ispD from 10403S complemented with ~200 bp upstream promoter
EDL248	L. monocytogenes	ΔhmgR	pPL2-ispD (FSL)	pPL2x	ispD from FSL N1-017 complemented with ~200 bp upstream promoter
EDL249	L. monocytogenes	ΔhmgR	pPL2-ispD (HPB)	pPL2x	ispD from HPB2262 complemented with ~200 bp upstream promoter
EDL250	L. monocytogenes	ΔhmgR	pPL2-ispD (Phyper)	pPL2x	ispD from 10403S complemented with Phyper promoter
EDL251	L. monocytogenes	ΔhmgR	pPL2-gcpE (10403S)	pPL2x	gcpE from 10403S complemented with ~200 bp upstream promoter
EDL252	L. monocytogenes	ΔhmgR	pPL2-gcpE (FSL)	pPL2x	gcpE from FSL N1-017 complemented with ~200 bp upstream promoter
EDL253	L. monocytogenes	ΔhmgR	pPL2-gcpE (HPB)	pPL2x	gcpE from HPB2262 complemented with ~200 bp upstream promoter
EDL254	L. monocytogenes	ΔhmgR	pPL2-gcpE (Phyper-HPB)	pPL2x	gcpE from HPB2262 complemented with Phyper promoter
EDL255	L. monocytogenes	ΔhmgR	pPL2-lytB (10403S)	pPL2x	lytB from 10403S complemented with ~200 bp upstream promoter
EDL256	L. monocytogenes	ΔhmgR	pPL2-lytB (FSL)	pPL2x	lytB from FSL N1-017 complemented with ~200 bp upstream promoter
EDL257	L. monocytogenes	ΔhmgR	pPL2-lytB (HPB)	pPL2x	lytB from HPB2262 complemented with ~200 bp upstream promoter
EDL258	L. monocytogenes	ΔhmgR	pPL2-lytB (Phyper-10403S)	pPL2x	lytB from 10403S complemented with Phyper promoter
EDL259	L. monocytogenes	ΔhmgR	pPL2-lytB (Phyper-FSL,HPB)	pPL2x	lytB from FSL N1-017 complemented with Phyper promoter
EDL260	L. monocytogenes	ΔgcpE hly::Tn917	pPL2-gcpE (10403S)	pPL2x	EDL189 with gcpE from 10403S complemented with ~200 bp upstream promoter
EDL261	L. monocytogenes	ΔgcpE hly::Tn917	pPL2-gcpE (FSL)	pPL2x	EDL189 with gcpE from FSL N1-017 complemented with ~200 bp upstream promoter
EDL262	L. monocytogenes	ΔgcpE hly::Tn917	pPL2-gcpE (HPB)	pPL2x	EDL189 with gcpE from HPB2262 complemented with ~200 bp upstream promoter
EDL263	L. monocytogenes	ΔgcpE hly::Tn917	pPL2-gcpE (Phyper-HPB)	pPL2x	EDL189 with gcpE from HPB2262 complemented with Phyper promoter
EDL264	L. monocytogenes	ΔlytB hly::Tn917	pPL2-lytB (10403S)	pPL2x	EDL190 with lytB from 10403S complemented with ~200 bp upstream promoter
EDL265	L. monocytogenes	ΔlytB hly::Tn917	pPL2-lytB (FSL)	pPL2x	EDL190 with lytB from FSL N1-017 complemented with ~200 bp upstream promoter
EDL266	L. monocytogenes	ΔlytB hly::Tn917	pPL2-lytB (HPB)	pPL2x	EDL190 with lytB from HPB2262 complemented with ~200 bp upstream promoter

EDL267	L. monocytogenes	ΔlytB hly::Tn917	pPL2-lytB (Phyper-10403S)	pPL2x	EDL190 with lytB from 10403S complemented with Phyper promoter
EDL268	L. monocytogenes	ΔlytB hly::Tn917	pPL2-lytB (Phyper-FSL,HPB)	pPL2x	EDL190 with lytB from FSL N1-017 complemented with Phyper promoter
EDL269	L. monocytogenes	ΔhmgR ΔgcpE	pPL2-gcpE (10403S)	pPL2x	gcpE from 10403S complemented with ~200 bp upstream promoter
EDL270	L. monocytogenes	ΔhmgR ΔgcpE	pPL2-gcpE (FSL)	pPL2x	gcpE from FSL N1-017 complemented with ~200 bp upstream promoter
EDL271	L. monocytogenes	ΔhmgR ΔgcpE	pPL2-gcpE (HPB)	pPL2x	gcpE from HPB2262 complemented with ~200 bp upstream promoter
EDL272	L. monocytogenes	ΔhmgR ΔgcpE	pPL2-gcpE (Phyper-HPB)	pPL2x	gcpE from HPB2262 complemented with Phyper promoter
EDL273	L. monocytogenes	ΔhmgR ΔlytB	pPL2-lytB (10403S)	pPL2x	lytB from 10403S complemented with ~200 bp upstream promoter
EDL274	L. monocytogenes	ΔhmgR ΔlytB	pPL2-lytB (FSL)	pPL2x	lytB from FSL N1-017 complemented with ~200 bp upstream promoter
EDL275	L. monocytogenes	ΔhmgR ΔlytB	pPL2-lytB (HPB)	pPL2x	lytB from HPB2262 complemented with ~200 bp upstream promoter
EDL276	L. monocytogenes	ΔhmgR ΔlytB	pPL2-lytB (Phyper-10403S)	pPL2x	lytB from 10403S complemented with Phyper promoter
EDL277	L. monocytogenes	ΔhmgR ΔlytB	pPL2-lytB (Phyper-FSL,HPB)	pPL2x	lytB from FSL N1-017 complemented with Phyper promoter
EDL278	E. coli (SM10)		pPL2-gcpE (Phyper-10403S)	pPL2x	gcpE from 10403S complemented with Phyper promoter
EDL279	L. monocytogenes	ΔgcpE	pPL2-gcpE (10403S)	pPL2x	EDL011 with gcpE from 10403S complemented with ~200 bp upstream promoter
EDL280	L. monocytogenes	ΔgcpE	pPL2-gcpE (FSL)	pPL2x	EDL011 with gcpE from FSL N1-017 complemented with ~200 bp upstream promoter
EDL281	L. monocytogenes	ΔgcpE	pPL2-gcpE (HPB)	pPL2x	EDL011 with gcpE from HPB2262 complemented with ~200 bp upstream promoter
EDL282	L. monocytogenes	ΔgcpE	pPL2-gcpE (Phyper-HPB)	pPL2x	EDL011 with gcpE from HPB2262 complemented with Phyper promoter
EDL283	L. monocytogenes	ΔlytB	pPL2-gcpE (10403S)	pPL2x	EDL012 with gcpE from 10403S complemented with ~200 bp upstream promoter
EDL284	L. monocytogenes	ΔlytB	pPL2-gcpE (FSL)	pPL2x	EDL012 with gcpE from FSL N1-017 complemented with ~200 bp upstream promoter
EDL285	L. monocytogenes	ΔlytB	pPL2-gcpE (HPB)	pPL2x	EDL012 with gcpE from HPB2262 complemented with ~200 bp upstream promoter
EDL286	L. monocytogenes	ΔlytB	pPL2-gcpE (Phyper-HPB)	pPL2x	EDL012 with gcpE from HPB2262 complemented with Phyper promoter
EDL287	L. monocytogenes	ΔgcpE	pPL2-gcpE (Phyper-10403S)	pPL2x	gcpE from 10403S complemented with Phyper promoter
EDL288	L. monocytogenes	ΔlytB	pPL2-gcpE (Phyper-10403S)	pPL2x	gcpE from 10403S complemented with Phyper promoter
EDL289	L. monocytogenes	ΔhmgR ΔgcpE	pPL2-gcpE (Phyper-10403S)	pPL2x	gcpE from 10403S complemented with Phyper promoter
EDL290	L. monocytogenes	ΔhmgR ΔlytB	pPL2-gcpE (Phyper-10403S)	pPL2x	gcpE from 10403S complemented with Phyper promoter
EDL291	E. coli (SM10)		pPL2-gcpE (P10403S FSL N1-017)	pPL2x	
EDL292	E. coli (SM10)		pPL2-gcpE (P10403S HPB2262)	pPL2x	

EDL293	E. coli (SM10)		pPL2-gcpE (PFSL 10403S)	pPL2x	
EDL294	E. coli (SM10)		pPL2-gcpE (PHPB 10403S)	pPL2x	
EDL295	L. monocytogenes	ΔhmgR	pPL2-gcpE (Phyper-10403S)	pPL2x	
EDL296	L. monocytogenes	ΔhmgR	pPL2-gcpE (P10403S FSL N1-017)	pPL2x	
EDL297	L. monocytogenes	ΔhmgR	pPL2-gcpE (P10403S HPB2262)	pPL2x	
EDL298	L. monocytogenes	ΔhmgR	pPL2-gcpE (PFSL 10403S)	pPL2x	
EDL299	L. monocytogenes	ΔhmgR	pPL2-gcpE (PHPB 10403S)	pPL2x	
EDL300	L. monocytogenes	ΔhmgR ΔgcpE	pPL2-gcpE (P10403S FSL N1-017)	pPL2x	
EDL301	L. monocytogenes	ΔhmgR ΔgcpE	pPL2-gcpE (P10403S HPB2262)	pPL2x	
EDL302	L. monocytogenes	ΔhmgR ΔgcpE	pPL2-gcpE (PFSL 10403S)	pPL2x	
EDL303	L. monocytogenes	ΔhmgR ΔgcpE	pPL2-gcpE (PHPB 10403S)	pPL2x	
EDL304	E. coli (SM10)		pPL2-gcpE (P10403S 10403S+FSL N1-017)	pPL2x	
EDL305	E. coli (SM10)		pPL2-lytB (P10403S + FSL N1-017)	pPL2x	KN
EDL306	E. coli (SM10)		pPL2-lytB (P10403S + HPB2262)	pPL2x	KN
EDL307	E. coli (SM10)		pPL2-lytB (P FSL + 10403S)	pPL2x	KN
EDL308	E. coli (SM10)		pPL2-gcpE (10403S, K291T/E293K/V294A)	pPL2x	Point mutations in gcpE to match 10403S more closely with clinical isolates
EDL309	E. coli (SM10)		pPL2-gcpE (10403S, I343V/D344E)	pPL2x	Point mutations in gcpE to match 10403S more closely with clinical isolates
EDL310	E. coli (SM10)		pPL2-gcpE (10403S, F357Y/V359E)	pPL2x	Point mutations in gcpE to match 10403S more closely with clinical isolates
EDL311	L. monocytogenes	ΔhmgR ΔgcpE	pPL2-gcpE (10403S, I343V/D344E)	pPL2x	Point mutations in gcpE to match 10403S more closely with clinical isolates
EDL312	L. monocytogenes	ΔhmgR ΔgcpE	pPL2-gcpE (10403S, F357Y/V359E)	pPL2x	Point mutations in gcpE to match 10403S more closely with clinical isolates
EDL313	L. monocytogenes	ΔhmgR ΔlytB	pPL2-lytB (P10403S + FSL N1-017)	pPL2x	KN
EDL314	L. monocytogenes	ΔhmgR ΔlytB	pPL2-lytB (P10403S + HPB2262)	pPL2x	KN

EDL315	L. monocytogenes	ΔhmgR ΔlytB	pPL2-lytB (P FSL + 10403S)	pPL2x	KN
EDL316	L. monocytogenes	ΔhmgR ΔgcpE	pPL2-gcpE (P10403S 10403S+FSL N1-017)	pPL2x	Chimera of 10403S and FSL (C-terminal) protein, starting at 250 AA
EDL317	L. monocytogenes	ΔhmgR ΔgcpE	pPL2-gcpE (10403S, K291T/E293K/V294A)	pPL2x	
EDL318	L. monocytogenes	ΔhmgR ΔlytB	pPL2-gcpE (10403S)	pPL2x	
EDL319	L. monocytogenes	ΔhmgR ΔlytB	pPL2-lytB (P HPB + 10403S)	pPL2x	KN
EDL320	E. coli (SM10)		pPL2-gcpE (10403S, K291T/E293K/V294A/I343V/D344E)	pPL2x	Point mutations in gcpE to match 10403S more closely with clinical isolates
EDL321	E. coli (SM10)		pPL2-gcpE (10403S, K291T/E293K/V294A/F357Y/V359E)	pPL2x	Point mutations in gcpE to match 10403S more closely with clinical isolates
EDL322	E. coli (SM10)		pPL2-gcpE (10403S, K291T)	pPL2x	Point mutations in gcpE to match 10403S more closely with clinical isolates
EDL323	E. coli (SM10)		pPL2-gcpE (10403S, E293K)	pPL2x	Point mutations in gcpE to match 10403S more closely with clinical isolates
EDL324	E. coli (SM10)		pPL2-gcpE (10403S, V294A)	pPL2x	Point mutations in gcpE to match 10403S more closely with clinical isolates
EDL325	L. monocytogenes	ΔhmgR ΔgcpE	pPL2-gcpE (10403S, K291T)	pPL2x	Point mutations in gcpE to match 10403S more closely with clinical isolates
EDL326	L. monocytogenes	ΔhmgR ΔgcpE	pPL2-gcpE (10403S, E293K)	pPL2x	*** Accidentally complemented in lytB?
EDL327	L. monocytogenes	ΔhmgR ΔgcpE	pPL2-gcpE (10403S, V294A)	pPL2x	Point mutations in gcpE to match 10403S more closely with clinical isolates
EDL328	L. monocytogenes	ΔhmgR fmnB::Tn917			hmgR strain with FLEET mutants (lmo2636)
EDL329	L. monocytogenes	ΔhmgR ndh2::Tn917			hmgR strain with FLEET mutants (lmo2638)
EDL330	L. monocytogenes	ΔhmgR ΔgcpE	pPL2-gcpE (10403S, K291T/E293K/V294A/I343V/D344E)	pPL2x	
EDL331	L. monocytogenes	ΔhmgR ΔgcpE	pPL2-gcpE (10403S, K291T/E293K/V294A/F357Y/V359E)	pPL2x	
EDL332	E. coli (SM10)		pKSV7-gcpE (K291T/E293K/V294A)	pKSV7x	Complements gcpE (K291T/E293K/V294A) onto the chromosome
EDL333	L. monocytogenes	pActA(999)-hmgS			Complements hmgS under mutated pActA (from Chen, on the chromosome)
EDL334	L. monocytogenes	gcpE (K291T/E293K/V294A)			Point mutations in gcpE (K291T/E293K/V294A) complemented onto the chromosome
EDL335	L. monocytogenes	ΔhmgR gcpE (K291T/E293K/V294A)			
EDL336	L. monocytogenes	ΔhmgR gcpE (K291T/E293K/V294A) lisK106A>G lmo1389::himar1			Adds lisK suppressor mutation into improved gcpE background

EDL337	L. monocytogenes	ΔhmgR gcpE (K291T/E293K/V294A) lisK826G>A lmo1389::himar1			Adds lisK suppressor mutation into improved gcpE background
EDL338	L. monocytogenes	ΔhmgR	pPL2-gcpE (10403S, E293K)		*** Accidentally complemented in lytB?
EDL339	E. coli (SM10)		pPL2-Phyper-iscSUAX-hSCBA (E. coli)	pPL2x	Contains ISC operon from K-12 E. coli to see if it complements aerobic ΔhmgR growth
EDL340	E. coli (SM10)		pPL2-Pnative-sufCDSUB	pPL2x	Contains sufCDSUB operon from B subtilis to see if it complements aerobic ΔhmgR growth
EDL341	E. coli (SM10)		pPL2-Phyper-sufCDSUB	pPL2x	Contains sufCDSUB operon from B subtilis to see if it complements aerobic ΔhmgR growth
EDL342	E. coli (SM10)		pKSV7-lytB (FSL)	pKSV7x	Complements gcpE (K291T/E293K/V294A) onto the chromosome
EDL343	L. monocytogenes	ΔhmgR	pPL2-Phyper-iscSUAX-hSCBA (E. coli)	pPL2x	Contains ISC operon from K-12 E. coli to see if it complements aerobic ΔhmgR growth
EDL344	L. monocytogenes	ΔhmgR ΔgcpE	pPL2-Phyper-iscSUAX-hSCBA (E. coli)	pPL2x	Contains ISC operon from K-12 E. coli to see if it complements aerobic ΔhmgR growth
EDL345	L. monocytogenes	ΔhmgR	pPL2-Pnative-sufCDSUB	pPL2x	Contains sufCDSUB operon from B subtilis to see if it complements aerobic ΔhmgR growth
EDL346	L. monocytogenes	ΔhmgR ΔgcpE	pPL2-Pnative-sufCDSUB	pPL2x	Contains sufCDSUB operon from B subtilis to see if it complements aerobic ΔhmgR growth
EDL347	L. monocytogenes	ΔhmgR	pPL2-Phyper-sufCDSUB	pPL2x	Contains sufCDSUB operon from B subtilis to see if it complements aerobic ΔhmgR growth
EDL348	L. monocytogenes	ΔhmgR ΔgcpE	pPL2-Phyper-sufCDSUB	pPL2x	Contains sufCDSUB operon from B subtilis to see if it complements aerobic ΔhmgR growth
EDL349	L. monocytogenes	ΔhmgR gcpE (K291T/E293K/V294A) ΔlytB			
EDL350	L. monocytogenes	ΔhmgR lmo1956::Tn			Transposon in Fur regulator
EDL351	L. monocytogenes	ΔhmgR ΔgcpE lmo1956::Tn			Transposon in Fur regulator
EDL352	L. monocytogenes	ΔhmgR gcpE (K291T/E293K/V294A) ΔlytB	pPL2-lytB (10403S)		Complements varying lytB genes in gcpE* background
EDL353	L. monocytogenes	ΔhmgR gcpE (K291T/E293K/V294A) ΔlytB	pPL2-lytB (FSL)		Complements varying lytB genes in gcpE* background
EDL354	L. monocytogenes	ΔhmgR gcpE (K291T/E293K/V294A) ΔlytB	pPL2-lytB (HPB)		Complements varying lytB genes in gcpE* background
EDL355	L. monocytogenes	ΔhmgR gcpE (K291T/E293K/V294A) ΔlytB	pPL2-lytB (Phyper-10403S)		Complements varying lytB genes in gcpE* background
EDL356	L. monocytogenes	ΔhmgR gcpE (K291T/E293K/V294A) ΔlytB	pPL2-lytB (Phyper-FSL,HPB)		Complements varying lytB genes in gcpE* background
EDL357	L. monocytogenes	ΔhmgR gcpE (K291T/E293K/V294A) ΔlytB	pPL2-lytB (P10403S + FSL N1-017)		Complements varying lytB genes in gcpE* background
EDL358	L. monocytogenes	ΔhmgR gcpE (K291T/E293K/V294A) ΔlytB	pPL2-lytB (P10403S + HPB2262)		Complements varying lytB genes in gcpE* background
EDL359	L. monocytogenes	ΔhmgR gcpE (K291T/E293K/V294A) ΔlytB	pPL2-lytB (P FSL + 10403S)		Complements varying lytB genes in gcpE* background

EDL360	E. coli (SM10)		pKSV7-ΔgcpE+kanR	pKSV7x	EDL009 with kanR cassette added in-frame after stop codon, for genetic linkage experiment
EDL361	E. coli (SM10)		pKSV7-ΔsufSU (lmo2412/2413)	pKSV7x	pKSV7 to delete sufSU (lmo2412/2413) in frame, without kanR cassette
EDL362	E. coli (SM10)		pKSV7-ΔsufSU+KanR inverted (lmo2412/2413)	pKSV7x	pKSV7 to delete lmo2412/2413 with kanR cassette added backwards
EDL363	E. coli (SM10)		pPL2-lytB (PHPB + 10403S)	pPL2x	
EDL364	L. monocytogenes	ΔhmgR gcpE (K291T/E293K/V294A) lytB (FSL)			hmgR knockout with manipulated gcpE and lytB from FSL N1-017
EDL365	L. monocytogenes	gcpE (K291T/E293K/V294A) hly::Tn917			
EDL366	E. coli (SM10)		pPL2-Phy-lytB (10403S/FSL chimera)	pPL2x	Split made at AA 221
EDL367	E. coli (SM10)		pPL2-Phy-lytB (HPB/10403S chimera)	pPL2x	Split made at AA 221
EDL368	E. coli (SM10)		pKSV7-ΔhmgR	pKSV7x	Remade, correct plasmid to delete hmgR
EDL369	E. coli (SM10)		pKSV7-ΔhmgR+KanR	pKSV7x	Makes hmgR deletion with KanR cassette fused directly behind
EDL370	E. coli (SM10)		pKSV7-HmgR+KanR	pKSV7x	Keeps hmgR gene with KanR cassette fused directly behind
EDL373	L. monocytogenes				DP-L7000
EDL374	L. monocytogenes	ΔhmgR gcpE (K291T/E293K/V294A)	pPL2-Phyper-iscSUAX-hSCBA (E. coli)	pPL2x	
EDL375	L. monocytogenes	ΔhmgR gcpE (K291T/E293K/V294A)	pPL2-Pnative-sufCDSUB	pPL2x	
EDL376	L. monocytogenes	ΔhmgR gcpE (K291T/E293K/V294A)	pPL2-Phyper-sufCDSUB	pPL2x	
EDL377	L.monocytogenes		pPL2-Phyper-sufCDSUB	pPL2x	
EDL378	E. coli (XL1 Blue)			pMV306	Integrating vector for cloning in M. tuberculosis
EDL379	L. monocytogenes		pPL2-Phyper-iscSUAX-hSCBA (E. coli)	pPL2x	Contains ISC operon from K-12 E. coli to see if it complements aerobic ΔhmgR growth
EDL380	L. monocytogenes	ΔgcpE ΔlytB			Nonmevalonate pathway double knockout
EDL381	L. monocytogenes	gcpE* (K291T/E293K/V294A) ΔlytB			LytB knockout with gcpE* chromosomal mutations
EDL382	E. coli (SM 10)		pKSV7 - ΔSufSU + KanR	pKSV7	Makes hmgR deletion with KanR casette fused directly behind. No stop codon
EDL383	L. monocytogenes	ΔactA pActA(999)-hmgS			Complements hmgS under mutated pActA (from Chen, on the chromosome); unknown actA deletion
EDL384	E coli (SM 10)		pPL2 - Prha - suf (lmo native)	pPL2x	
EDL385	E. coli (SM 10)		pPL2 - Phyper - suf (lmo native)	pPL2x	NOPE but i'm keeping the placeholder in the lab inventory
EDL386	L. monocytogenes	WT	pPL2 - Phyper suf(lmo native)	pPL2x	NOPE, BUT i'm keeping the placeholder for now.

EDL387	L. monocytogenes	ΔhmgR	pPL2 - Phyper - suf(lmo native)	pPL2x	NOPE but keeping placeholder
EDL388	L. monocytogenes	WT	pPL2 - Prhamnose - suf (lmo native)	pPL2x	two frozen in bottom of box waiting for further screening
EDL389	L. monocytogenes	ΔhmgR	pPL2 - Prhamnose - suf (lmo native)	pPL2x	two frozen in bottom of box waiting for further screening